ATMOSPHERIC PROCESSES RELATED TO

DEEP PERSISTENT SLAB AVALANCHES IN THE WESTERN UNITED STATES

by

Andrew Robert Schauer

A thesis submitted in partial fulfillment
of the requirements for the degree

of

Master of Science

in

Earth Sciences

MONTANA STATE UNIVERSITY
Bozeman, Montana

May 2019

ACKNOWLEDGEMENTS

I would like to thank Jordy Hendrikx, Karl Birkeland, and Megan Higgs for their guidance during this project, and for helping me transform an idea into a Master's thesis. Cary Mock provided invaluable feedback with respect to atmospheric processes and classification. I would like to thank Rob Payn for direction and feedback while developing the methodology of this project. I am extremely grateful to the Bridger Bowl Ski Patrol- notably Pete Maleski, Ella Darham, Richard Griffen, and Doug Richmond- for providing records, and sharing their insight regarding weather patterns and big avalanches at Bridger Bowl. Thank you to Ned Bair and the Mammoth Mountain Ski Patrol for compiling, sharing, and discussing weather and avalanche records from Mammoth Mountain. Thanks to Chris McCollister, Bob Comey, Patrick Wright, Grand Targhee Ski Patrol, and Jackson Hole Ski Patrol for doing the same for Jackson Hole and Grand Targhee. Their input, guided by decades of experience in the arena, helped solidify my understanding of this project.

Thank you to everybody at the Gallatin National Forest Avalanche Center for your guidance and mentorship, and for a good excuse to get outside while I was buried in this thesis. I am especially grateful for the motivation and support from Alex Marienthal. I would not have made it this far without his help.

Most importantly, I would like to thank my entire family for their support and encouragement from day one, and for the countless hours they spent editing my writing.

This research was funded in part by two separate grants from the American Avalanche Association.

TABLE OF CONTENTS

TABLE OF CONTENTS CONTINUED

LIST OF TABLES

Table Page

LIST OF FIGURES

Figure Page

LIST OF FIGURES CONTINUED

Figure Page

LIST OF FIGURES CONTINUED

Figure Page

ABSTRACT

Deep persistent slab avalanches are a natural hazard that are particularly difficult to predict. These avalanches are capable of destroying infrastructure in mountain settings, and are generally unsurvivable by humans. Deep persistent slab avalanches are characterized by a thick (> 1 m) slab of cohesive snow overlaying a weak layer in the snowpack, which can fail due to overburden stress of the slab itself or to external triggers such as falling cornices, explosives, or a human. While formation of such snowpack structure is controlled by persistent weather patterns early in the winter, a snowpack exhibiting characteristics capable of producing a deep persistent slab avalanche may exist for weeks or months before a specific weather event such as a heavy precipitation or rapid warming pushes the weak layer to its breaking point. Mountain weather patterns are highly variable down to the local scale (1-10 m), but they are largely driven by atmospheric processes on the continental scale (1000 km). This work relates atmospheric circulation to deep persistent slab events at Mammoth, CA; Bridger Bowl, MT; and Jackson, WY. We classify 5,899 daily 500 millibar geopotential height maps into 20 synoptic types using Self-Organizing Maps. At each location, we examine the frequency of occurrence of each of the 20 types during November through January during major deep persistent slab seasons and compare those frequencies to seasons without deep persistent slab avalanches. We also consider the 72-hour time period preceding deep persistent slab avalanches at each location and identify synoptic types occurring frequently, as well as those rarely occurring prior to onset of activity. At each location, we find specific synoptic types that tend to occur at a higher rate during major deep persistent slab years, while minor years are characterized by different circulation patterns. We also find a small number of synoptic types dominating the 72-hour period prior to onset of deep slab activity. With this improved understanding of the atmospheric processes preceding deep persistent slab avalanches, we provide avalanche practitioners with an additional tool to better anticipate a difficult to predict natural hazard.

INTRODUCTION

Background

Deep persistent slab avalanches are a destructive and difficult to predict natural hazard. These events are capable of causing severe damage to infrastructure and are often unsurvivable for people caught in them. Persistent Slab avalanches occur when a persistent weak layer in the snowpack that is overlain by a cohesive slab collapses due to overburden stress from the slab itself, or applied stresses from external loads such as new and wind-deposited snow, falling cornices, explosives, or humans. (Schweizer et al., 2016; McClung and Schaerer, 2006). Formation of a snowpack conducive to slab avalanches results from weather patterns operating on time scales from hours to months (Birkeland, 1998; Lang et al., 1984; Marienthal et al. 2015), which can exhibit a large amount of geographic and interannual variability (Mock and Birkeland, 2000). Similarly, the onset of slab avalanche activity is commonly accompanied with certain meteorological conditions including severe loading from snow and wind, rain-on-snow events, or rapid warming (Atwater, 1954; LaChapelle, 1966; LaChapelle, 1980). Although mountain weather is a complex and spatially variable phenomenon, these meteorological processes are largely driven by circulation patterns occurring in the upper atmosphere on the synoptic scale (Aguado and Burt, 2015). The field of synoptic climatology relates atmospheric processes to environmental responses such as precipitation, air quality, and natural disasters (Yarnal, 1993), and will provide the framework for this study.

Avalanche Impacts

Snow avalanches killed 1083 people in the United States between 1950/51 and 2017/18 (CAIC, 2019). Between 1951 and 1970 there were 4.9 fatalities on average annually (Figure 1). With the advent of more advanced backcountry skiing technology and subsequent increased backcountry usage beginning in the early1970's, 12.5 people were dying in avalanches per year on average between 1970 and 1990. Beginning in the early 1990's the average rate increased again, with development of snowmobiles that enabled an even larger population of backcountry users to access dangerous terrain. During the period from 1990 to 2005, the average annual fatality rates jumped to 22.4 deaths per year. Since 2005, that increasing trend has leveled off despite a continued exponential increase in backcountry usage (Figure 1). This may be attributed to improvements in avalanche education, increased usage of backcountry avalanche advisories, and advances in backcountry rescue equipment and techniques (Birkeland et al., 2017). During the winter seasons from 2004/05-2017/18, the average annual fatality rate in the U.S. was 26 deaths per year. Between 1925 and 1975, the annual mortality rate from avalanches was larger than the annual rates for all other mass wasting events combined (National Research Council, 1990). Snow avalanches also have important economic impacts including rescue costs, property damage, destruction of infrastructure, litigation costs, and operational expenses related to avalanche mitigation and road maintenance (National Research Council, 1990).

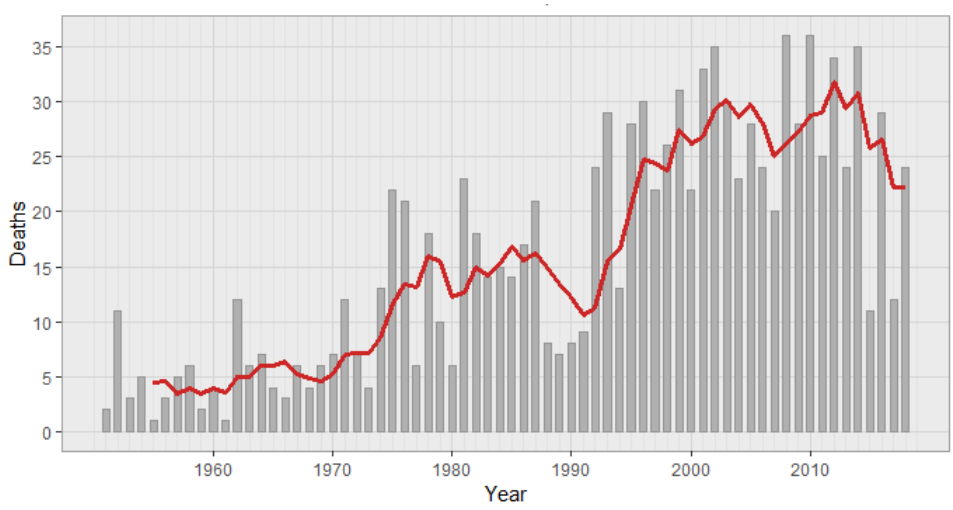

Figure 1: Time series plot of annual U.S. avalanche fatalities since 1951. Bars represent the number of fatalities for a given season. The red line represents a 5-year moving average. For example, the moving average value for 2018 is the average of the annual fatalities from 2014-2018.

Slab Avalanche Mechanics

Slab avalanches result from a complex interaction between a cohesive slab of snow (referred to hereafter as a slab) and a poorly bonded, relatively weaker layer deeper in the snowpack (referred to hereafter as a weak layer). Slab avalanches may be separated into two distinct groups: dry slab avalanches and wet slab avalanches. Schweizer et al. (2016) describe four steps that are prerequisite for a dry slab avalanche: fracture initiation, onset of crack propagation, rapid dynamic propagation, and slab tensile failure and release. In the first step, a fracture is initiated in the weak layer. This initial failure may occur slowly and on the scale of millimeters as a weak layer is loaded incrementally via new or wind-transported snow. Alternatively, larger initial fractures (centimeters to decimeters) may be initiated rapidly by applying an external load such as a falling cornice, an explosive, or a human. As this initial crack grows the overlying slab begins to

bend, which generates compressive and shear stress at the slab-weak layer interface. Once the initial crack reaches a critical length, stress concentrations at the crack tip generated by slab bending exceed the amount of stress the weak layer is able to support. At this point, the energy generated by the slab bending is sufficient to break the bonds in the weak layer and the crack is able to propagate without any additional load (Gaume et al., 2017). If the slab has enough tensile strength to remain intact during bending, the crack is able to propagate for long distances (10's to 100's of meters) and dynamic propagation ensues. However, if the slab is not strong enough to remain intact while bending, the slab will fracture before the crack can propagate through the weak layer and the weak layer fracture will arrest (Reuter and Schweizer, 2018). If the slab and the weak layer are capable of sustaining dynamic propagation, the physical bonds keeping the slab coupled with the slope will be destroyed. If the slope angle is great enough to overcome the forces of residual friction, the slab will undergo tensile failure at the top of the slope and slide downhill. If the slope is not steep enough to overcome friction, the weak layer will still collapse, but the slab will settle in place.

Whereas dry slab avalanches are a result of failure due to applied loads increasing stress on a weak layer, wet slab avalanches typically occur when weak layer strength decreases, and may be independent of additional loading. Weak layer strength can decrease when liquid water is introduced to a winter snowpack through melting or rain-on-snow events, altering the structure of the snowpack such that the weak layer may no longer able to support the weight of the overlying slab (McClung and Schaerer, 2006; Pietzsch, 2009). Baggi and Schweizer (2009) and Marienthal et al. (2012) observed that

liquid water tends to accumulate at capillary boundaries within the snowpack between relatively fine grains in slabs and large- grained weak layers during wet slab activity. These field observations have subsequently been supported by cold lab experiments which documented high liquid water content at capillary boundaries in snow samples (Avanzi et al., 2016). When there is enough liquid water available at the slab-weak layer boundary, liquid water is able to flow downslope, deteriorating the fragile bonds between the slab and the weak layer and resulting in a wet slab avalanche.

Onset of a slab avalanche depends on the properties of both the slab and the weak layer. Birkeland et al. (2014) demonstrated through a series of field experiments that a slab is capable of sustaining fracture propagation even when large portions of the weak layer are interrupted or removed. They also observed fracture arrest when portions of the weak layer were supported to prevent collapse, or if enough of the slab was removed that the slab fractured under tensile failure. Gaume et al. (2017) supported these results numerically by modeling crack propagation using the mechanical properties of both the slab and the weak layer. They found that the length of the crack required for onset of fracture propagation depends on the slab elastic modulus, which is a measure of slab stiffness, as well as the weak layer specific fracture energy, a measure of the resistance of the weak layer to collapse. Birkeland et al. (2019) conducted a series of field experiments that confirmed this, finding critical crack lengths to be proportional to slab modulus and weak layer specific fracture energy. Gaume and Reuter (2017) highlighted the importance of considering layering within the slab when modeling critical crack length as well as the length of the initial crack resulting from the stress applied by a skier on the snow surface.

Reuter and Schweizer (2018) further demonstrated that they were better able to predict slab collapse in the field by incorporating slab tensile strength as well as fracture initiation in the weak layer and propagation propensity.

The relationship between slab depth and snow stability is complex. Generally, as slab depth increases it becomes more difficult to initiate a critical crack in a weak layer, but more likely to propagate a fracture once a crack in the weak layer is initiated. Although critical crack length tends to decrease with slab thickness and density, crack length tends to increase with increasing slab stiffness (Gaume et al. 2017). Further complicating the process is the influence of external loads on a deeply buried weak layer. Schweizer and Camponovo (2001) used load cells to measure normal stress at depths up to one meter within the snowpack while applying a load at the surface approximately equal to that of a skier. They found that as depth increases, the area affected by the applied load increases, which results in a decrease in the magnitude of stress with depth. In their experiments, stresses measured at one meter depth were equal to roughly 10% of the applied load at the surface (Figure 2). As slab stiffness increases, stress is more effectively dispersed with depth, which results in decreased applied stress at the buried weak layer (Thumlert and Jamieson, 2014). The result of these processes is that as the depth to the weak layer increases, fracture initiation becomes more difficult yet propagation becomes more likely. This makes deep slab avalanches particularly difficult to predict, and uncertainty increases as the slab thickness, and subsequently the potential size of the avalanche, increases.

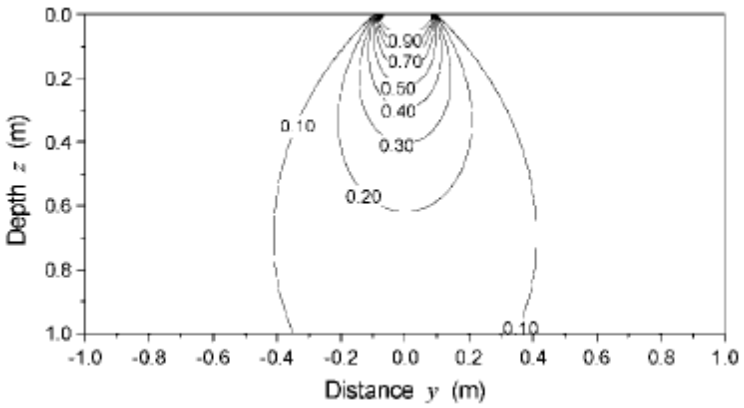

Figure 2: Vertical cross section of the stress distribution for an applied surface stress approximate to that of a skier. Labeled contour lines represent the percent of the surface load measured at different depths in the snowpack. Taken from Schweizer and Camponovo (2001).

Meteorological Drivers of Deep Slab Avalanches

The process by which snow crystals on the ground change form over time is referred to as snow metamorphism. Metamorphism is driven by vapor pressure gradients within the snowpack, and the rate of metamorphism has important implications regarding snow stability. Vapor pressure gradients are primarily driven by differences in temperature in the snowpack and by the radius of curvature of individual grains. Saturation vapor pressure over a curved surface increases as radius of curvature decreases. Additionally, saturation vapor pressure is higher over convex surfaces compared to concavities. In the absence of large temperature gradients, this means that water vapor will sublimate off the corners of snow grains and deposit in the bonds that join them in a process called sintering (Colbeck, 1983a; Armstrong and Brun, 2008). This sintering process results in a cohesive layer of rounded, well-bonded grains. The rate of

diffusion for sintering and rounding is very slow relative to the rate of vapor transfer due to an imposed temperature gradient. In the presence of a temperature gradient exceeding 0.1 - 0.2 ^{o}C/cm, snow grains move towards equilibrium by transporting vapor from areas of high saturation pressure (high temperature) to areas of low vapor pressure (low temperature). This results in sublimation off of the warmer grains and deposition on the colder grains. Deposition occurs rapidly, forming individual faceted crystals. Since the sintering process is slow relative to crystal growth, these new grains tend to be large and poorly bonded relative to rounded grains formed in the absence of a large temperature gradient (Colbeck, 1983b). Thus, the faceting process results in a relatively weak layer in the snowpack, which can lead to slab avalanches.

In the Northern Hemisphere, the formation of a snowpack conducive to deep slab avalanches often results from observed weather in November through January. Onset of slab avalanche activity is commonly preceded by new or wind-transported snow loading, rapid warming, or rain-on-snow events. Marienthal et al. (2015) investigated meteorological factors associated with deep slab avalanches failing on persistent weak layers in an intermountain snowpack in southwest Montana. They found November-January total snow water equivalence (SWE), as well as December-only SWE to be the best indicator of deep slab activity later in the season, with lower December SWE totals more commonly associated with deep slab cycles. They also found deep slab avalanches to be preceded by warm temperatures and large precipitation totals in the days leading to the event. Conlan et al. (2014) found wind speed and direction, warming temperatures, and 1, 3, 6, and 12-day cumulative precipitation totals to be related to deep slab activity

in the Coastal and Columbia mountains of British Columbia. However, they noted that the relationship was not strong enough to be used as a forecasting tool due to high false-alarm ratios and suggested they might find stronger relationships by grouping the events based on early/late season events, location, weak layer type, and type of trigger. Savage (2006) investigated deep slab avalanches on the south face of Lone Mountain at Big Sky Resort in Montana. He described a common early season weather scenario for seasons with major deep slab problems in which early season (October – November) snowfall is transported by S-SW winds, creating a smooth bed surface that remains intact for the remainder of the season. He noted that the problem may be exacerbated if the wind event is followed by a warm, sunny period which can form an ice crust in start zones that is subsequently buried and persists for the season. Additionally, he found 3- and 5- day wind direction and cumulative storm totals to be closely related to deep slab activity.

Atmospheric Processes

Much of the weather we observe at the surface is driven by circulation patterns in the mid troposphere, at altitudes around 5000-6000 m. At these altitudes, air pressure is approximately 500 mb, or roughly half the pressure at sea level. Meteorologists commonly incorporate maps of 500 mb geopotential heights in their forecasts. One utility of the 500 mb geopotential height map is its ability to illustrate north-south migration of polar and tropical air masses (i.e. meridional flow), which control surface temperatures. Since cooler temperatures increase density in a fluid, a colder air mass will not expand as much vertically and is therefore associated with lower 500 mb heights. When a polar air

mass migrates southward, these lower geopotential heights create a depression, or trough. Alternatively, warm air will expand and push the 500 mb level higher. It follows that as warm air masses move northward, they generate an upper-level ridge.

Upper-level wind speed and direction are a product of pressure gradients as well as the Coriolis effect. Windspeeds increase with greater pressure gradients, and at the 500 mb height direction is always perpendicular to the gradient. This results from an enhanced Coriolis effect with high wind speeds due to the lack surface friction at high altitudes. On a map of 500 mb geopotential heights, this means that winds will flow parallel to the isobars. These winds are referred to as geostrophic winds. Wind direction influences vapor transport in the atmosphere, and therefore influences the storm track, or the general direction in which storms migrate (Barry and Chorley, 2003). The direction of the storm track has been shown to have a strong relationship with precipitation in the mountainous western U.S. (e.g. McGinnis, 2000; Mock and Birkeland, 2000; Wise, 2012). However, these regional-scale atmospheric circulation patterns are unable to fully explain precipitation distribution without also incorporating the effects of local-scale topography (Mock, 1996; Price et al., 2013).

Five hundred millibar geopotential heights also provide information related to vertical motion of air masses. This vertical motion plays a major role in precipitation. As rising air cools adiabatically, it decreases in its ability to retain moisture. When an air mass reaches its lifting condensation level, it is unable to store all of the water molecules as vapor. The excess water vapor then condenses or freezes in the atmosphere, and becomes available for precipitation. Alternatively, air warms as it descends, increasing its

capacity to hold water vapor. As the air warms, liquid or solid water in the atmosphere evaporates or sublimates, and is stored as vapor in the atmosphere. This water is no longer available for precipitation (Aguado and Burt, 2015). At the 500 mb height, vertical motion is controlled by divergence and vorticity. Divergence may be driven by diffluence, the physical action of two air streams moving apart from one another. This would manifest itself on a 500 mb geopotential height map as isobars moving from tightly to widely spaced moving in the direction of air flow. The alternative of this setup, referred to as confluence, is associated with upper-level convergence. Geostrophic winds also experience divergence as wind speeds accelerate, or confluence as wind speeds decelerate. When air diverges aloft it leaves an area of relatively low pressure, resulting in uplift of air from the surface. Alternatively, when air converges aloft it tends to undergo subsidence (descending vertical motion).

Vorticity is a measure of the rotation of any fluid mass. Although air masses rotate in three dimensions, the horizontal component about an axis perpendicular to Earth's surface is of particular importance in terms of uplift and subsidence. Vorticity may be broken into two components: relative and absolute. Relative vorticity refers to the direction in which the air parcel is rotating. An air parcel is said to have positive vorticity if it is rotating counter clockwise in the Northern Hemisphere (i.e. cyclonic motion), and negative vorticity if it is rotating clockwise (i.e. anticyclonic motion). Therefore, positive vorticity is observed around troughs, while negative vorticity is observed around ridges. Absolute vorticity is driven by the Coriolis effect, and increases with distance from the equator. As vorticity becomes increasingly positive, uplift is more likely. Maximum

uplift is therefore observed immediately downstream of the bottom of an upper-level trough, with large positive vorticity due to cyclonic motion and increasing absolute vorticity as the parcel moves northward. These areas are commonly associated with precipitation. The opposite occurs immediately downstream of a ridge, as air is undergoing anticyclonic motion (i.e. negative relative vorticity) and moving southward (i.e. decreasing absolute vorticity). It follows that these regions are typically dry (Barry and Chorely, 2003).

Wise (2012) investigated synoptic-scale drivers of precipitation across the intermountain west. She found precipitation distribution was strongly linked with magnitudes and positions of a semi-permanent high pressure cell over the sub-tropical Pacific and a low pressure cell above the Aleutian Islands. There was also a strong connection with the latitude of the North American storm track, characterized by enhanced east-west, or 'zonal', flow and generally located either between 45-50^{o} N, over the Snake River Basin, or along the U.S.- Mexican border. The location of the storm track can shift on time scales from days to seasons. The strength of the Pacific-North American teleconnection (PNA) was found to be another key factor in precipitation across the intermountain west. A strong positive PNA phase is characterized by a strong Aleutian low with a blocking ridge over the western U.S. and western Canada (Wallace and Gutzler, 1981), and is generally associated with lower precipitation across the intermountain west. In contrast, the Aleutian low and western North American ridges diminish during PNA negative phases, resulting in increased zonal flow and subsequent increased precipitation in the intermountain west. Wise (2012) also described strong

relationships between the El Niño Southern Oscillation (ENSO) and the location of the storm track as well as the strength of the PNA pattern. During periods of positive ENSO anomalies, the storm track tends to shift south and PNA index trends positive. Alternatively, during negative ENSO periods, PNA weakens and the storm track shifts north.

Synoptic Climatology

The field of synoptic climatology relates synoptic-scale upper atmospheric circulations to the surface environment (Yarnal, 1993), and has been used as a framework to study precipitation patterns (Esteban et al., 2005; Grundstein, 2003; Hartley and Keables, 1998; McGinnis, 2000; Schuenemann et al., 2009;), snow structure (Yokley, 2014), describe regional weather (Jiang, 2004; Kidson, 2000), and to characterize avalanche activity (Birkeland et al., 2001; Fitzharris, 1987; Fitzharris and Bakkehøi, 1986; Keylock, 2003; Martin and Germain, 2017). The latter five studies identify significant avalanche events based on magnitude, frequency, destruction, or fatalities, which are primarily characterized by direct-action events resulting mainly from heavy snowfall or wind loading.

Yarnal (1993) describes two fundamental approaches to a synoptic climatology study: environment-to-circulation and circulation-to-environment. In the former, an environmental variable such as snowfall or air quality is measured repeatedly, and time periods with similar environmental measurements are grouped together. These groups are then used to classify circulation patterns. In the latter, groups are formed by aggregating days with similar atmospheric setups first, and environmental responses are then

measured for each group. Additionally, there are two primary ways atmospheric conditions may be described. One is by using measurements of air mass characteristics such as temperature, relative humidity, and wind velocity. The other is by using map patterns of geopotential heights. This study will use the framework of a circulation-to-environment approach using 500 mb geopotential heights to describe circulation patterns, and examining deep persistent slab avalanches as the environmental response.

The crux of circulation-to-environment studies using map pattern classification lies in the task of generating the synoptic types. Initially, patterns were classified manually by climatologists using expert judgement. Examples of these classifications include Lamb's classification of daily synoptic patterns over the British Isles (Lamb, 1972) and the Grosswetterlagen, which classifies surface pressure and upper-air charts across Europe and the North Atlantic. The Grosswetterlagen was originally developed in 1944 (Baur et al., 1944) and has been updated several times since, most recently in Werner and Gerstengarbe (2010) (Hoy et al., 2013). Two major drawbacks of manual classification are the amount of time required to generate a classification and the dependence of the resulting synoptic types on the individual performing the classification. In order to reduce subjectivity and improve reproducibility, synoptic climatologists began using principal components analysis (PCA) and clustering algorithms to generate synoptic types. There is extensive research investigating the utility of PCA in generating synoptic types, (e.g. Huth, 1996; Kalkstein et al., 1987; Key and Crane, 1986; Richman, 1981), and it remained a popular classification tool from the 1980's through the early 2000's. More recently, scientists have explored the utility of

self-organizing maps (SOM) (Kohonen, 1998) to classify synoptic map patterns (Hewitson and Crane, 2002; Reusch et al., 2005; Schuenemann et al., 2009; Sheridan and Lee, 2011; Wise and Dannenberg, 2014). The SOM approach improves on the PCA in that the map types generated are considered to be generalizations of real patterns that exist on a continuum, rather than as discrete, independent phenomena. This mitigates the consequences of choosing too few or too many synoptic types, as increasing the number of synoptic patterns effectively increases the spatial resolution of the patterns generated, but does not introduce any new patterns. A SOM generates a user-specified number of 'nodes' which are generalizations of all of the different modes of variability across the dataset. Each node may be thought of as a model that represents a unique synoptic type representing a group of days with a similar circulation pattern. These synoptic types are then arranged in a two-dimensional array such that similar map patterns are plotted adjacent to each other and dissimilar patterns are plotted on opposite ends of the array. The array is an organized display of synoptic types that summarize the spectrum atmospheric circulation patterns, including a transition from zonal to meridional flow, migration of semi-permanent pressure centers, latitudinal shifts in the storm track, and more subtle changes that will vary with geographic extent. The SOM array provides an effective means of visualizing high dimensional data in a way that is easy to interpret.

Research Questions

The previously mentioned studies have established direct connections from weather to snow metamorphism to snowpack structure and mechanics, which collectively

control snow stability. There is also extensive research investigating the connections between regional-scale circulation patterns in the upper atmosphere and meteorological responses at the surface. There have been several studies that draw connections between circulation patterns and avalanche activity, but none have specifically addressed deep slab avalanches failing on persistent weak layers, which remain difficult to predict. This research aims to fill this knowledge gap by addressing the following questions:

1. What circulation patterns in the early winter are commonly associated with deep persistent slab avalanche activity later in the season?
2. What patterns are frequently observed in the days leading to deep persistent slab avalanches?
3. How do these relationships change at different geographical locations across the western U.S?

I hypothesize that early winters commonly associated with deep persistent slabs will have limited snowfall, that days leading to deep persistent avalanching will be associated with either rapid loading (for dry slabs) or rapid warming and/or rain (for wet slabs), and that these relationships will vary geographically depending on how the broad atmospheric patterns interact with local terrain at the different locations. This work uses weather and avalanche records maintained by Ski Patrols at Bridger Bowl Ski Area, Montana, Jackson Hole Mountain Resort, Wyoming, and Mammoth Mountain, California.

References Cited

Aguado, E. and Burt, J., 2015. Understanding Weather and Climate. Seventh ed., Pearson Education, Inc.

Armstrong, R.L., and Brun, E., 2008. Snow and Climate: Physical processes, surface energy exchange and modeling. Cambridge University Press. 256 pp.

Atwater, M., 1954. Snow Avalanches. *Scientific American, 190 (1),* 26-31.

Avanzi, F., Hirashima, H., Yamaguchi, S., Katsushima, T., De Michele, C., 2016. Observations of capillary barriers and preferential flow in layered snow during cold laboratory experiments. The Cryosphere, 10, 2013-2026.

Baggi, S., and Schweizer, J., 2009. Characteristics of wet-snow avalanche activity: 20 years of observations from a high alpine valley (Dischma, Switzerland). *Natural Hazards, 50,* 97-108.

Barry, R., Chorley, R., 2003. Atmosphere, Weather and Climate. Eighth ed., Routledge. pp 112-122.

Baur, F., Hess, P., Nagel, H., 1944. Calendar of European Grosswetterlagen 1881-1939; in German/ Bad Homburg v.d. H., 35 pp.

Birkeland K.W., van Herwijnen A., Reuter B., Bergfeld B., 2019. Temporal changes in the mechanical properties of snow related to crack propagation after loading. *Cold Regions Science and Technology.* https://doi.org/10.1016/ j.coldregions.2018.11.007

Birkeland, K.W., Greene, E.M., Logan, S., 2017. In response to avalanche fatalities in the United States by Jekich et al. ([Epub ahead of print]) Wilderness and Environmental Medicine 18 (4).

Birkeland, K., van Herwijnen, A., Knoff, E., Staples, M., Bair, E., Simenhois, R., 2014. The role of slabs and weak layers in fracture arrest. *Proceedings of the 2014 International Snow Science Workshop*, Breckenridge, CO, USA.

Birkeland, K., Mock, C., and Shinker, J., 2001. Avalanche extremes and atmospheric circulation patterns. *Annals of Glaciology, 32,* 135-140.

Colbeck, S.C., 1983 (a). Ice crystal morphology and growth rates at low supersaturations and high temperatures. *Journal of Applied Physics, 54 (5),* 2677-2682.

Colbeck, S.C., 1983 (b). Theory of metamorphism of dry snow. *Journal of Geophysical Research, 88 (C9),* 5475-5482.

Colorado Avalanche Information Center, 2019. Avalanche Accident Statistics. [Dataset]. Retrieved from https://avalanche.state.co.us/accidents/statistics-and-reporting.

Conlan, M., Tracz, D., Jamieson, B., 2014. Measurements and weather observations at persistent deep slab avalanches. *Cold Regions Science and Technology*, 97, 104-112.

Esteban, P., Jones, P., Martín-Vide, J., Mases, M., 2005. Atmospheric circulation patterns related to heavy snowfall days in Andorra, Pyrenees. *International Journal of Climatology, 25,* 319-329.

Fitzharris, B.B., 1987. A climatology of major avalanche winters in Western Canada. *Atmosphere-Ocean,* 25 (2), 115-136.

Fitzharris, B.B., Bakkehøi, S., 1986. A synoptic climatology of major avalanche winters in Norway. *Journal of Climatology, 6,* 431-446.

Gaume, J., Reuter, B., 2017. Assessing snow instability in skier-triggered snow slab avalanches by combining failure initiation and crack propagation. *Cold Regions Science and Technology*, 144, 6-15.

Gaume, J., van Herwijnen, A., Chambon, G., Wever, N., Schweizer, J., 2017. Snow fracture in relation to slab avalanche release: critical state for the onset of crack propagation. *The Cryosphere*, 11, 217-228.

Grundstein, A., 2003. A synoptic-scale climate analysis of anomalous snow water equivalent over the norther Great Plains of the USA. *International Journal of Climatology, 23,* 871-886.

Hartley, S., Keables, M., 1998. Synoptic associations of winter climate and snowfall variability in New England, USA, 1950-1992. *International Journal of Climatology, 18,* 281-298.

Hewitson, B.C., and Crane, R.G., 2002. Self-organizing maps: applications to synoptic climatology. *Climate Research, 22 (1)*, 13-26.

Hoy, A., Sepp, M., Matschullat, J., 2013. Atmospheric circulation variability in Europe and northern Asia (1901 to 2010). *Theoretical and Applied Climatology, 113 (1-2),* 105-106.

Huth, R., 1996. Properties of the circulation classification scheme based on rotated principal component analysis. *Meteorology and Atmospheric physics, 59,* 217-233.

Jiang, N., Hay, J.E., Fisher, G.W., 2004. Classification of New Zealand synoptic weather types and relation to the Southern Oscillation Index. *Weather and Climate, 23,* 3-24.

Kalkstein, L., Tan, G., Skindlov, J., 1987. An evaluation of three clustering procedures for use in synoptic climatological classification. *Journal of Climate and Applied Meteorology, 26,* 717-730.

Key, J., and Crane, R., 1986. A comparison of synoptic classification schemes based on 'objective' procedures. *Journal of Climatology, 6,* 375-388.

Keylock, C.J., 2003. The North Atlantic Oscillation and snow avalanching in Iceland. *Geophysical Research Letters, 30 (5).*

Kidson, J., 2000. An analysis of New Zealand synoptic types and their use in defining weather regimes. *International Journal of Climatology, 20,* 299-316.

Kohonen, T., 1998. The Self-organizing map. *Neurocomputing, 12,* 1-6.

LaChapelle, 1980. The fundamental processes in conventional avalanche forecasting. *Journal of Glaciology*, 26 (94), 75-84.

LaChapelle E., 1966. Avalanche forecasting- A modern synthesis. IAHS Publication 69: 350-356.

Lamb H., 1972 British Isles weather types and a register of the daily sequences of circulation patterns 1861-*1971 Geophysical Memo No. 116 (85)* HMSO, London.

Lang, R.M., Leo, B.R., Brown, R.L., 1984. Observations on the growth process and strength characteristics of surface hoar. Proceedings of the 1984 International Snow Science Workshop, Aspen, CO.

Marienthal, A., Hendrikx, J., Birkeland, K., Irvine, K., 2015. Meteorlogical variables to aid forecasting deep slab avalanches on persistent weak layers. *Cold Regions Science and Technology*, 120, 227-236.

Marienthal, A., Hendrikx, J., Chabot, D., Maleski, P., Birkeland, K., 2012. Depth Hoar, Avalanches, and Wet Slabs: A case study of the historic March 2012 wet slab avalanche cycle at Bridger Bowl, Montana. Proceedings of the International Snow Science Workshop, Anchorage, AK, USA.

Martin, J.P., Germain, D., 2017. Large-scale teleconnection patterns and synoptic climatology of major snow-avalanche winters in the Presidential Range (New Hampshire, USA). *International Journal of Climatology, 37,* 109-123.

McClung, D., and Schaerer, P., 2006. The Avalanche Handbook. 3rd ed. The Mountaineers Books.

McGinnis, D., 2000. Synoptic controls on upper Colorado River Basin snowfall. *International Journal of Climatology, 20,* 131-149.

Mock C., and Birkeland, K., 2000. Snow Avalanche Climatology of the Western United States Mountain Ranges. *Bulletin of the American Meteorological Society, 87 (10),* 2367-2392.

National Research Council (U.S.). (1990). *Snow Avalanche Hazards and Mitigation in the United States. Washington, D.C.: National Academies Press*. Retrieved from http://search.ebscohost.com.proxybz.lib.montana.edu/login.aspx?direct=true&db=nlebk&AN=14505&site=ehost-live

Pietzsch, E.H., 2009. Water movement in a stratified and inclined snowpack: Implications for wet slab avalanches. MSc thesis, Montana State University, Bozeman, MT, USA.

Price, M.F., Byeres, A.C., Friend, D.A., Kohler, T., Price, L.W., 2013. Mountain Geography: Physical and human dimensions, University of California Press.

Reusch, David B., Alley, Richard B., Hewitson, Bruce C., 2005. Relative performance of self-organizing maps and principal component analysis in pattern extraction from synthetic climatological data. *Polar Geography,* 29:3, 188-212. DOI: 10.1080/789610199

Reuter, B., and Schweizer, J., 2018. Describing snow instability by failure initiation, crack propagation, and slab tensile support. *Geophysical Research letters*, 45, 7019-7027. https://doi.org/10.1029/2018GL078069

Richman, M. 1981. Obliquely rotated principal components: An improved meteorological map typing technique? *Journal of Applied Meteorology, 20,* 1145-1159.

Savage, S., 2006. Deep slab avalanche hazard forecasting and mitigation: the south face at Big Sky ski area. Proceedings of the 2006 International Snow Science Workshop, Telluride, CO, pp. 483–490.

Schuenemann, C., Cassano, J., Finnis, J., 2009. Synoptic forcing of precipitation over Greenalnd: Climatology for 1961-99. *Journal of Hydrometeorology*, 10, 60-78.

Schweizer, J., Reuter, B., van Herwijnen, A., Gaume, J., 2016. Avalanche release 101. Proceedings of the International Snow Science Workshop, Breckenridge, CO.

Schweizer, J., Camponovo, C., 2001. The skier's zone of influence in triggering slab avalanches. *Annals of Glaciology, 32,* 314-320.

Sheridan, S.C., Lee., C.C., 2011. The self-organizing map in synoptic climatological research. *Progress in Physical Geography, 35 (1),* 109-119.

Thumlert, S., Jamieson, B., 2014. Stress measurements in the snow cover below localized dynamic loads. *Cold Regions Science and Technology, 106-107,* 28-35.

Wallace, J.M., and Gutzler, D.S., 1981. Teleconnections in the geopotential height field during the Northern Hemisphere winter. *Monthly Weather Review, 109,* 784-812.

Werner, P.C., and Gerstengarbe, F.W., 2010. Catalog of European Grosswetterlagen; in German, 7th edtion. PIK Report 119. 140 pp.

Wise, E.K., 2012. Hydroclimatology of the US intermountain west. *Progress in Physical Geography, 36 (4),* 458-479. DOI: 10.1177/030913312446538.

Yarnal, B. 1993. Synoptic Climatology in Environmental Analysis: A Primer. Bellhaven Press, London, UK. 195 pp.

Yokley, L., Hendrikx, J., Birkeland, K., Williams, K., Leonard, T., 2014. Role of synoptic atmospheric conditions in the formation and distribution of surface hoar. Proceedings of the 2014 International Snow Science Workshop, Banff, Alberta, CA.

ATMOSPHERIC PROCESSES RELATED TO DEEP PERSISTENT SLAB AVALANCHES IN THE WESTERN UNITED STATES

Abstract

Deep persistent slab avalanches are destructive natural hazards that pose a threat to infrastructure, transportation, and recreationists in cold mountain regions around the world. Formation of a snowpack conducive to deep persistent slab avalanches is typically driven by weather occurring in the beginning weeks to months of the winter season. While the exact timing of deep persistent slab avalanches is difficult to predict, onset of avalanche activity is commonly preceded by rapid warming, heavy precipitation, or abnormal wind events. Previous work has identified local meteorological factors contributing to deep persistent slab avalanches, but there is little work exploring the atmospheric processes controlling them. This work addresses this knowledge gap by investigating the synoptic drivers of deep persistent slab avalanches at Bridger Bowl, Montana; Jackson, Wyoming; and Mammoth Mountain, California. We use self-organizing maps to generate 20 synoptic types that summarize 5,899 daily 500 mb geopotential height maps for the winters (November – March) of 1979/80 – 2017/18. For each of the three locations, we identify major and minor deep persistent slab avalanche seasons, and analyze the number of days represented by each synoptic type during the beginning (November – January) of the major and minor seasons. We also examine number of days assigned to each synoptic type during the 72 hours preceding deep persistent slab avalanche activity. Each of the three sites exhibits a unique distribution of

the number of days assigned to each synoptic type during November – January of major and minor seasons, and for the 72-hour period preceding deep persistent slab avalanche activity. This work identifies the atmospheric circulation patterns contributing to deep persistent slab instabilities, and the patterns that commonly precede deep persistent slab avalanche activity. By identifying these patterns, we provide practitioners with an additional tool to anticipate the timing of these difficult to predict events.

Introduction

Deep persistent slab avalanches are capable of destroying infrastructure and are usually unsurvivable to those who are caught in a slide. The exact timing of deep persistent slab avalanches is difficult to predict, which results in a great deal of uncertainty when assessing avalanche danger due to deep persistent problems. A deep persistent slab avalanche can occur when a weak layer in the snowpack fails due to applied stress from an external load such as a falling cornice, explosives, or the weight of a human. Failure can also initiate from the stress of an overlying slab of cohesive snow without any artificial trigger. In some cases, the weak layer fails without the addition of any new or wind transported snow by means of the introduction of liquid water to the snowpack, deteriorating the fragile bonds between grains in the weak layer such that the weak layer is no longer able to support the weight of the overlying slab. As slab thickness and stiffness increase throughout the winter season, applied stress at the surface is dissipated within the slab, which makes it more difficult to initiate failure in a deeply buried weak layer (Schweizer and Camponovo, 2001; Thumlert and Jamieson, 2015).

The series of processes resulting in deep persistent slab avalanches is complex, which makes these events particularly difficult to predict.

Formation of a snowpack conducive to deep persistent slab avalanches is typically controlled by weather patterns occurring during the early months of the winter season (Marienthal et al. 2015), and onset of slab avalanche activity is commonly preceded by new or wind-transported snow loading, rapid warming, or rain-on-snow events (Conlan, 2014; Davis et al., 1999; Marienthal et al., 2012). Associations between these meteorological events and slab avalanche activity have long been used as a tool to aid in avalanche forecasting (Atwater, 1954; LaChapelle, 1966; LaChapelle, 1980). Although mountain weather is a product of processes operating on a wide range of scales (Price et al., 2013), a large amount of variability in surface meteorology, and subsequently snow stratigraphy, is driven by synoptic-scale upper atmospheric circulation patterns (Barry and Chorley, 2003). Wallace and Gutzler (1981) describe a teleconnection they refer to as the Pacific/North American pattern, which is characterized by a blocking ridge over the western U.S. and enhanced troughing over the Aleutian Islands and the eastern U.S. Wise (2012) and Mock (1996) identified an increase in annual winter precipitation during seasons exhibiting a negative PNA pattern, and relatively dry seasons during the positive PNA phase. Furthermore, winter precipitation over the western U.S. is typically unevenly distributed between northern and southern regions, with positive precipitation anomalies in one region coinciding with negative anomalies in the other (Dettinger et al., 1998). This has been attributed to seasonal shifts in the position of the storm track over the western U.S., which may be pushed southward by a strong Aleutian low, or may favor

the northern region with a weak Aleutian low and resulting troughing over the western U.S. The center at which this north-south precipitation dipole pivots is fairly narrow, occurring between 40°N and 42°N (Wise, 2010).

The field of synoptic climatology relates synoptic-scale upper atmospheric circulations to the surface environment (Yarnal, 1993), and has been used as a framework to study precipitation patterns (Esteban et al., 2005; Grundstein, 2003; Hartley and Keables, 1998; McGinnis, 2000; Schuenemann et al., 2009; Wise, 2012), snow structure (Yokley, 2014), describe regional weather (Jiang, 2004; Kidson, 2000), and to characterize avalanche activity at four sites in the western U.S. located in Montana, Wyoming, Utah, and New Mexico (Birkeland et al., 2001), the Selkirk Mountains of British Columbia, Canada (Fitzharris, 1987), Norway (Fitzharris and Bakkehøi, 1986), Iceland (Keylock, 2003), and the Presidential Range in the northeast U.S. (Martin and Germain, 2017). The latter five studies identify significant avalanche events based on magnitude, frequency, destruction, or fatalities. They do not explicitly distinguish between events failing on deep persistent weak layers and events occurring within new snow layers or interfaces between old and new snow after heavy snowfall or wind loading. There is very little research relating upper atmosphere circulation patterns to deep slab avalanches failing on persistent weak layers. This work addresses that knowledge gap, with the goal of improving the ability of practitioners to anticipate these difficult to predict events through a better understanding of the processes that drive them. Specifically, we aim to answer the following three questions:

1. What circulation patterns in the early winter are commonly associated with deep persistent slab activity later in the season?
2. Which patterns are frequently observed in the days leading to deep persistent slab avalanches?
3. How do these relationships change at different locations across the western U.S?

We predict that early season patterns will typically be associated with low precipitation and colder temperatures during seasons with deep persistent slab avalanches, while the patterns in the days leading to the events will facilitate heavy precipitation for dry slabs, and warmer temperatures for wet slab events. The circulation patterns driving deep persistent slab activity should be different at each site, and will be influenced by the interaction between atmospheric circulation and local to regional topography.

Methods

Study Location

This research focuses on three ski areas in the western U.S.: Bridger Bowl, Montana, Jackson Hole, Wyoming, and Mammoth Mountain, California. Bridger Bowl ski area is located on the east side of the Bridger mountain range in southwest Montana approximately 27 km north of Bozeman (45.8174° N, -110.8966° W) with a summit elevation of 2652m and base elevation of 1859m (Figure 3). Jackson Hole is located in western Wyoming in the Teton Range (43.833° N, -111.871° W). The base elevation at Jackson Hole is 1924 m and the summit rises to 3185 m. Grand Targhee ski area is located in the same mountain range approximately 20 km (12 mi) northwest of Jackson Hole. Due to their close proximity, the records for both of these ski areas are used to describe avalanche activity in the Jackson area for this analysis. Mammoth Mountain ski area is located in the Sierra Nevada range in central California (37.630° N, -119.050° W)

with a summit elevation of 3698 m and a base elevation of 2424 m. Bridger Bowl and Jackson Hole typically fall within the intermountain snow climate regime, characterized by cool winter temperatures and moderate to heavy seasonal snowfall. Mammoth Mountain lies within the coastal snow climate zone, with high seasonal snowfall totals, relatively warm temperatures, and somewhat regular rainfall events during the winter season (Mock and Birkeland, 2000). The study sites were selected such that they cover a broad geographical extent within the western U.S., and on the basis that they have the longest and most consistent weather and avalanche data available.

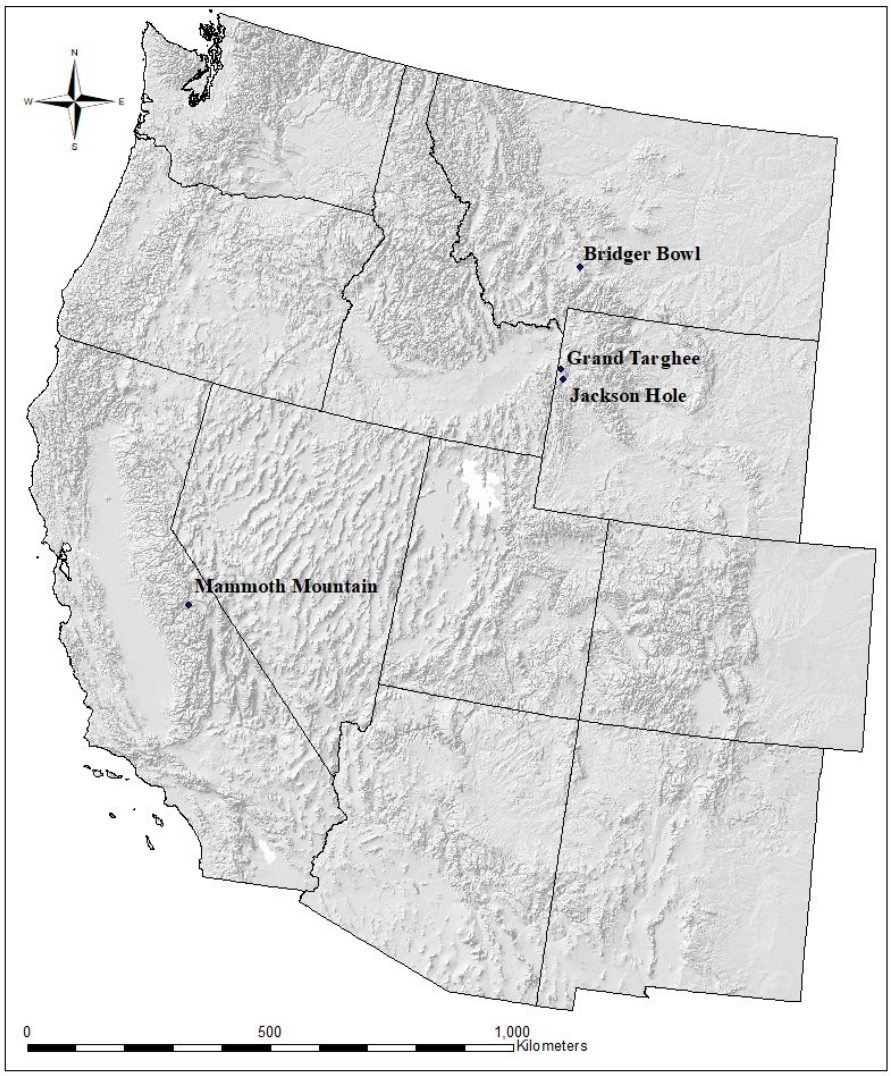

Figure 3: Location map of the sites used in this study. Geographic data from US Census Bureau (2016) and USGS National Center for EROS (2005).

Weather and Avalanche Records

Daily weather and avalanche logs are maintained by professional ski patrol at each study site. This research uses the daily data from November 1 to March 31 for each operational season. The operational season is limited based on snow coverage, and data are somewhat sparse in November for most seasons, depending on the opening date for the season. The duration of weather and avalanche records for each site ranges from 32 to 39 seasons (Table 1). Earlier data are available at each site but were not used in this project to align with the atmospheric data discussed in the next section, and to reduce apparent state changes in the record due to migration of instrument location and changes in recording practices.

Crown depth, bed surface, avalanche type, and relative (R) size are used to describe individual avalanches after American Avalanche Association (2016). In most cases, observers record some, but not all of these values for an avalanche. Ski patrol maintains data records as a means to communicate between practitioners on a day-to-day basis. They are used as part of a holistic approach to assess snowpack stability from an operational perspective. The observations are recorder-dependent and do not necessarily involve direct measurements or a thorough examination of the avalanche. Although this does result in some measurement uncertainty, it remains the best available data source for historical avalanche activity, as it is virtually the only dataset in the US which has a recording rate that is not dependent on fatalities, injuries, or damage to infrastructure. In light of this uncertainty, we do not interpret precise measurements of crown depth in the analysis. Rather, we use the observation to separate large and small events (described in

the Avalanche Classification section). Additionally, the size classification (also described in the Avalanche Classification section) uses the R-size record and operates on a scale which varies on a range of up to two orders of magnitude larger than the crown depth measurement. This reduces the magnitude of error propagated as a result of measurement uncertainty. We performed a sensitivity analysis that assessed the impact of these measurement uncertainties on our study, and found that our results were minimally impacted by errors of +/- one step in R-size and +/- one foot in crown depth. A thorough summary of the sensitivity analysis is given in Appendix E. There is also a high level of uncertainty in the bed surface records. Specifically, the designation of avalanches failing within the old snow versus at the interface between old and new snow is suspect. For this reason, we only use the "old snow" bed surface designation in conjunction with other indicators of deep persistent slabs (i.e. type = "hard slab", crown depth $\geq$ 0.9m, and R-size $\geq$ 4). The designation of bed surface as "ground" is somewhat more straightforward, and would indicate that an avalanche failed deep within the snowpack, even if there is some uncertainty as to exactly which layer failed. The record for avalanche type is used only to separate slab and loose avalanches, as well as wet and dry. Both distinctions are straightforward and have little ambiguity. R size is a size designation given based on a visual assessment of size relative to the entire slide path. This method is used regularly by avalanche professionals, and scores are taken as recorded (except for apparent errors as noted in Appendix B).

Table 1: Length of avalanche and weather records used at each study site.

Location	Avalanche Record	Weather Record
Bridger Bowl	1979/80 – 2017/18	1979/80 - 2017/18
Jackson Hole	1979/80 - 2017/18	1979/80 - 2017/18
Mammoth Mountain	1979/80 - 2017/18	1982/83 - 2013/14

The avalanche dataset for the Jackson area was obtained through the Bridger-Teton National Forest Avalanche Center (BTAC), and contains records of events from Jackson Hole, Grand Teton National Park (GTNP), Grand Targhee ski resort, Teton Pass, and the surrounding backcountry. However, the backcountry zones including GTNP and Teton Pass generally exhibit a snowpack that is very different from that of an operating ski area due to less skier traffic and more importantly, much less active avalanche mitigation. Furthermore, backcountry avalanches frequently go unreported unless there is damage to infrastructure, an injury or fatality, or it is an unusually large event. These two considerations would make it inappropriate to compare avalanche events between backcountry settings and within the boundaries of an operating ski area, so the backcountry records are omitted from this analysis.

Atmospheric Data

Atmospheric data are obtained from the National Center for Environmental Prediction/ National Center for Atmospheric Research (NCEP/NCAR) Reanalysis data set (Kalnay et al., 1996). Daily 500mb geopotential height values are recorded on a 2.5^{o} x 2.5^{o} grid extending from 20^{o} N to 70^{o} N latitude and 160^{o} E to 60^{o} W longitude. Thus, each day is represented by a 1197-cell grid which describes the spatial distribution of the atmospheric condition for that day. The size of this study area is

similar to previous synoptic studies (e.g. Birkeland et al., 2001; Mock and Birkeland, 2000; Wise and Dannenberg, 2014). We used daily data for the winter season only (November 1 – March 31) in order to correspond with the weather and avalanche data and to avoid a seasonal signal in the circulation patterns after Yarnal (1993). The reanalysis data extend back to 1948, but the atmospheric measurements forcing the reanalysis models evolved as better techniques were developed in the 1950s through the 1970s. The last major change in data availability occurs in 1979, with the addition of satellite measurements. This research uses the reanalysis data for the winter seasons from 1979/80 through 2016/17 to maintain consistency in the atmospheric measurements.

Avalanche Classification

Avalanches are classified as deep slab events failing on persistent weak layers based on the bed surface, crown depth, avalanche type, R-size, and 72-hour storm totals. All events with a recorded bed surface as "ground" and crown depth greater than 0.9 m are flagged as deep slab events. An event recorded as failing in the old snow is retained if crown depth exceeds 0.9 m and is greater than 150% of the mean crown depth for the day. We also consider events using a scaling factor representing the ratio of crown height to 72-hour new snow totals:

$$C = \frac{D}{HN_{72}}$$

where D is the crown depth and HN72 is the 72-hour new snow total. At each location, we plot a histogram of this crown depth scaling factor *C* for all of the events where crown depth exceeds 0.9 m and storm snow exceeds 0.15 m. We then assign a threshold that

retains the events in the tail of the distribution and eliminates a majority of the events (Figure 4). This distinction operates under the assumption that most of the events recorded as failing in the old snow are either storm slab or wind slab avalanches, and events failing on persistent weak layers deeper in the snowpack should be less common in a snowpack that is actively mitigated.

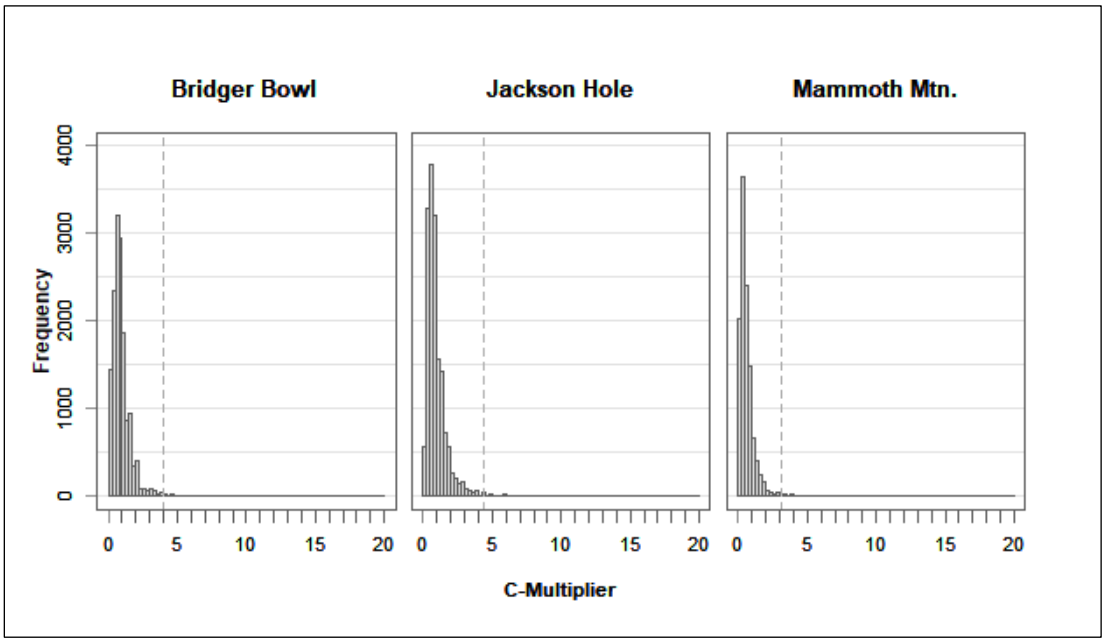

Figure 4: Histograms of C-multipliers for Bridger Bowl (left), Jackson Hole (center), and Mammoth Mountain (right). Dashed line indicates C-multiplier threshold used to distinguish deep slab events.

By considering the tail of the distribution with the larger values for *C*, we retain the events where the crown depth is large relative to the new snow, which should represent deep slab avalanches failing on persistent weak layers. Thus, any avalanches that failed in the old snow and had a crown depth greater than *C* times the 72-hour accumulated snow were treated as deep slab avalanches. For each site, we select the value of *C* corresponding with the 99th percentile of the distribution shown in Figure 4 to

indicate a deep persistent slab event. This gives *C*-values of 4.0 for Bridger Bowl, 4.4 for Jackson Hole, and 3.1 for Mammoth Mountain.

There are multiple extended periods of missing weather data, particularly in November and December (e.g. 1979-80 at Bridger Bowl, 1982-83 at Jackson Hole, or 1982-83 at Mammoth Mountain). For avalanches where there are three consecutive days of missing precipitation data, we add another set of events for which crown depth exceeds 0.9 m, the avalanche is classified as a hard slab, the bed surface is designated as "old snow", and the R-size is greater than or equal to 4.

As a final step, we inspect events identified using our classification criteria manually to ensure that the events retained are in fact deep persistent events. By only retaining the events identified with our criteria, we are confident that the events we are studying are in fact deep persistent slab avalanches, rather than large direct-action events such as storm slabs or wind slabs failing at the old snow interface immediately following a storm. It is possible that this criteria may omit a small number of ambiguous or smaller magnitude events. However, we maintain that including such events in our record of deep persistent slab events would increase uncertainty in our analysis and make it difficult to assess atmospheric patterns related specifically to deep persistent slab events.

Deep Slab Activity Index

Each avalanche classified as deep slab event is assigned a score based on the size of the avalanche using the avalanche activity index (AAI) from Schweizer et al. (1998). Since any event not classified as a deep slab avalanche receives a score of 0, we refer to this score as the deep slab activity index (DSAI):

$$DSAI = \sum_{i=1}^{n} 10^{R-3}$$

where *R* is the R-size of event *i*, and *n* is the number of deep slab events occurring in a given year. The size weighting scheme developed in Schweizer et al. (1998) was developed using the Canadian D-size classification that estimates the mass of each event, which increases logarithmically with size. In this case, the available records describe each event using the American R-size (American Avalanche Association, 2016), which estimates the size of the avalanche relative to the path. Birkeland and Landry (2002) conclude that the relative mass of an avalanche also increases logarithmically with R-size, despite the fact that there is no way to convert R-size to an approximate mass for a given avalanche. Furthermore, they demonstrate that the frequency of avalanche occurrence decreases logarithmically as R-size increases. Therefore, despite the difference in the nature of the two size classifications, we assume it is reasonable to apply the Schweizer et al. (1998) AAI index to the R-sizes recorded in our dataset. DSAI score for each R-size is summarized in Table 2. The scores are summed up for each season and thresholds are identified to separate major and minor deep slab seasons by looking at scatterplots of seasonal DSAI score.

Table 2*:* DSAI score for each R-size designation.

Avalanche R-size	DSAI Score
1	.01
2	.1
3	1
4	10
5	100

Self-Organizing Maps

A self-organizing map (SOM) is a type of neural network that generates a set of descriptive models, or nodes, from a multidimensional dataset. The distribution of these nodes describes the range of variability across the dataset, and each node summarizes a collection of observations that are objectively determined by the neural network model to be categorically similar (Kohonen, 1998). The SOM provides a clear way of summarizing multidimensional data, as the algorithm takes into account the similarity between nodes as they are generated and then displays them on a two-dimensional array such that adjacent nodes are similar, while distant nodes are not. Recently, SOMs are being used in the field of synoptic climatology (Hewitson and Crane, 2002; Reusch et al., 2007; Schuenemann et al., 2009; Sheridan and Lee, 2011; Wise and Dannenberg, 2014) to classify atmospheric variability. The optimal SOM configuration is identified by minimizing the variability among map patterns represented by the same node and maximizing variability among groups of maps represented by different nodes.

Each node generated by the SOM is characterized by 1197 grid point values on the same 2.5^{o} x 2.5^{o} grid used by the NCEP/NCAR daily 500-mb geopotential height maps. Within-group variability is measured by calculating the root mean square error (RMSE) between grid points of the node and the corresponding grid points for a given day, so each day has one associated RMSE value. These RMSE values are then averaged over all days in the record. Between-group variability is measured by calculating a RMSE value for each combination of two nodes in the SOM, and averaging all the RMSE values over all node-to-node combinations. The SOM is implemented in R using the Kohonen

package (Wehrens and Buydens, 2007) to generate 20 synoptic types summarizing the atmospheric circulation patterns observed over the study area. This is similar to the number of synoptic types used in previous studies (e.g. Esteban et al., 2005; Kidson, 2000; Schuenemann et al., 2009). The synoptic types generated by the SOM are discussed further in the results section. A thorough discussion of the SOM optimization procedure is presented in Appendix A.

Using the synoptic classification scheme and the daily weather and avalanche record, we quantify distributions of daily maximum and minimum temperature and new snow water equivalence (SWE) for each synoptic type at each of the three study sites. Additionally, we consider the number of days assigned to each synoptic type in the beginning of the winter season (November-January) when deep persistent weak layers tend to form (Marienthal et al., 2015), and compare differences in the frequency distribution of daily synoptic types for major and minor deep slab years at all three study sites. We then count the number of days assigned to each synoptic type in the three days preceding deep slab avalanche activity to identify any relationships between circulation patterns and onset of deep slab avalanches. For each location, we compare frequency distributions that summarize the number of days assigned to each synoptic type from November to January over all major seasons to all minor seasons on the record. Finally, we identify similarities and differences between atmospheric setups prior to wet and dry slab activity. We analyze synoptic type frequency at each study site to explore the influence of geographic location on the response to atmospheric circulation.

Results

Map Pattern Classification

The SOM-generated 500 mb map pattern classification scheme shows a gradual transition from meridional flow in the top rows to zonal flow in the bottom rows (Figures 5 and 6). There is also a transition from a negative PNA phase in the lower left corner to a positive phase in the upper right, characterized by a trough over the Aleutian Islands, and a blocking ridge over western North America. There is also a low-pressure center over Hudson Bay in the upper left of the array, which becomes weaker moving diagonally to the lower right. A ridge over the eastern Pacific Ocean in the leftmost columns migrates eastward moving to the right across the array, until it lies over North America (e.g. patterns D, G, H, and L). The eastward migration of this ridge is coupled with a transition from a more northwesterly flow over the continental U.S. in the leftmost columns to a more west-southwest flow in the patterns in the rightmost columns. Finally, there is a distinct transition from a high-pressure ridge over the Aleutian Islands and eastern Siberia in the leftmost columns to a low-pressure trough in the columns on the right side of the array.

At first glance, synoptic type L seems to be oddly out of place in the array, with an omega block situated over the Bearing Straight and southcentral Alaska that closely resembles the setup in pattern A on the opposite side of the array, while all adjacent types feature a low-pressure trough in this region. However, the map also features a ridge over the Rocky Mountains and a low pressure center just north of Hudson Bay, which closely resembles adjacent patterns G, H, and K.

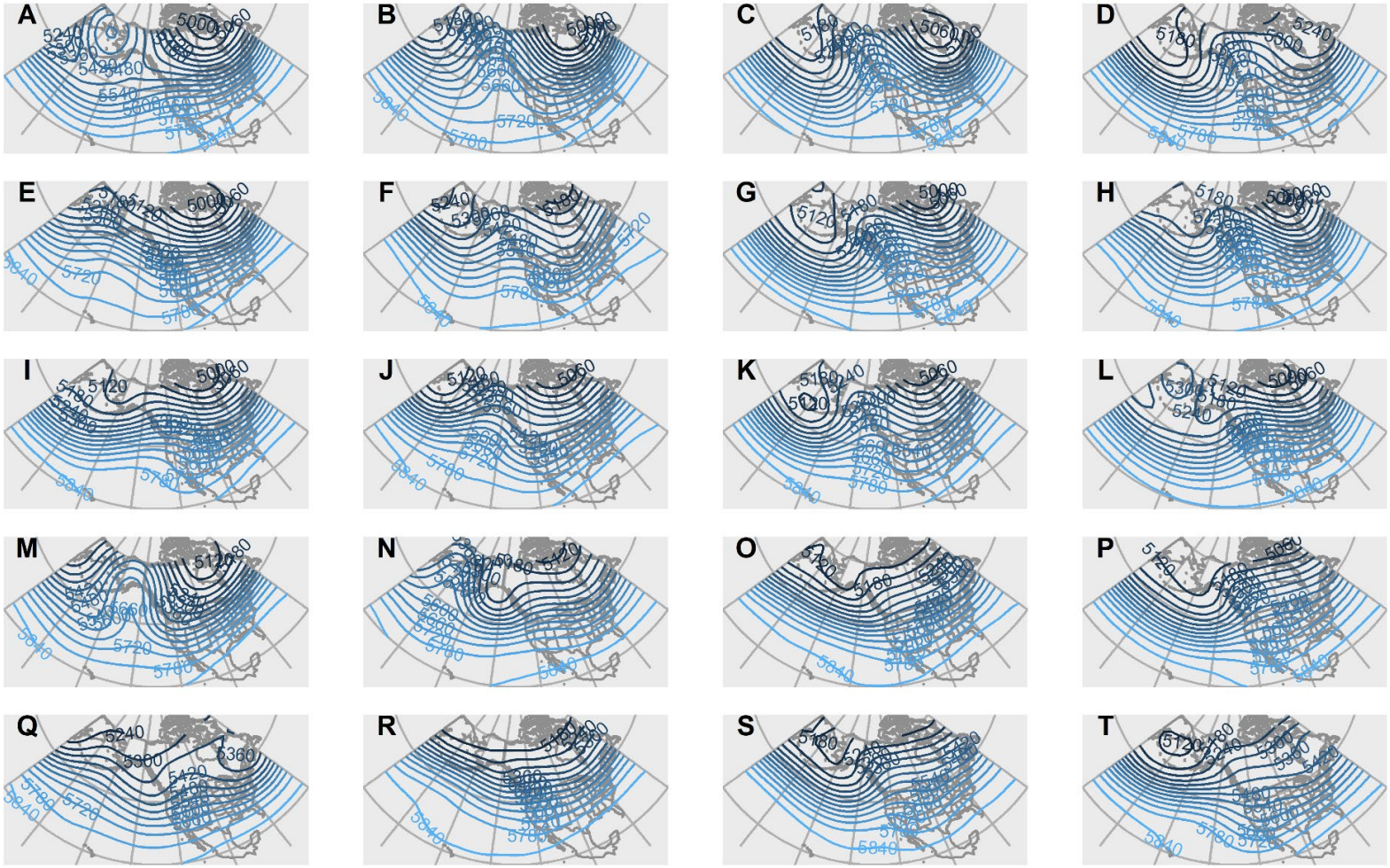

Figure 5: Array of 500 mb geopotential height map patterns generated using self-organizing maps. Each map pattern, or synoptic type, is a generalization of a group of days exhibiting a similar circulation pattern.

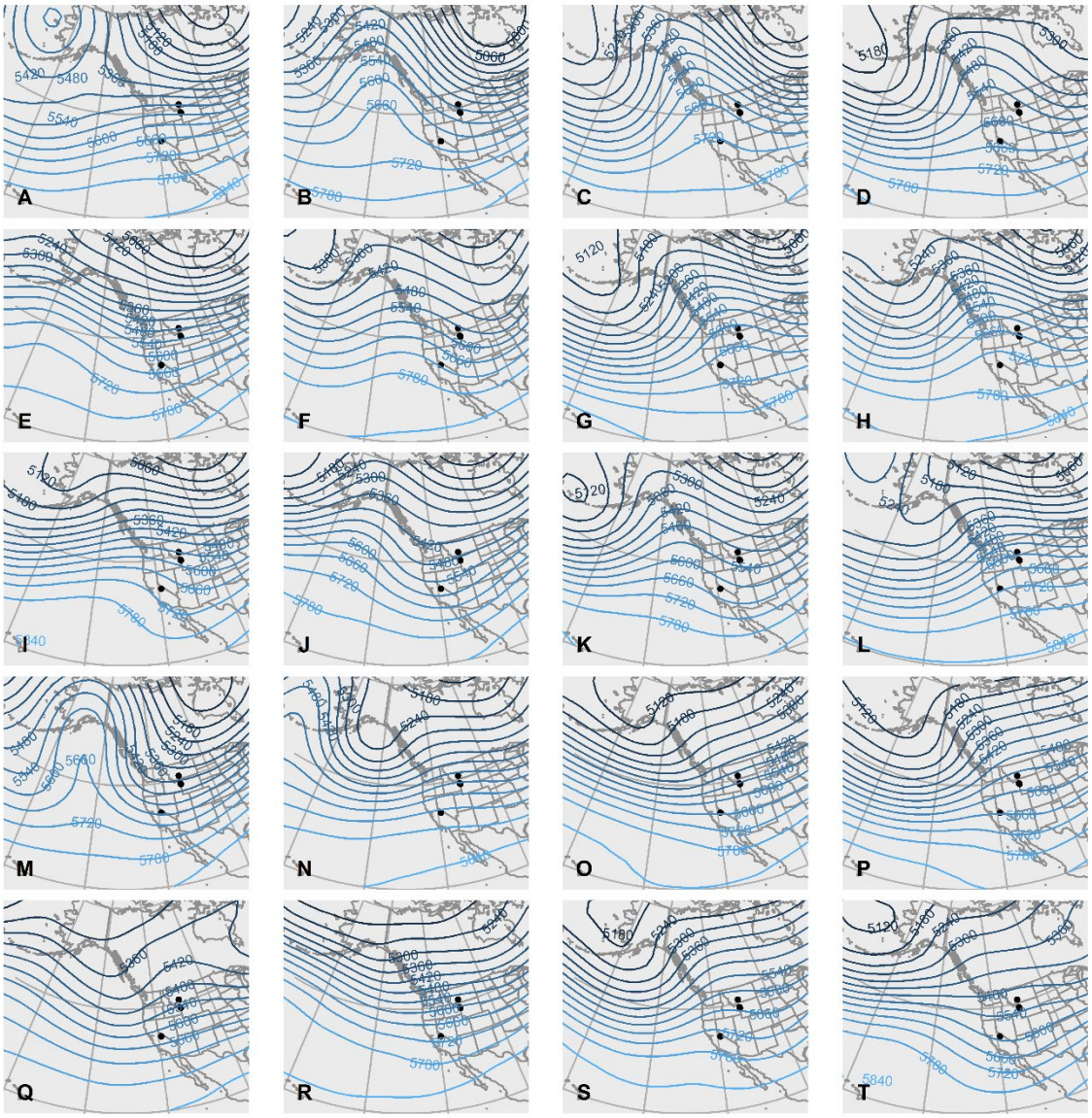

Figure 6: The same array as in Figure 5, zoomed over a smaller geographic extent in to emphasize local circulation patterns over the study sites. Points represent the locations used in this study.

Meteorological Characteristics for Synoptic Types

Bridger Bowl. Histograms of daily maximum and minimum temperature at Bridger Bowl, MT highlight types A, B, E, F, J, K and M as having the coldest temperatures (Figure 7, Table 3). All of these synoptic types are characterized by a strong north-to-south airmass trajectory over the northwest U.S. (Figures 5 and 6). Types G, H, L, N, and S show the warmest daily temperature distributions. These patterns feature ridging over the Rocky Mountains, and a southerly flow direction.

Map patterns for types B, F, J, K, and M observe the most frequent precipitation events at Bridger Bowl (Table 3). All of these types feature a ridge over the eastern Pacific or west coast of the U.S and some amount of troughing over Hudson Bay, which results in localized northwest flow over Bridger Bowl. Type F has the second highest median storm total and the highest percentage of days with precipitation of all synoptic types. The Pacific ridge for type F is less pronounced than the other five types, which results in a more zonal flow pattern and thus more efficient vapor transport. Types G, H, P, and S have the lowest percentage of days with precipitation. These four types are characterized by a moderate to strong ridge over the western U.S. and a southwest flow trajectory. SWE distributions for patterns H and S show a low percentage of precipitation days but a high median precipitation total, suggesting that storms occurring during these patterns are infrequent but can be large. The SWE distribution for type M is noteworthy because although the percentage of days during which precipitation is recorded is the second highest of all types, the median daily precipitation total is among the lowest overall. Additionally, there are multiple events in which 24-hour SWE total exceeded 50

mm. This map pattern shows the strongest ridge over the east Pacific, and the most intense northerly flow trajectory.

Jackson Hole. Types B, E, I, J, K, and M have the coldest distributions of daily maximum and minimum temperature (Figure 8, Table 4). Similar to the trends observed at Bridger Bowl, these map patterns all exhibit an eastern Pacific ridge, a trough over Hudson Bay, and a resulting northerly flow trajectory. Types G, H, L, N, and S have the warmest daily temperature distributions, and are characterized by a southerly flow direction and moderate to strong ridging over the Rockies.

Types B, E, J, M, and O have the highest percentage of days with precipitation at Jackson Hole. With the exception of type O, the map patterns are characterized by a moderate to strong ridge over the east Pacific and a trough over the Hudson Bay region, and storm totals are modest. Type O shows a very different configuration, with a trough over the Gulf of Alaska and zonal flow over eastern Canada, which results in zonal flow slightly out of the southwest over the continental U.S. Type O has one of the highest percentage of days with precipitation and one of the highest median daily precipitation totals of all synoptic types. Types C, G, H, I, N, and S have the smallest percentage of days with precipitation. Types C, G, and H feature enhanced troughs over the Aleutians and Hudson Bay, and a ridge over the western U.S. In patterns I, N, and S, the ridge over the continental U.S. is not as pronounced. For Type N, the southwest zonal flow with a weak to moderate ridge is associated with relatively infrequent, but larger storm events. Type M features strong ridge over Gulf of Alaska and trough extending from Hudson

Bay over the continental U.S, and has a high percentage of precipitation days, but relatively low daily precipitation totals.

Mammoth Mountain. Types E, J, K, M, and T have the coldest daily temperature distributions at Mammoth Mountain (Figure 9, Table 5). Types E, J, K, and M both show up as the colder synoptic types at Bridger Bowl and Jackson Hole as well, characterized by a ridge over the east Pacific, a trough extending to the southwest from Hudson Bay, and resulting in a strong northwest flow. Type T is one of the coldest synoptic types at Mammoth, but it is also associated with average temperatures at Jackson Hole and above average temperatures at Bridger Bowl. This map pattern shows a split flow at approximately 45^{o} N, with a weak ridge extending to the north and a trough extending to the south. The result is that Mammoth Mountain experiences a northwest flow pattern while Jackson Hole and Bozeman see more directly west or southwest patterns. Types C, F, H, L and S feature a southwest flow with moderate to strong ridging over the coast, resulting in warm daily temperature distributions. For type F, Jackson and Bridger are situated farther downstream of the ridge, which leads to average or below average at each site, respectively. Types N and R are also relatively warm, but they are characterized by a more direct westerly zonal flow.

Types A, J, L, M, O, P and Q have the wettest daily SWE distributions. Types O, P, and Q see among the highest percentage of days with recorded precipitation, and the highest median daily precipitation amounts. These types are all characterized by a trough over the Gulf of Alaska, with southwest zonal flow patterns over the western U.S. Types A and L see a smaller percentage of days with precipitation, but record high daily

precipitation totals during storms. These patterns feature a split flow, with an omega block over the Bearing Sea and zonal flow over the continental U.S. At Mammoth Mountain, both types result in southwest flow trajectory. Types J and M show a more northwesterly flow trajectory, with a ridge over the east Pacific. Precipitation during days associated with these types is common, but precipitation totals are usually moderate. Types C, F, H, and I have the smallest percentage of days with precipitation. Mammoth Mountain is situated on the downstream end of an upper-level ridge during days associated with these synoptic types, which results in blocking and a northwest flow trajectory. Types R and S see a slightly higher percentage of days with precipitation, but precipitation totals for days associated with the two patterns is among the lowest of all synoptic types. These patterns are again associated with enhanced northwest flow (Type R) and a blocking ridge (Type S).

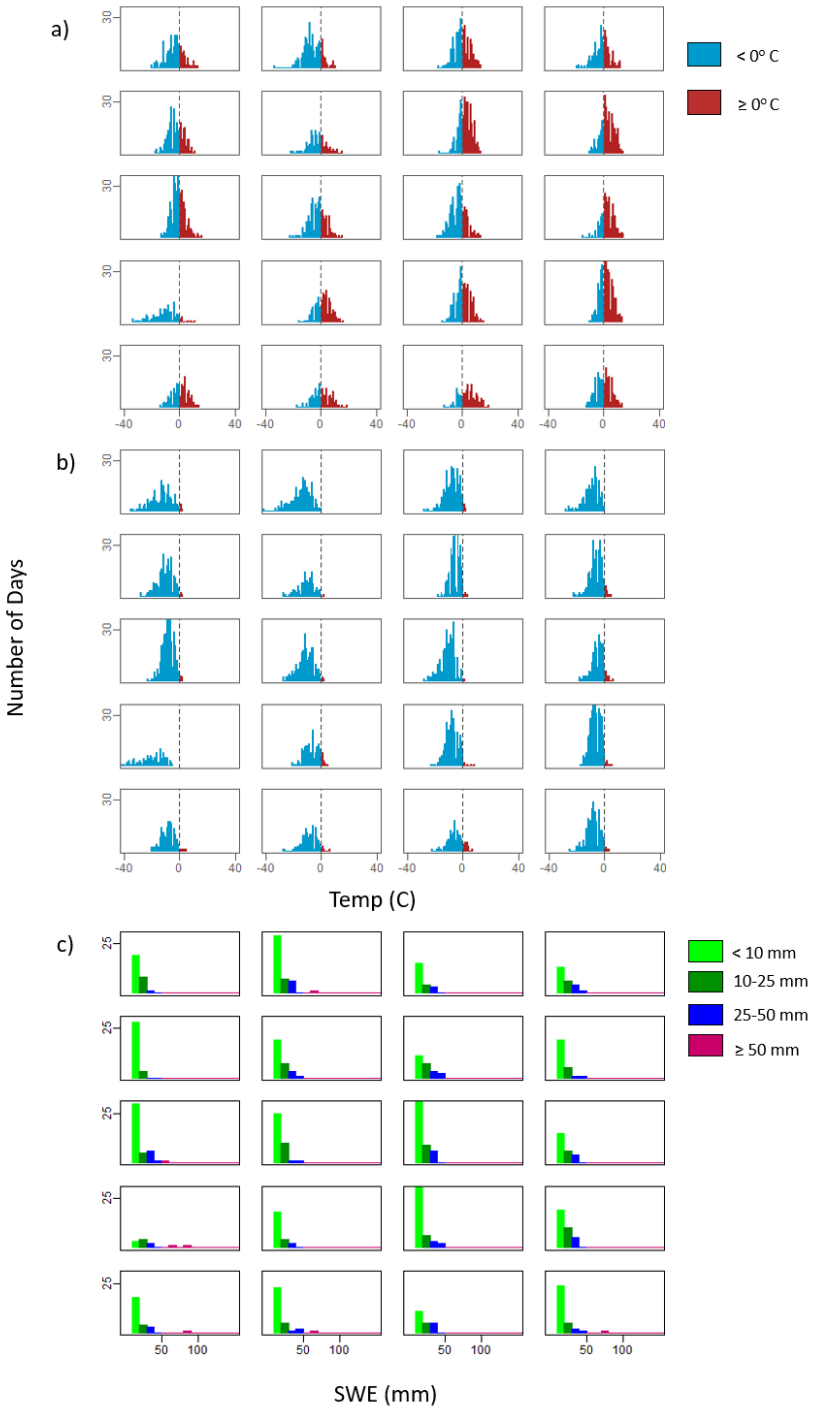

Figure 7: Histograms of daily maximum temperature (a), minimum temperature (b), and snow water equivalence totals for Bridger Bowl, MT. For each array (a-c), the position of the plot corresponds with the map pattern shown in Figures 5 and 6. For example, the histograms located in the upper left corner of each array (a-c) correspond with synoptic type A.

Table 3: Descriptive statistics for weather metrics at Bridger Bowl. Summaries of Daily SWE totals are given using 50th, 75th, and 90th percentiles, along with percent of total days during which any amount of precipitation was recorded (> 0). Daily maximum and minimum temperatures are summarized using 25th, 50th, and 75th percentiles. For each column, values equal to or greater than the upper quartile (i.e. wettest or warmest types) are bold and highlighted in dark grey, while those less than the lower quartile (i.e. driest or coldest types) are italicized and highlighted in light grey.

	SWE (mm)				**Max T (C)**			**Min T (C)**		
	50	**75**	**90**	**% >0**	**25**	**50**	**75**	**25**	**50**	**75**
A	*4.0*	*10.0*	*15.8*	53	*-7.0*	*-3.0*	*0.8*	*-18.0*	*-12.0*	*-7.3*
B	5.0	10.8	19.0	**59**	*-10.0*	*-6.0*	*-1.0*	*-18.7*	*-13.0*	*-9.0*
C	*3.8*	*9.5*	17.6	*32*	-3.3	0.0	4.0	-12.0	-7.0	-4.0
D	*4.0*	*9.3*	19.9	46	-5.0	-1.0	2.0	-12.0	-9.0	-6.0
E	5.0	**12.0**	*16.4*	43	-6.0	*-3.0*	2.0	-13.8	*-10.0*	-6.5
F	**6.0**	**13.0**	**24.1**	**61**	*-7.0*	*-3.0*	*1.0*	-13.8	*-10.0*	*-7.0*
G	5.0	10.0	**22.3**	*29*	**-1.0**	**2.0**	**6.0**	**-8.3**	**-6.0**	**-3.0**
H	**6.0**	**11.4**	19.0	*30*	**-0.6**	**2.0**	**6.0**	**-8.5**	**-6.0**	**-3.0**
I	5.0	11.0	18.0	41	-4.0	-1.0	2.0	-11.0	-8.0	-6.0
J	5.0	10.0	18.0	**58**	-6.7	-2.0	*1.0*	*-14.0*	*-11.0*	*-7.0*
K	5.0	11.0	18.0	**55**	*-7.0*	*-3.0*	*1.0*	*-14.0*	*-10.0*	*-7.2*
L	**6.0**	*9.3*	20.2	42	**0.0**	**3.0**	**6.0**	**-7.0**	**-4.0**	**-2.0**
M	*3.4*	*6.0*	*17.1*	**59**	*-14.5*	*-9.0*	*-4.4*	*-25.2*	*-19.0*	*-13.5*
N	5.1	11.0	19.0	43	-2.0	**2.0**	**6.0**	-11.0	**-6.6**	**-2.9**
O	**6.0**	11.0	18.8	50	-3.0	0.0	4.0	-11.0	-8.0	-4.4
P	5.0	10.0	**21.4**	*37*	**-1.1**	**2.0**	4.8	**-9.0**	-7.0	-3.5
Q	5.0	11.0	*15.0*	50	-4.0	1.0	4.0	-12.0	-8.0	-6.0
R	**8.0**	**15.1**	**22.2**	52	-4.0	1.0	**6.0**	-11.3	-8.0	-4.0
S	**8.0**	**12.5**	**27.4**	*39*	**-1.0**	**4.0**	**8.0**	**-9.0**	**-6.0**	**-2.5**
T	5.0	10.0	*17.0*	54	-4.0	0.0	4.0	-11.0	-8.0	-5.0

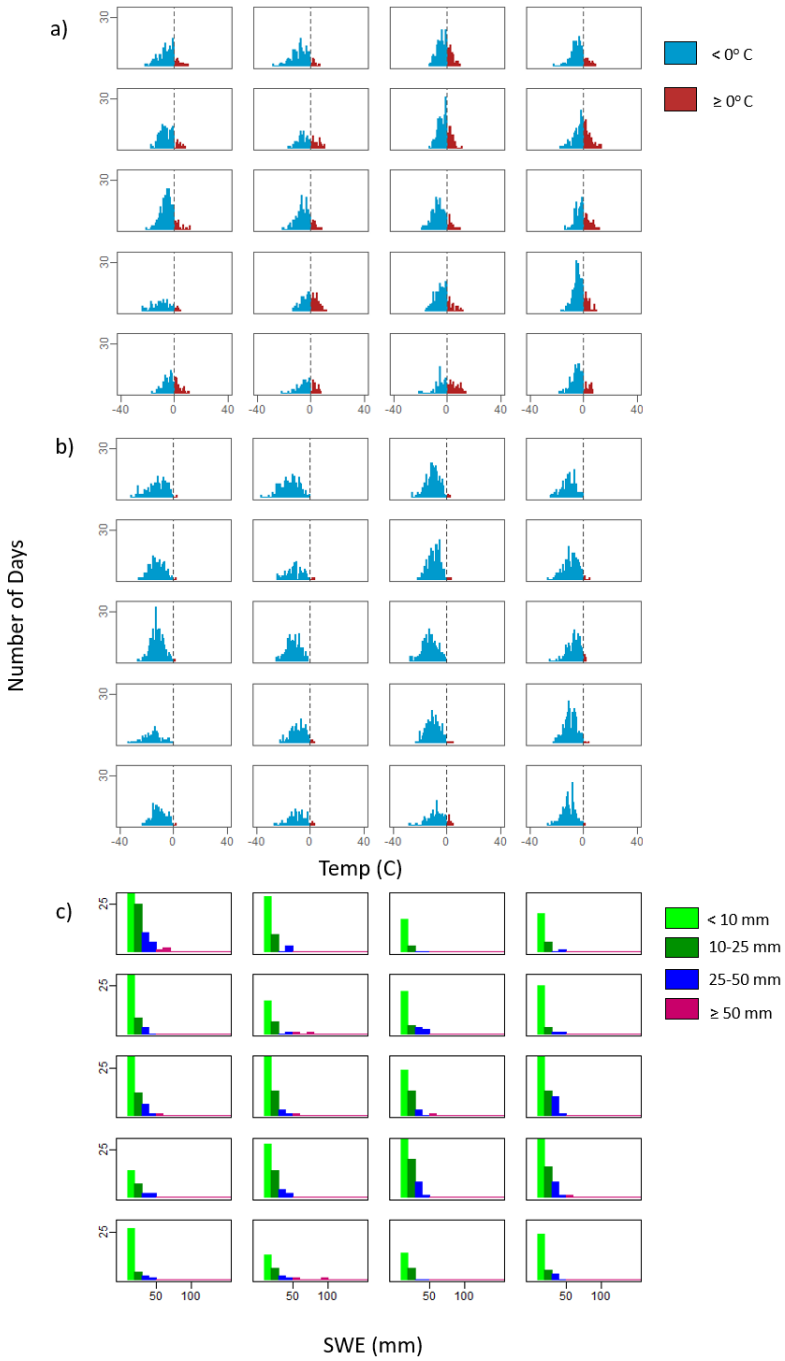

Figure 8: Histograms of daily maximum temperature (a), minimum temperature (b), and snow water equivalence totals for Jackson, WY. For each array (a-c), the position of the plot corresponds with the map pattern shown in Figures 5 and 6. For example, the histograms located in the upper left corner of each array (a-c) correspond with synoptic type A.

Table 4: Descriptive statistics for weather metrics at Jackson, WY. Summaries of daily SWE totals are given using 50th, 75th, and 90th percentiles, along with percent of total days during which any amount of precipitation was recorded (%> 0). Daily maximum and minimum temperatures are summarized using 25th, 50th, and 75th percentiles. For each row, values equal to or greater than the upper quartile (i.e. wettest or warmest types) are bold and highlighted in dark grey, while those less than the lower quartile (i.e. driest or coldest types) are italicized and highlighted in light grey.

	SWE (mm)				Max T (C)			Min T (C)		
	50	**75**	**90**	**%> 0**	**25**	**50**	**75**	**25**	**50**	**75**
A	**7.6**	**18.7**	**28.9**	75	*-8.9*	-4.4	-1.1	*-16.7*	-11.1	-6.7
B	3.2	8.5	*14.0*	**77**	*-11.7*	*-7.8*	*-3.3*	*-19.4*	*-14.4*	*-10.0*
C	*2.5*	*6.4*	*12.6*	*40*	-6.1	-2.8	0.6	-13.3	-10.0	-7.2
D	*2.5*	*6.4*	*13.7*	64	-7.2	-4.4	*-2.2*	-15.0	-11.1	-7.2
E	4.6	10.3	17.4	**78**	*-9.4*	*-6.1*	*-2.2*	*-16.1*	*-12.8*	-8.3
F	*3.0*	8.8	17.5	68	-7.8	-3.9	0.6	-15.0	-11.7	-7.8
G	3.3	*6.7*	*12.7*	*53*	**-5.6**	**-2.2**	0.0	**-12.8**	**-9.2**	-6.5
H	*2.5*	*7.6*	15.4	*44*	**-5.0**	**-1.7**	**1.1**	**-12.8**	**-8.9**	**-5.6**
I	**5.6**	**11.4**	17.8	69	-8.3	*-5.6*	*-2.8*	-15.6	*-12.8*	*-9.9*
J	4.1	8.9	17.8	**82**	*-8.9*	*-5.6*	*-2.2*	-15.6	-12.2	*-8.9*
K	*3.0*	*7.6*	14.2	76	*-8.9*	*-6.1*	*-2.2*	*-16.7*	*-13.3*	*-9.4*
L	**8.1**	**15.2**	**22.6**	68	**-4.4**	**-1.7**	**1.1**	**-10.6**	**-6.7**	**-3.9**
M	3.8	8.9	17.8	**85**	*-13.3*	*-8.9*	*-4.4*	*-20.8*	*-15.6*	*-12.2*
N	**5.8**	**12.4**	**21.2**	*62*	**-5.6**	**-1.7**	**2.2**	**-12.8**	**-8.9**	**-5.0**
O	**6.1**	**11.4**	**21.6**	**79**	-7.8	-4.4	-1.1	-14.4	-10.6	-6.7
P	4.8	10.2	18.9	71	-6.1	-3.9	-0.6	**-12.8**	-10.0	-6.7
Q	3.8	8.9	*14.0*	75	-6.7	-2.8	0.1	-14.4	-11.1	-7.2
R	5.1	10.9	**23.6**	65	-6.1	-3.1	**1.1**	-14.0	-10.0	**-6.1**
S	3.8	8.0	16.5	*53*	**-5.6**	**-0.6**	**4.4**	**-11.4**	**-7.8**	**-3.9**
T	*2.5*	*6.4*	*12.1*	72	-6.7	-3.9	-1.1	-13.9	-11.1	-8.3

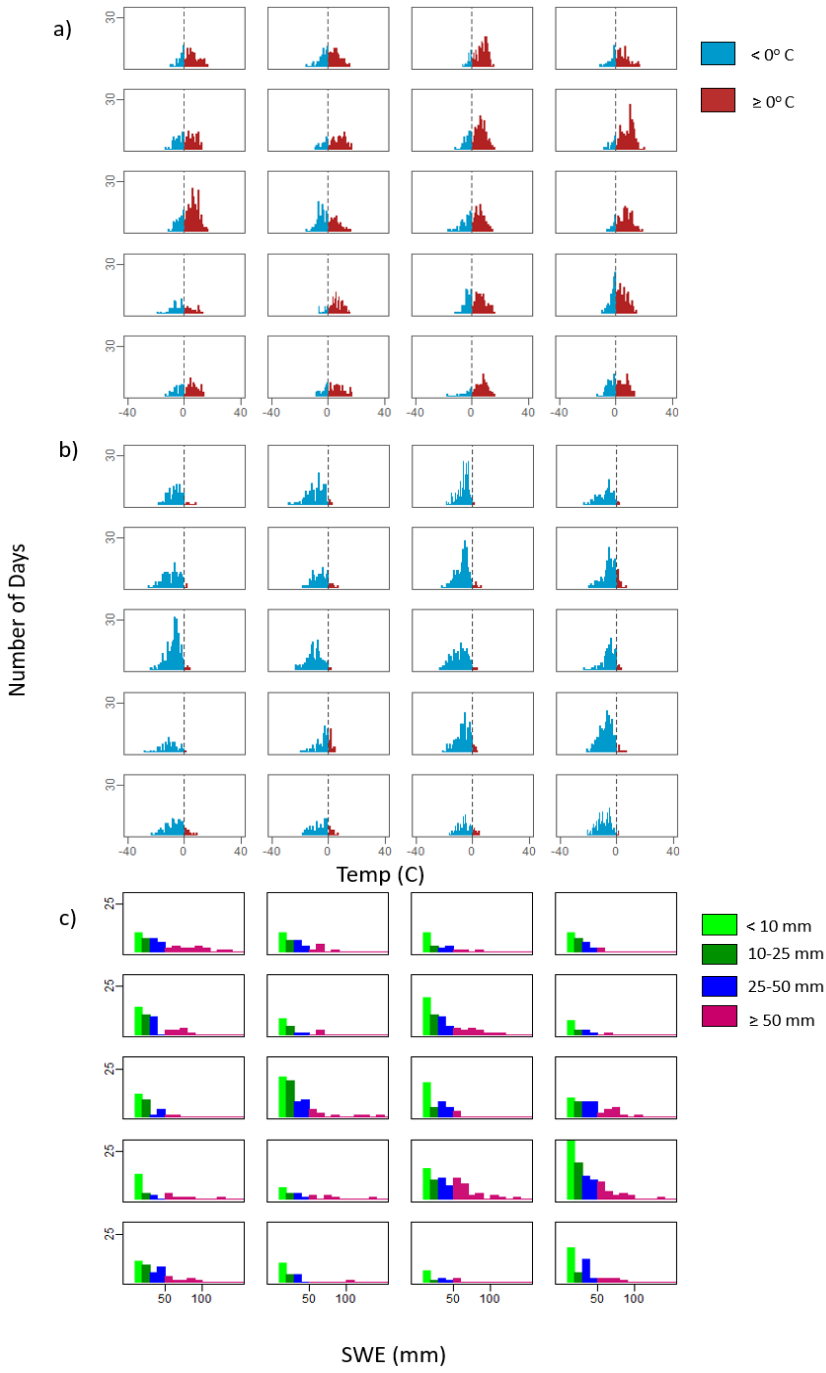

Figure 9: Histograms of daily maximum temperature (a), minimum temperature (b), and snow water equivalence totals for Mammoth Mtn., CA. For each array (a-c), the position of the plot corresponds with the map pattern shown in Figures 5 and 6. For example, the histograms located in the upper left corner of each array (a-c) correspond with synoptic type A.

Table 5: Descriptive statistics for weather metrics at Mammoth, CA. Summaries of daily SWE totals are given using 50th, 75th, and 90th percentiles, along with percent of total days during which any amount of precipitation was recorded (%> 0). Daily maximum and minimum temperatures are summarized using 25th, 50th, and 75th percentiles. For each column, values exceeding the upper quartile (i.e. wettest or warmest types) are highlighted in dark grey and bold, while those less than the lower quartile (i.e. driest or coldest types) are highlighted in light grey and italicized.

	SWE (mm)				**Max T (C)**			**Min T (C)**		
	50	**75**	**90**	**%> 0**	**25**	**50**	**75**	**25**	**50**	**75**
A	**25.4**	**50.8**	**95.1**	39	-0.6	2.8	7.2	-10.0	-6.7	-3.9
B	15.2	33.0	59.9	29	*-2.2*	2.2	6.1	*-13.3*	-8.3	-4.4
C	*9.4*	*19.9*	45.2	*21*	**2.8**	**6.7**	**10.0**	**-8.9**	**-5.6**	-3.9
D	12.7	23.6	*36.1*	36	-0.7	2.8	6.7	-11.7	-6.7	-4.4
E	**17.3**	34.3	58.4	35	*-3.8*	*1.4*	*5.6*	*-13.3*	*-8.9*	*-5.0*
F	11.8	23.2	*40.0*	*20*	0.0	**6.1**	**10.4**	-10.6	-5.8	-2.8
G	13.0	30.5	**66.0**	37	0.0	5.0	8.3	-10.0	-6.7	-4.4
H	*7.6*	*18.4*	*31.8*	*15*	**3.3**	**8.3**	**11.1**	**-7.2**	**-5.0**	**-2.2**
I	*8.9*	21.6	40.1	*19*	0.6	4.7	7.9	-10.0	-6.7	-4.4
J	12.1	26.2	46.9	**58**	*-5.0*	*-1.1*	*3.3*	*-13.3*	*-10.6*	*-7.2*
K	*9.1*	*20.4*	*38.6*	36	*-2.2*	2.2	*6.0*	*-13.2*	*-8.9*	*-5.6*
L	**27.9**	**41.9**	**70.4**	35	**1.8**	**6.7**	**9.9**	**-6.7**	**-4.4**	**-2.2**
M	11.4	23.9	54.6	**44**	*-6.1*	*-1.7*	*3.9*	*-13.9*	*-10.0*	*-6.7*
N	11.0	37.1	**65.4**	*22*	**2.8**	5.6	**9.4**	**-5.7**	**-2.8**	**-0.6**
O	**19.1**	**49.5**	**63.8**	**48**	*-2.2*	2.2	6.7	-10.0	-6.7	-3.3
P	**18.3**	**38.5**	56.5	**49**	-1.1	*1.7*	*5.6*	-11.1	-7.2	-4.4
Q	14.5	**38.3**	51.4	**47**	*-2.2*	3.3	6.7	-11.1	-6.7	-2.8
R	10.7	*19.2*	*34.0*	29	0.0	4.4	8.3	-11.1	**-5.6**	**-1.7**
S	*9.5*	*20.1*	43.8	24	**2.4**	**6.1**	8.9	**-9.4**	**-5.6**	**-2.2**
T	11.7	34.0	42.5	37	*-3.3*	*1.1*	6.1	-12.8	*-8.9*	*-5.6*

Early Season Patterns for Major and Minor Seasons

In this section, we refer to one operational winter season (i.e. November through March) by the year in which it started. For example, the winter of 1984-85 is referred to hereafter as the 1984 season. At each location, we use scatterplots of seasonal cumulative DSAI score to identify clear breaks that separate seasons with high scores from the rest of the seasons (Figure 10a). These seasons are hereafter referred to as "major seasons". Additionally, we designate any season with a cumulative DSAI score of zero as a "minor season". The threshold separating major seasons from the rest varies by site, as does the number of years designated as major seasons. However, there is a distinct group of seasons with exceptionally high DSAI scores at each site, indicating these seasons had a particularly large number of events or large magnitude events. Time series plots do not indicate any apparent temporal trend in deep persistent slab activity at the three sites (Figure 10b). At Bridger Bowl, there are four seasons with DSAI scores equal to or exceeding 284.3, representing the 90^{th} percentile for annual DSAI scores at that site (Table 6). There are four seasons with a DSAI score of zero at Bridger Bowl. We also include the 2014 and 1997 seasons as minor seasons, which had seasonal scores of 0.01 and 0.1, respectively. At Jackson Hole, we find ten seasons with DSAI scores exceeding 209.3, representing the 75^{th} percentile at that site. Similarly to Bridger Bowl, there were only two seasons (1993 and 2003) with seasonal DSAI scores of zero so we include an additional three seasons with DSAI less than or equal to 0.1 as minor seasons (1999, 2005, and 2016). We find seven seasons at Mammoth Mountain with DSAI scores equal

to or greater than 100.1, which corresponds with the 82nd percentile at that site. We found 18 seasons with seasonal a DSAI score of zero at Mammoth Mountain.

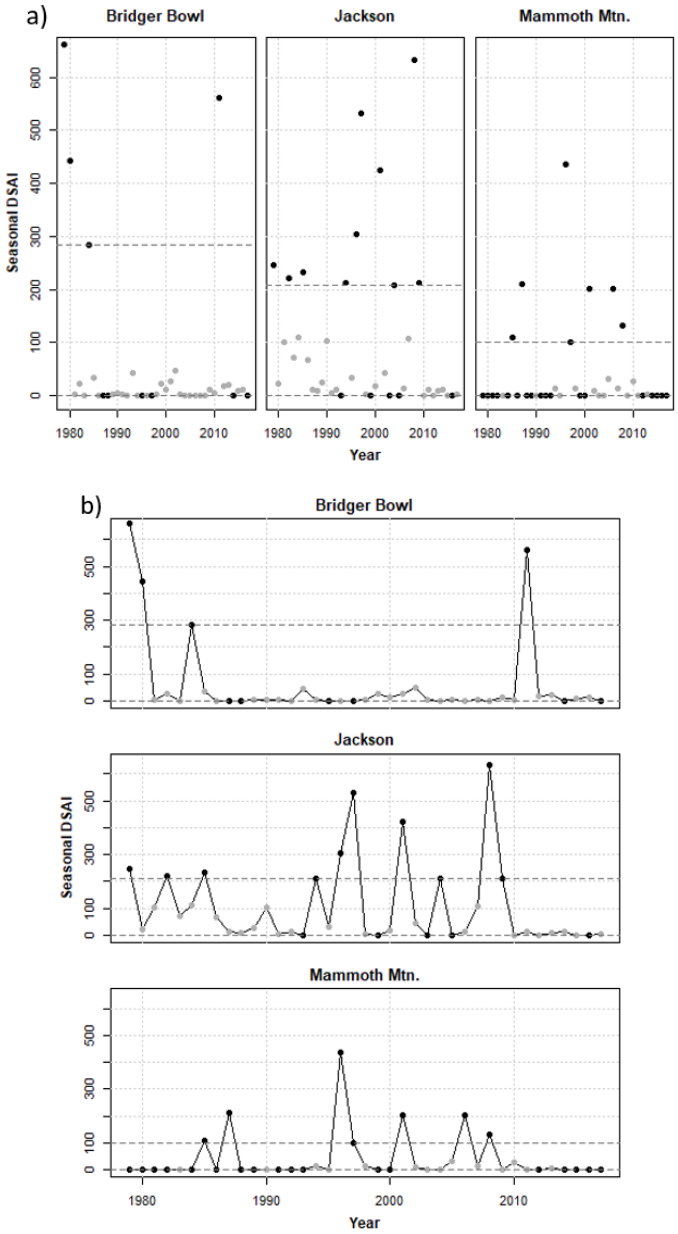

Figure 10: (a) Scatterplots of seasonal deep slab activity index scores for Bridger Bowl, MT (left), Jackson Hole (center), and Mammoth Mountain, CA (right). Highlighted points represent the years considered as major and minor deep persistent avalanche seasons, and dashed lines represent the cutoff thresholds used to identify those points. (b) The same time series is plotted with a line to assess a temporal trend in deep persistent slab activity.

Table 6: Major and minor deep slab avalanche seasons for the three study sites, determined by cumulative seasonal DSAI score.

Location	Major Seasons	Minor Seasons
Bridger Bowl	1979, 1980, 1984, 2011	1987, 1988, 1995, 1997, 2014, 2017
Jackson Hole	1979, 1982, 1985, 1994, 1996, 1997, 2001, 2004, 2008, 2009	1993, 1999, 2003, 2005, 2016
Mammoth Mountain	1985, 1987, 1996, 1997, 2001, 2006, 2008	1979-1982, 1984, 1986, 1988, 1989, 1991-1993, 1999, 2000, 2012, 2014-2017

Bridger Bowl. Heat maps for the major deep slab seasons 1979, 1980, 1984, and 2011 show the number of days assigned to each synoptic type during November through January of each season (Figure 11). During the major deep slab seasons 1979, 1980, and 1984, there is a noteworthy concentration of higher counts in the upper rows of the array, which are represented by patterns exhibiting strong blocking patterns. The 1979 season saw high counts for days associated with types A, E, and F- all of which show a ridge over the east Pacific, resulting in enhanced north to south airflow and subsequent colder temperatures. The 1980 season also saw a large number of days associated with Type A, while 1984 had a large number of days associated with type E. This is not the case for the 2011 season, which was dominated by types I and R, both of which are zonal patterns with direct westerly flows.

The minor deep slab seasons of 1987, 1988, and 1997 exhibit a distinct lack of the blocking patterns in the upper rows of the SOM array during November-January (Figure 12). The 1987, 1997, and 2014 seasons also show a high number of days assigned to the

synoptic types on the right side of the SOM array, which are associated with a moderate ridge over the western U.S. and above normal temperatures. The 2014 season had a large number of days represented by types B and F, two of the synoptic types more commonly associated with precipitation. The 1995 and 2017 seasons were unlike the other four minor deep slab seasons in that they had a relatively large number of days assigned to synoptic types in the upper right corner of the array, which are characterized by a blocking ridge over the western U.S. and more commonly associated with the major seasons. Both seasons had a large number of days assigned to type N, while the 1995 season also had a large number assigned to type L. Both synoptic types are associated with southwesterly flow and relatively warm temperatures at Bridger Bowl.

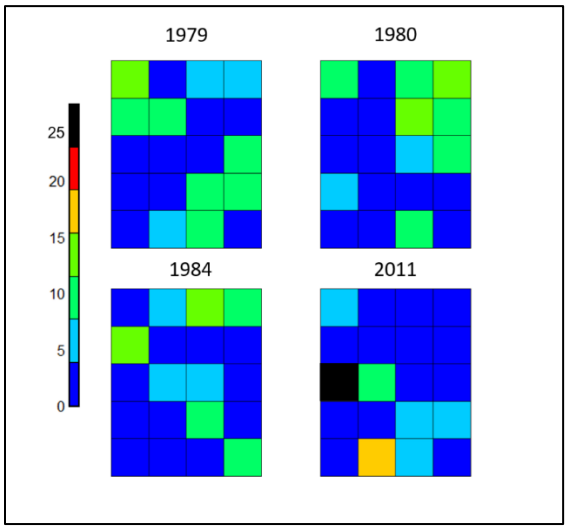

Figure 11: Heat maps displaying counts for number of days assigned to each synoptic type during November through January of major deep slab avalanche seasons at Bridger Bowl. The scale bar on the left represents the number of days each synoptic type was observed. Each square on a heatmap for a given season corresponds with the synoptic type in the same location of the array in Figures 5 and 6.

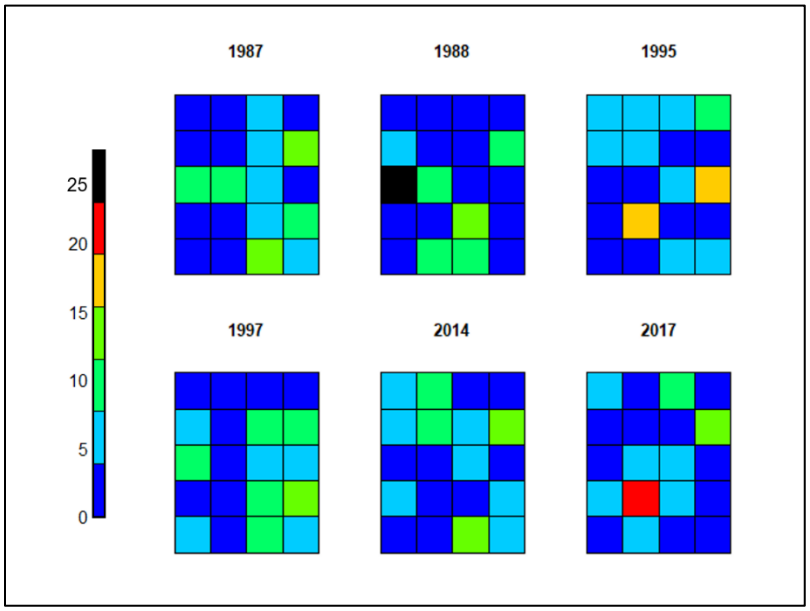

Figure 12: Heat maps for the number of days assigned to each synoptic type during November-January of the six minor deep slab seasons at Bridger Bowl, MT. Each square on a heatmap for a given season corresponds with the synoptic type in the same location of the array in Figures 5 and 6.

By considering relative frequency of each synoptic type for the early winter (i.e. the number of days assigned to each synoptic type divided by the total number of days from November to January over all major seasons and over all minor seasons), a shift towards increased meridional flow during the beginning of major seasons becomes apparent (Figure 13). This meridional shift during major deep slab seasons is especially noteworthy in the large increase in frequencies for types A, C, D, and E and the dramatic decrease in counts for types N and P. Major seasons also see a decrease in frequency for type B, which is characterized by enhanced northwest flow over Bridger Bowl and is commonly associated with increased precipitation. During minor seasons, there are a large number of days represented by types H, N, and S. All three types are characterized

by a southwesterly airflow pattern, and they are among the warmest synoptic types at Bridger Bowl.

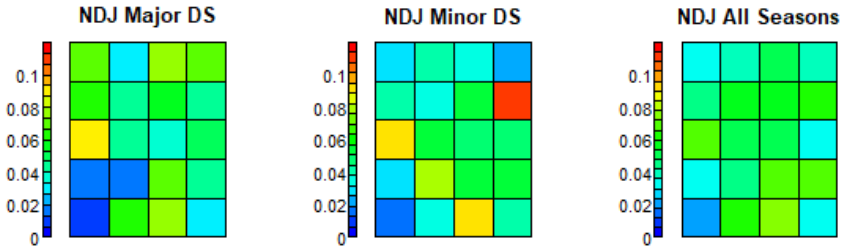

Figure 13: Relative frequencies for each synoptic type from November-January over all major deep persistent slab seasons (left), all minor seasons (center) and all seasons (right) at Bridger Bowl. Frequencies are calculated by summing counts of days assigned to each synoptic type over all major (minor) seasons and dividing by total number of days for all major (minor) seasons.

Barplots of the difference in relative frequencies for each synoptic type during major and minor deep persistent slab seasons further highlight the general shift towards meridional flow during major years and zonal flow during minor seasons (Figure 14). In these plots, we calculate the change in relative frequency by subtracting the relative frequency of days associated with each type for November – January of all seasons from the relative frequency during November – January of major (minor) seasons. We also subtract the relative frequency of each synoptic type during minor seasons from the relative frequency during major seasons.

These barplots illustrate the transition toward blocking patterns during major seasons and zonal patterns during minor seasons. There is an increase in the number of days assigned to types A, C, D, E, and F during major seasons relative to minor seasons, all of which are located in the upper rows of the SOM array and are associated with meridional circulation. Alternatively, the plots demonstrate an increase in relative

frequencies of days associated with types H, N, S, and T during minor seasons. Type H is associated with an upper-level ridge over the western U.S., while types N, S, and T are all predominately zonal patterns. Type T is characterized by a northwesterly flow, while the storm tracks in types N and S come out of the southwest. Median daily maximum and minimum temperatures for types H, N, and S are in the upper quartile of all synoptic types at Bridger Bowl.

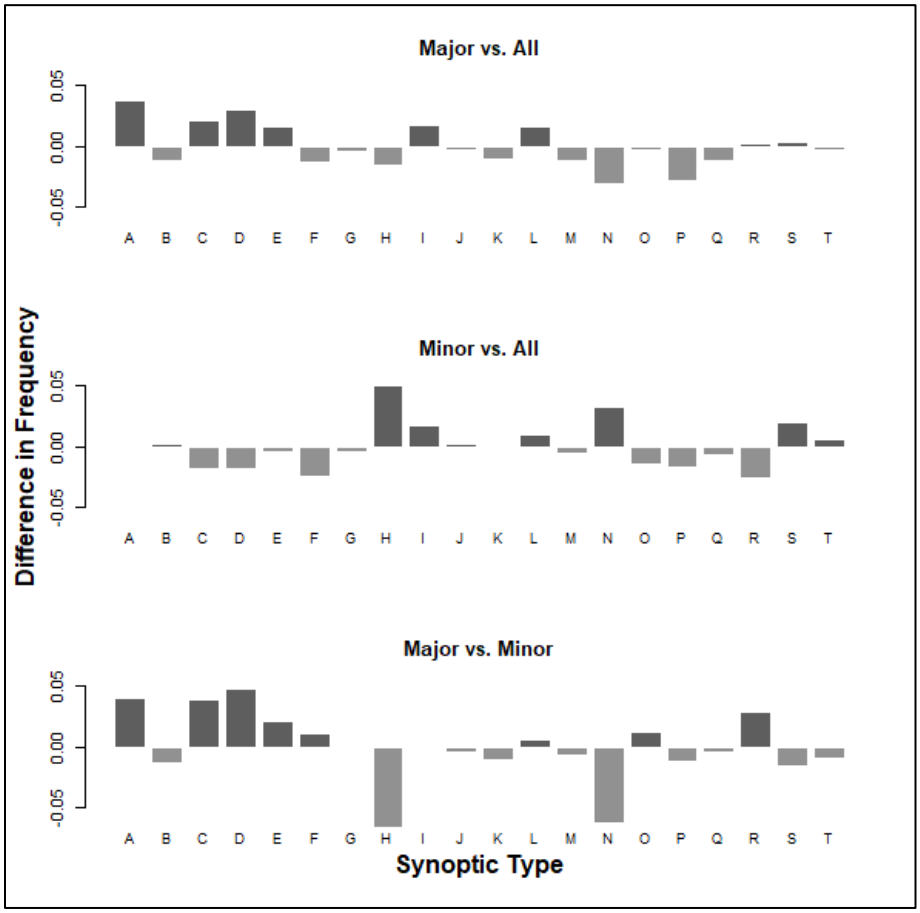

Figure 14: Barplots for the difference in relative frequency for each synoptic type during November-January between major seasons and all seasons (top), minor seasons and all seasons (center), and major seasons and minor seasons (bottom) at Bridger Bowl. Positive values indicate an increase in relative frequency during the first category in the title of each chart. For example, a positive value for type A in the top chart indicates a higher relative frequency for that synoptic type during major deep slab seasons relative to all seasons.

Jackson Hole. Heat maps for November-January synoptic type counts during major deep slab years indicate high counts for the number of days assigned to patterns associated with an enhanced ridge over the western U.S. for the seasons 1985, 1996, 1997, 2001, and 2009 (Figure 15). The 1997 and 2001 seasons also had relatively high counts for types O, P, and S, which are more zonal patterns, although they still feature a weak ridge over the western U.S. The 2009 season was dominated by a high pressure ridge extending from central California northward along the west coast of Canada. For most major deep slab seasons, the synoptic types with the largest number of days have a weak to moderate low pressure trough over Hudson Bay.

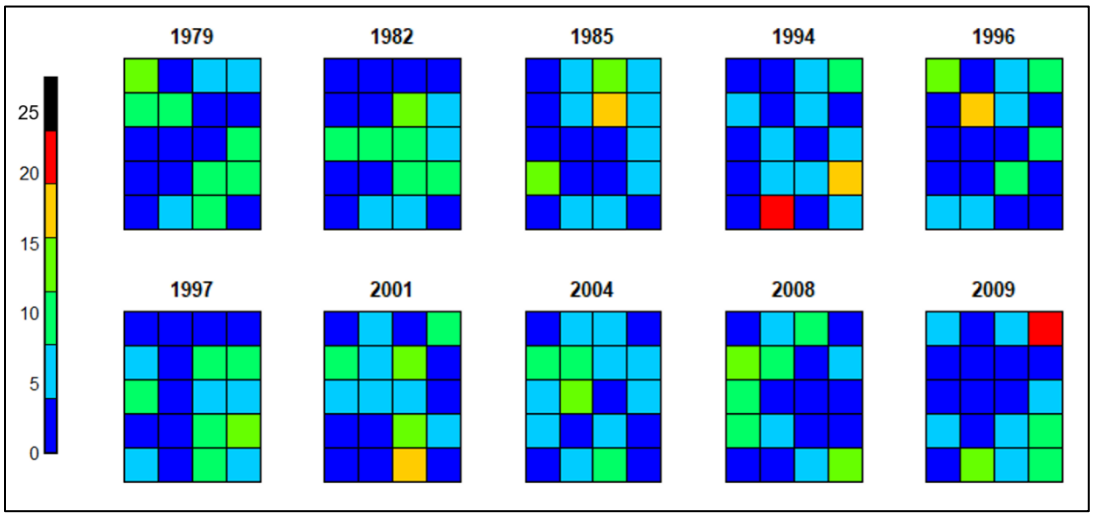

Figure 15: Heat maps displaying counts for the number of days each synoptic type was observed Nov.- Jan. during major deep slab years at Jackson Hole. For each season in the figure, a colored square on the array corresponds to the map pattern at the same location in the array in Figures 5 and 6.

The map patterns for the synoptic types assigned the most days during November-January of minor deep slab years in Jackson Hole feature enhanced zonal flow, with very few days assigned to the synoptic types representing blocking patterns in the upper row of the SOM array (Figure 16). The 1993 season appears to be the exception to the rule, with moderate counts for types B, C, and K. These patterns are characterized by a ridge near the Gulf of Alaska and the Pacific coast. However, the season also exhibited high counts for days assigned to type O, a direct westerly zonal pattern frequently associated with precipitation at Jackson, and type H, in which the upper-level ridge is situated above the intermountain west, commonly resulting in above-average temperatures and dry weather. During the 1999, 2003, and 2016 seasons, there were high counts for days assigned to types R and S. These patterns also showed up frequently during several major seasons. However, during 1999 and 2016 there were also high counts for types A, E, and/or I. All of which are characterized by zonal westerly flow over the U.S. and regularly lead to precipitation at Jackson Hole. November-January of 2003 saw a large number of days assigned to types M and O, which are characterized by zonal west/southwest flow, and commonly result in precipitation at Jackson Hole.

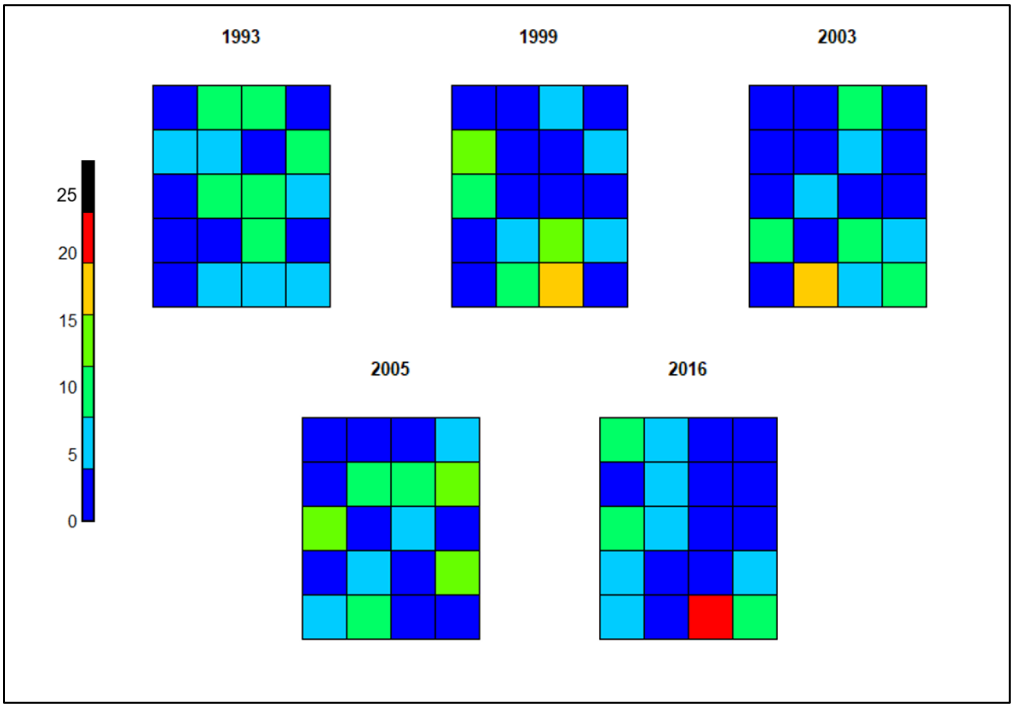

Figure 16: Heat maps displaying counts for the number of times each synoptic type was observed Nov.- Jan. during minor deep slab years at Jackson Hole. For each season in the figure, a colored square on the array corresponds to the map pattern at the same location in the array in Figures 5 and 6.

There is a notable increase in the number of days assigned to synoptic types D, G, and L during the beginning of major deep slab seasons in the Jackson area, and a decrease in the number of days assigned to the same types during minor seasons (Figure 17). All three of these types are characterized by a strong ridge over the western U.S. Major seasons also have very low frequencies for types I and N, which exhibit a zonal flow pattern with a westerly or slightly southwesterly trajectory over Jackson. Minor seasons exhibit high frequencies for synoptic types R, S, and T which may be attributed

to above average temperatures or frequent precipitation observed during those circulation patterns.

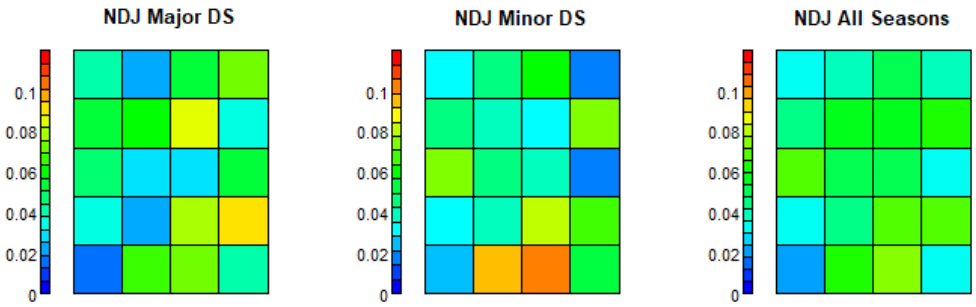

Figure 17: Relative frequencies for each synoptic type during November- January of all major deep persistent slab seasons (left), all minor seasons (center), and all seasons during the study period (right) at Jackson Hole. Frequencies are calculated by summing number of days assigned to each synoptic type over all major (minor) seasons and dividing by total number of days for all major (minor) seasons.

Barplots of the difference in relative frequencies for each synoptic type during major and minor seasons also indicate an increase in frequency tor types D, G, and L during the beginning of major seasons, which all decrease during minor seasons (Figure 18). There is a marked increase in the number of days assigned to patterns R, S, and T during minor seasons. This implies a shift towards increased meridional flow during the beginning of major seasons, and a transition towards increased zonal flow during minor seasons.

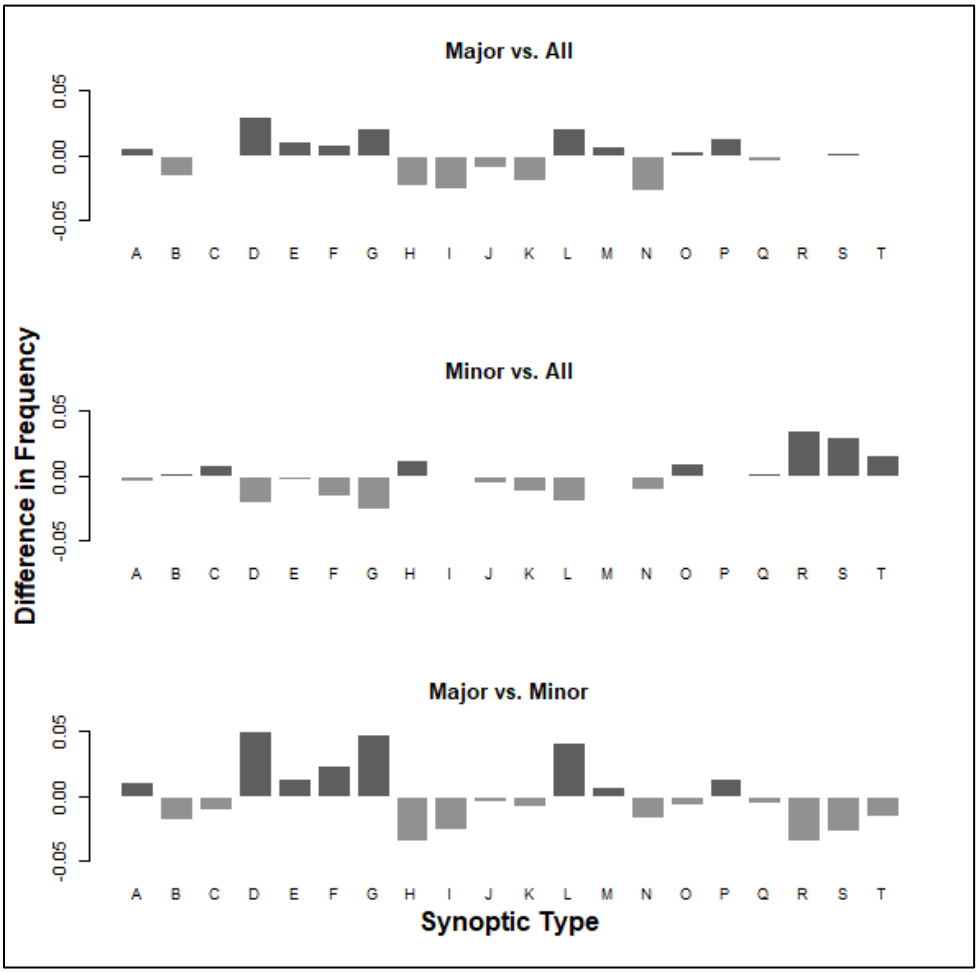

Figure 18: Barplots for the difference in relative frequency for each synoptic type during November-January between major seasons and all seasons (top), minor seasons and all seasons (center), and major seasons and minor seasons (bottom) at Jackson Hole. Positive values indicate an increase in relative frequency during the first category in the title of each chart. For example, a positive value for type D in the top chart indicates a higher relative frequency for that synoptic type during major deep slab seasons relative to all seasons.

Mammoth Mountain. For four of the seven major deep slab seasons (1985, 1997, 2001, and 2006) at Mammoth Mountain, November-January circulations were largely dominated by patterns with west to southwest flow directions and zonal to weak blocking patterns (Figure 19). The 2008 season had a different pattern, with relatively large

number of days assigned to types E, F, M, and T, which have varying degrees of a northwest flow direction. During the early winter of 1996, type F had the largest number of days, which again is associated with a northwest pattern. However, the season also recorded large numbers of days assigned to types A, D, L, and O, which all have a weak to moderate ridge over the west coast, and a resulting southwest flow direction. The beginning of 2006 had a large number of days assigned to types N and P, which both show a trough over the east Pacific. Type N is typically warmer and drier than type P, which is one of the wettest patterns for Mammoth Mountain and has a median daily maximum temperature that is in the lowest quartile for the site.

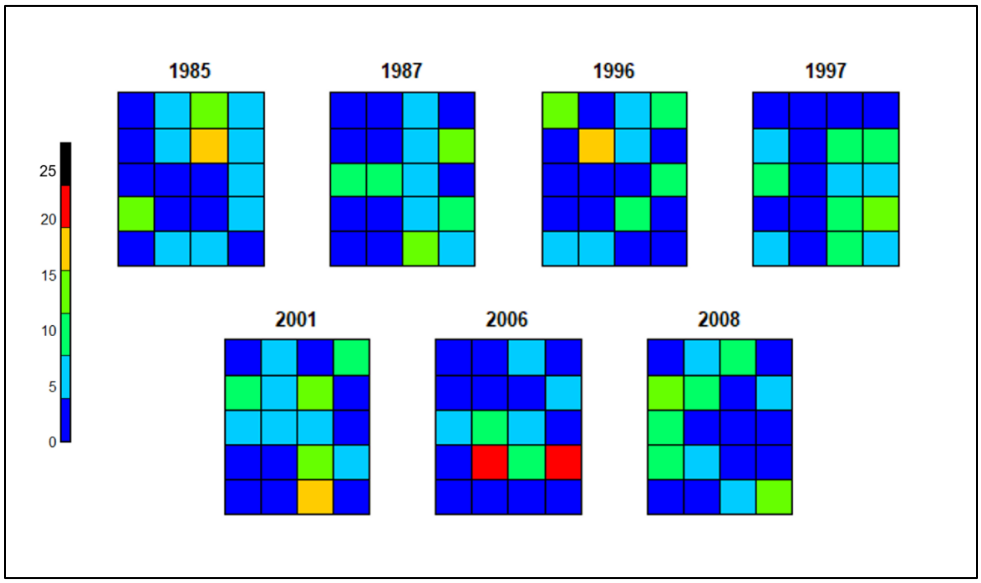

Figure 19: Heat maps displaying counts for the number of days assigned to each synoptic type for Nov.- Jan. during major deep slab seasons at Mammoth Mountain. For each season in the figure, a colored square on the array corresponds to the map pattern at the same location in the arrays in Figures 5 and 6.

There was not a single deep slab event in 18 of the 35 seasons at Mammoth Mountain with complete weather and avalanche records. For many of these seasons, the dominant synoptic types were primarily zonal (Figure 20). This is true during the 1979, 1981, 1982, 1999, 2004, 2012, 2015, 2016, and 2017 seasons. Seasons 1980, 1988, 1989, 1991, 2000, and 2002 all had high counts of synoptic types characterized by a ridge over the west coast, while during the seasons 1982 and 1983 Mammoth was more frequently situated under an upper level trough, and the 1993 season had periods of both.

Seasons 1982, 1988, 1989, 1991, 1999, and 2004 had a large number of days assigned to type I, which was mostly absent in the major deep slab seasons. The seasons 1991, 1999, 2015, 2016, and 2017 all had a large number of days represented by patterns R, O, or S, which are zonal patterns with a general northwesterly flow over the Pacific, but localized westerly flow over Mammoth Mountain. None of the minor seasons had large counts for days associated with type M or Q. Type M is characterized by a strong ridge over the eastern Pacific, with enhanced northwesterly flow over Mammoth Mountain, while type Q has a slight ridge further to the west over the Aleutians. Both patterns tend to be associated with cold temperatures at Mammoth Mountain.

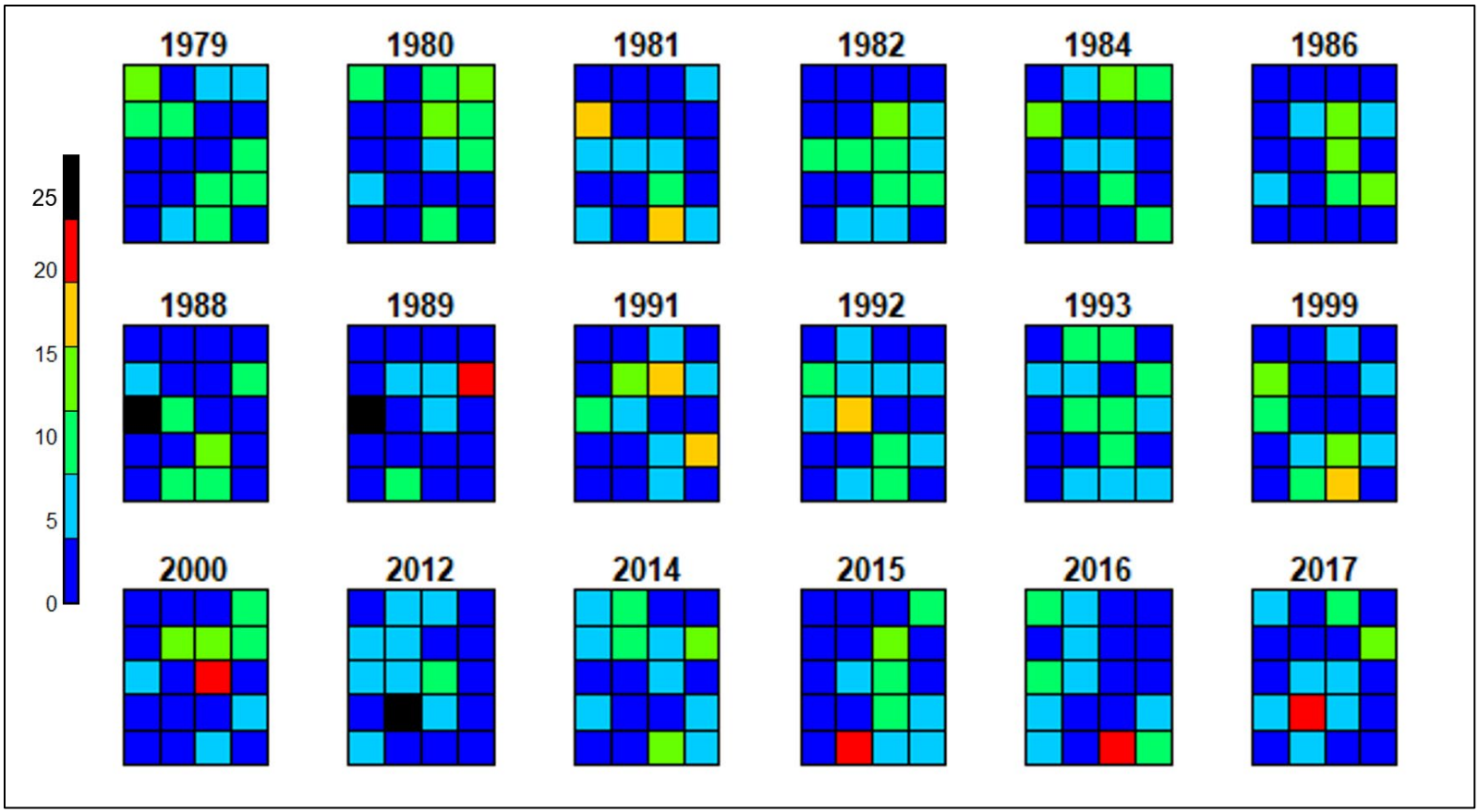

Figure 20: Heat maps displaying counts for the number of days assigned to each synoptic type from Nov.- Jan. during minor deep slab seasons at Mammoth Mountain. For each season in the figure, a colored square on the array corresponds to the map pattern at the same location in the arrays in Figures 5 and 6.

There is an increase in frequencies for types G, O, and P during major deep persistent slab seasons at Mammoth (Figure 21). Type G is characterized by enhanced ridging over the West Coast, while types O and P are zonal patterns with localized southwest flow. Minor deep slab seasons have a large number of days assigned to types H, I, and S, which are associated with direct zonal flow and a slight ridge over the California Coast.

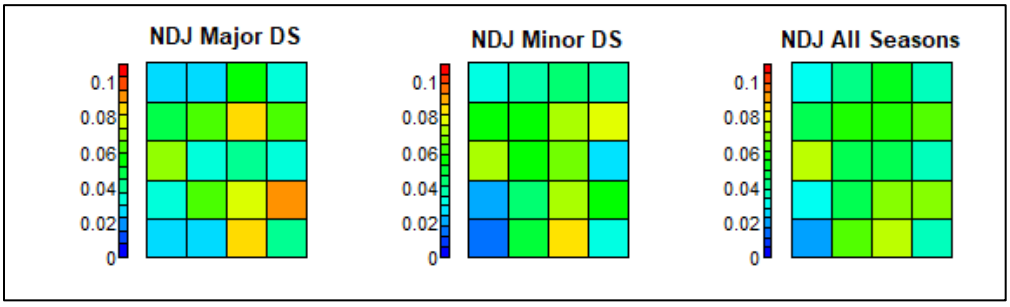

Figure 21: Relative frequencies for each synoptic type during all major deep persistent slab seasons (left) and all minor seasons (center) at Mammoth Mountain, and all seasons during the study period (right). Frequencies are calculated by summing counts for each synoptic type over all major (minor) seasons and dividing by total number of days for all major (minor) seasons.

Barplots of the difference in relative frequencies for each synoptic type during major and minor years show a slight decrease in early season frequencies for patterns H-K during major seasons, while the same patterns appear more frequently during minor years (Figure 22). The same holds true for type R. Types C, M, N, P and Q have the opposite tendencies, with more days assigned to these types in the beginning of major seasons and fewer days assigned early in the minor seasons.

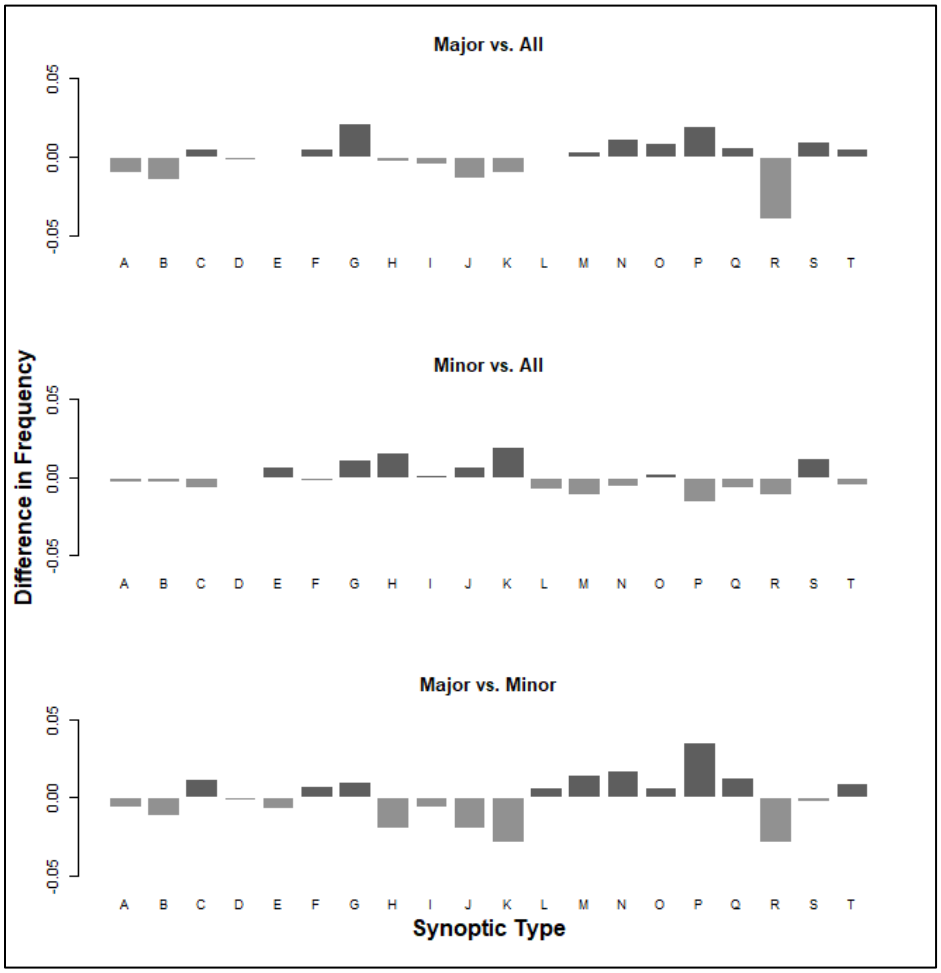

Figure 22: Barplots for the difference in relative frequency for each synoptic type during November-January between major seasons and all seasons (top), minor seasons and all seasons (center), and major seasons and minor seasons (bottom) at Mammoth Mountain. Positive values indicate an increase in relative frequency during the first category in the title of each chart. For example, a positive value for type G in the top chart indicates a higher relative frequency for that synoptic type during major deep slab seasons relative to all seasons.

Atmospheric Condition Prior to Deep Slab Activity

Total number of avalanches during the study period ranges from approximately 20,000 to just over 40,000 at each site, while the number of deep slab events is roughly 2-3 orders of magnitude smaller (Table 7). While the deep slab events are primarily dry

slab avalanches, there are a small number of deep persistent events classified as wet slabs at Bridger Bowl and Jackson. Each of the three study sites displays a unique distribution of the number of days assigned to each synoptic type in the 72 hours prior to deep slab activity for dry and wet slabs (Figures 23 and 24). At each site there is a small group of synoptic types that occur much more frequently than the rest in the three days leading to deep slab activity. The relative frequencies for each type during the 72 hours preceding deep persistent slab activity differ from the overall relative frequency distribution during the study period, which indicates a unique circulation preference for deep persistent slab avalanches at each study site.

Table 7: Summary of number of total avalanches, all deep slab events, dry deep slab events, and wet deep slab events. The number of days each type of avalanche was recorded is given in parentheses.

Site	All Avalanches	All Deep Slab	Dry Deep Slab	Wet Deep Slab
Bridger Bowl	31455 (2161)	314 (176)	287 (169)	27 (7)
Jackson Hole	20180 (2343)	293 (173)	284 (168)	9 (5)
Mammoth Mountain	41751 (1177)	92 (60)	92 (60)	0 (0)

Dry Slab Events Types I, P, and T are associated with the greatest number of days at Bridger Bowl in the 72 hours prior to dry deep slab events (Figure 23). All three types are zonal patterns with varying degrees of troughing over the Aleutian Islands and slightly different north-south orientations. Type T is almost directly out of the west, with a slight

northwest orientation above the northwest U.S. Type P has more of a southwest flow direction, with a slight ridge over Montana. In pattern I, this gentle ridge shifts towards the North American west coast and a trough develops over northeast Canada, which results in a distinct northwest flow pattern over Montana. Type F was recorded less than ten times in the days leading to dry deep slab events, while type R was never observed. Type F is characterized by a strong ridge over the east Pacific and trough over Hudson Bay, which results in strong north-south flow over the western U.S., while type R shows strong zonal flow from eastern Siberia all the way across to the Atlantic, with a direct westerly trajectory.

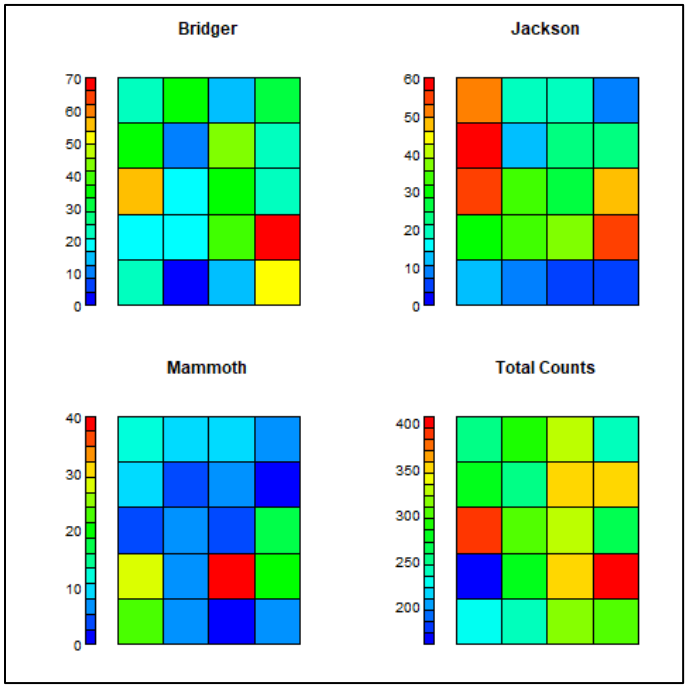

Figure 23: Heat maps displaying the number of days assigned to each synoptic type within 72 hours prior to a day with dry deep slab avalanches recorded at Bridger Bowl (upper left), Jackson Hole (upper right), Mammoth Mountain (lower left), and total counts for the duration of the study period.

Types A, E, I, L and P dominate the period immediately prior to dry deep slab activity at Jackson Hole. Patterns A, E, and I are characterized by zonal flow over the western U.S. coming slightly out of the north, and moderate to strong troughing over Hudson Bay. In patterns A and L there is a split flow, with an omega block over the Aleutians and western Alaska and more zonal flow over the continental U.S. However, the two patterns differ in that pattern L also shows a weak upper-level ridge over the Rockies, whereas type A does not. This leads to a more southwesterly flow in type L, whereas the trajectory for type A is more directly out of the west, and even slightly northwest over Jackson. Pattern P shows more enhanced troughing over the Aleutians and the east Pacific, which results in a zonal pattern over the western U.S. with enhanced southwesterly flow. There are very few days associated with types R, S, and T during the period leading to dry deep slab avalanches at Jackson Hole. These patterns are all primarily zonal. Patterns R and T have a north to south trajectory over the western U.S., while pattern S has a slight trough over the east Pacific, which leads to increased southwesterly flow.

The 72-hour period prior to dry deep slab events at Mammoth is dominated by types M and O, which are two very different patterns. Type M has the strongest ridge over the Pacific up towards the Gulf of Alaska, while type O shows a trough over the Gulf of Alaska that transitions into a direct zonal pattern moving southward into the Pacific. Type Q was the third most frequent pattern observed in the three days prior to dry deep slab events. This pattern closely resembles type O in the southwest quarter of the study area, especially over the central and west Pacific and the California coast. The

lack of synoptic types with more intermediate counts at Mammoth Mtn. may be attributed to the smaller number of dry deep slab events compared to the other sites over the duration of the study period.

Wet Slab Events. Of the 314 deep persistent slab events recorded at Bridger Bowl, 27 were classified as wet slab avalanches. These occurred on five different days in the record. Nine of the 293 deep slab avalanches were wet slabs at Jackson on six different days, while there were no deep slab events classified as wet slab avalanches at Mammoth Mountain (Table 7). The heatmaps for the synoptic types leading to the days with wet slabs at Bridger Bowl shows a large number of days associated with type P, which was also a frequently observed type during dry deep slab events (Figures 23 and 24). The second most common pattern was type O, which was not as pronounced in the dry deep slab record. Types L, O, and P were assigned the highest number of days prior to deep wet slab avalanches at Jackson. For both Bridger Bowl and Jackson, the synoptic types assigned the most days prior to deep wet slab activity are characterized by a distinct trough over the Gulf of Alaska, which is coupled with enhanced southwesterly zonal flow over the continental U.S.

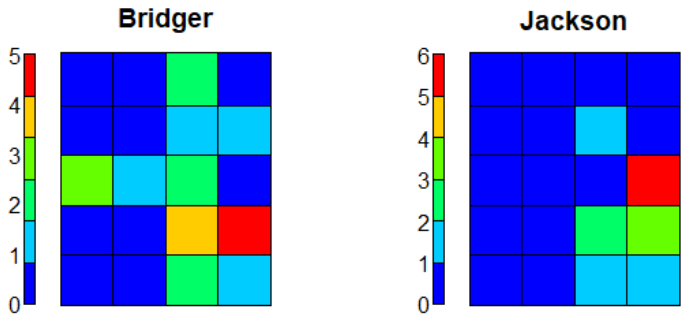

Figure 24: Heat maps for the number of times each synoptic type was recorded within the 72 hours prior to deep wet slab avalanches at Bridger Bowl (left) and the Jackson area (right).

Discussion

Each site exhibits different synoptic types that favor precipitation based on the trajectory of storm tracks. Bridger Bowl tends to have frequent and large storms during the synoptic configurations with a slight ridge over the East Pacific and a storm track moving out of the northwest over Montana. This supports the findings of Birkeland and Mock (1996), which studied atmospheric circulation at the 500-mb level for 44 large precipitation events at Bridger Bowl between 1968 and 1993. They concluded that increased precipitation during these northwest zonal flow patterns is a result of regional and local topography, as there are fewer orographic barriers to the northwest of the Bridger Range. The canyons on the west side of the range are also oriented such that they channel moisture moving in from the Northwest, which maximizes efficiency in orographic uplift, resulting in more frequent and larger storms. Contrary to the other two sites, precipitation at Bridger Bowl is less frequent during storms that come in directly from the west or from the south, even with enhanced zonal flow. Birkeland and Mock

(1996) also attributed this to regional topography, as there are multiple large orographic barriers immediately west and southwest of Bridger Bowl that inhibit moisture transport. This is not the case at Jackson Hole, which is situated at the head of the Snake River plain and benefits from the storms out of the west-southwest that are able to efficiently transport moisture inland with relatively few topographic barriers. Birkeland et al. (2001) found heavy precipitation and increased avalanche activity commonly occur at Jackson Hole during atmospheric circulation events characterized by direct westerly zonal flow, due largely to this lack of major orographic barriers to the west and southwest. Mammoth also receives increased precipitation with airflow out of the southwest, which is likely due in part to the perpendicular orientation of the Sierra Nevada range to such storms.

Each location experiences the coldest temperatures with a strong ridge over the Pacific and a trough over the west, resulting in migration of cold polar airmasses southward. This is indeed the case with types E and M, which are among the coldest patterns at all three sites. However, due to the geographic separation of the three study locations there are some cases where sites experience very different temperatures under the same circulation patterns. This is manifested with type F, in which Mammoth Mountain lies below an upper level ridge and subsequently experiences warm temperatures, whereas Jackson Hole and Bridger are farther to the west and downstream of the ridge. This leads to a more northerly flow over the latter two sites, and subsequent cooler temperatures. This pattern also tends to result in increased precipitation over Bridger Bowl due to local topography, while Mammoth will more commonly remain dry.

The major deep slab seasons at Bridger Bowl and Jackson Hole observed a large number of days assigned to synoptic types that are associated with low frequency of precipitation events in the beginning of the season. Some of these dry patterns are controlled by a blocking ridge over the continental U.S. (e.g. types C, D, and G), which are assigned to a large number of days during major deep slab seasons at both locations and are much less common during minor seasons. Major deep slab seasons at both sites tend to shift towards a positive PNA pattern, with a high concentration of synoptic types in the upper right corner of the SOM array. This has previously been identified to be associated with reduced snowfall totals in the western U.S (Wise, 2012), which is supported by weather records at Bridger and Jackson (Figures 7 and 8). Low snowfall totals in the beginning of the season have been previously shown to lead to development of persistent weak layers by means of increasing the bulk temperature gradient in intermountain and continental snowpacks (Mock and Birkeland, 2000). There is also a notable increase in synoptic types more commonly associated with mild temperatures during the beginning of minor seasons. Warmer early season temperatures would effectively reduce temperature gradients within the snowpack, thereby preventing the development of depth hoar or near-surface faceted layers.

The major deep slab seasons at Mammoth are slightly different. Due to its proximity to the Pacific and the lower latitude at which it is located, Mammoth Mountain experiences higher precipitation totals and warmer temperatures on average than the other two sites. A deeper snowpack, coupled with the mild and consistent coastal temperatures, impedes formation of faceted persistent weak layers and thus changes the

character of deep slab avalanches in coastal snow climates during most years. Under the right conditions, depth hoar and smaller faceted grains may still form in coastal snow climates, but these layers are much less common in a coastal snowpack than they are in continental or intermountain climates. Most large avalanches in coastal areas fail within the storm snow or at the interface between old and new snow. In these cases, the early season snowpack has very little to do with the likelihood of triggering a large avalanche (Mock and Birkeland, 2000). However, this research has effectively omitted this large portion of events by focusing only on the avalanches where the crown depth exceeded three times the three-day storm totals.

There are a large number of days assigned to synoptic types characterized by cold temperatures (e.g. types E and M) or infrequent precipitation (type G) during November-January of major deep persistent slab seasons at Mammoth Mountain. This characteristic is consistent with Bridger Bowl and Jackson Hole. However, unlike the other two study sites, there are also a substantial number of days in November-January of major seasons assigned to synoptic types that are associated with frequent or heavy precipitation (e.g. patterns M, P, and Q). Additionally, there are a large number of days assigned to the drier synoptic types (H, K, and R) during the beginning of minor seasons. Given the processes driving dry snow metamorphism, one would expect the exact opposite- less frequent precipitation leading to enhanced faceting and depth hoar during major seasons, and increased precipitation with less faceting during minor seasons. However, the majority of the deep persistent slabs at mammoth mountain are recorded in December and January. Thus, it would be necessary to have enough precipitation events early in the season to

build a slab thick enough to be classified as a deep slab according to our criteria. Additionally, some of the precipitation events provide the necessary load to push a deep persistent weak layer to its breaking point. Indeed, type M is associated with regular precipitation at Mammoth Mountain and it shows up frequently during the beginning of major seasons as well as in the 72 hours preceding deep persistent slab events. Alternatively, it is often the case during minor seasons that there is simply never enough snow to develop a snowpack conducive to deep persistent slab avalanches. This was the case during the 1988 and 1989 seasons, which were dominated by northwest zonal flow (type I) and the 1991 and 1993 seasons, which had a persistent blocking ridge over the west coast (types G, C, and H). There also exists a subset of minor seasons with little to no precipitation during the beginning of the season, but subsequent heavy precipitation for the rest of the season (1992 and 1999). In the coastal climate of Mammoth Mountain, even if there was a persistent weak layer, it may have simply been buried so deep that no load applied at the surface would be able to initiate a fracture in the weak layer. For the major seasons of 1987, 1996, 1997, and 2001, there was an initial dry period followed by intermediate snowfall. This provided a period during which a persistent weak layer could develop, and enough snow to subsequently bury the persistent weak layer deep enough to form a deep persistent slab, but shallow enough that it remained prone to large applied loads. For these four seasons, all of the deep slab events occurred from November-January.

Conlan et al. (2014) performed a field study of 41 deep persistent slabs in western Canada and found the layers immediately above the failure layer were either 0.5-1mm

rounded grains, 0.5-1mm facets, or a melt-freeze crust. Grain types for layer immediately below the failure layer were similar: 0.5-1 mm rounded grains, 0.5- 2 mm facets, melt-freeze crusts, ice or ground. While this work did not focus specifically on coastal climates, it did include three coastal sites. Hammonds et al. (2015) measured localized temperature gradients immediately above and below an ice lens that were up to an order of magnitude larger than the bulk temperature gradient imposed on a snow sample in a laboratory setting. This supports field observations that weak layers commonly form adjacent to ice crusts within the snowpack. Furthermore, a buried ice crust has very low friction, which would provide an efficient bed surface in an avalanche. There are a large number of days assigned to types O and P in November-January of major seasons at Mammoth. These types both have frequent precipitation events at Mammoth. Type S is one of the patterns with the highest counts in November – January during major deep persistent seasons at Mammoth include and is not commonly associated with precipitation. Days associated with type S and type G, which also represented a large number of days during the beginning of major deep slab seasons, tend to have above-freezing daily maximum temperatures with subfreezing minimum temps. An early season with alternating low precipitation and alternating warm and cold temperatures would facilitate near-surface faceting and ice lens formation, which would act as a low-friction bed surface conducive to avalanches later in the season. This may explain another process in which November-January circulation can favor precipitation even during major deep persistent slab avalanche seasons.

At all three sites, there is increased frequency of counts in the 72 hours prior to dry deep slab events for synoptic types that are commonly associated with higher levels of precipitation. Again, these patterns differ by site depending on latitude, proximity to the coast, and local and regional topography. At Bridger Bowl, the types occurring most commonly during this time period have either enhanced zonal flow (types P and T) or localized northwesterly storm track (type I). The relatively high counts for types I and P mimic the frequency pattern for the entire study period. This suggests that these two types show up frequently in this 72-hour window due to their high frequency of occurrence overall, rather than an association with deep persistent avalanches. This is not the case with type T, which has a very high frequency of occurrence preceding deep persistent slab avalanches despite exhibiting relatively low counts for the duration of the study period. The types with a northwesterly storm track dominate the period prior to deep slabs at Jackson as well; however, there are also very high counts for type L, which is characterized by a strong southwesterly storm track that would channel warm, moist air directly over the Snake River Plain. There is a distinct spike in patterns A, E, and L during the 72 hours preceding deep slab activity at Jackson, which stands out when compared to the relatively low counts for all three patterns during the overall duration of the study period. This suggests that these three patterns may indeed be good indicators for increasing likelihood of deep persistent slab avalanches at Jackson Hole. The patterns with the highest count for this 72-hour period at Mammoth (types M and O) exhibit localized west-southwesterly flow. However, the two patterns differ greatly over the full extent of the study area, with a strong ridge over the Pacific in type M, and a mild trough

in the same area for type O. Both patterns have frequently recorded high levels for 24-hour precipitation, albeit somewhat less frequently with type M than type O. This may be one reason why type M shows up more frequently than type O in the days leading to deep slab avalanches. Similarly to Bridger and Jackson, the heat map for the 72-hour period preceding deep persistent slab avalanches at Mammoth looks very different than the overall frequency distribution. There is a notable lack of days associated with patterns G and H at both sites during the 72 hours prior to dry deep persistent slab avalanches, which are both characterized by a strong blocking ridge that extends over all three study sites. This usually results in little or no precipitation for all three sites. The apparent difference in the distribution of days assigned to all synoptic types at each of the three sites indicates a unique atmospheric configuration during the period immediately prior to onset of deep persistent slab avalanches at Mammoth Mountain.

Bridger Bowl records a large number of days associated with the warmer synoptic types with a strong southwest flow and a mild ridge over the western U.S. in the days leading to deep slab events. Combined with the large number assigned to wetter synoptic types, this suggests two mechanisms leading to deep slab events. One is that a deeply buried weak layer is pushed to its breaking point by adding a large enough load in the form of new snow. The other is that the weak layer fails due to liquid water that is introduced in the snowpack through rapid warming. The latter case would provide an explanation for the large number of days assigned to relatively warm synoptic types not commonly associated with precipitation. By isolating the wet slab events from the record, we identify a large number of days assigned to types O and P at Bridger Bowl and

Jackson Hole in the 72 hours leading to the event. These patterns are characterized by zonal flow with a slight southwesterly component, which results in warm temperatures and frequent precipitation at both sites, although the precipitation totals at Bridger Bowl are usually somewhat modest during these circulation patterns. Jackson Hole also shows a high frequency of type L, which has a stronger southwest component, usually resulting in even warmer temperatures than types O and P.

There is a notable lack of circulation patterns with a ridge over the Gulf of Alaska during the time leading up to the wet slab events at both sites. This is particularly interesting because types A and E showed up among the types with the highest counts for dry deep slab events at Jackson. The ridge over the Gulf of Alaska is coupled with a northwesterly flow over the continental U.S., and often results in cold temperatures at both Jackson and Bridger Bowl, which would be unlikely to result in liquid water in the snowpack.

Marienthal et al. (2012) investigated a historic wet deep slab avalanche cycle at Bridger Bowl that occurred in late March of 2012 and found that the key factors leading to onset of avalanche activity included poor snow structure with depth hoar near the ground, a rapid warming event beginning on March 24th, and a large loading event on the evening of March 26th, during which 20 cm of snow (38mm SWE) fell on a recently warmed snowpack, which insulated the snowpack and prevented liquid in the snowpack from refreezing. This created an unstable condition in which there was a supply of liquid water in the snowpack and a large load applied at the surface. Looking back on the beginning of the season, we find that the upper-level circulation was dominated by

synoptic types I and R (Figure 25). Both synoptic types are characterized by west-northwesterly airflow trajectory and are associated with modest snowfall and near-average temperatures. The combination of low snowfall and average temperatures in November and December facilitated facet growth at the bottom of the snowpack, which eventually developed into depth hoar. This remained an active weak layer in the snowpack until February, when it was buried deep enough that applied surface loads (e.g. explosives and humans) were unable to initiate collapse.

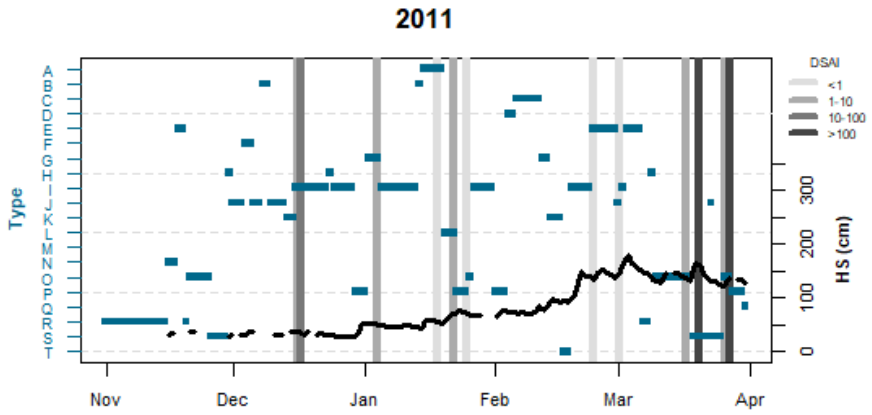

Figure 25: Seasonal plot of daily synoptic type classification (blue rectangles), accumulated snow depth (black line), and daily DSAI score (vertical bars) for the 2011-2012 winter season at Bridger Bowl. The vertical bars representing DSAI score are color-coded such that darker bars indicate a higher daily score. A similar plot for each season at each location may be found in Appendix D.

The warming event on March 24th coincided with consecutive days of synoptic type S, which indeed is often associated with warmer temperatures. The precipitation event during the evening prior to the wet slab cycle was facilitated in part by synoptic type O, which has the perfect combination of slightly warmer temperatures and frequent precipitation that resulted in liquid water movement in the snowpack. On the morning of

the 27th, this combination of warming and precipitation was enough to push the snowpack to its breaking point, and Bridger Bowl Ski Patrol was able to trigger multiple massive wet slab avalanches with explosives during their morning control routes. This case study provides an example of how our work may be used in conjunction with previous research to summarize the atmospheric processes related to deep persistent slab avalanches, and identify potentially dangerous conditions that lead to them.

February 1986 was marked by an avalanche cycle that extended throughout much of the western United States, with major events in Washington, Oregon, California, Utah, Montana, Wyoming, and Colorado. Birkeland and Mock (2001) previously investigated this event and found that it was primarily a result of a large precipitation event in mid-February, rather than from an anomalously weak snowpack. Out of the 20 sites that were investigated in the study, Bridger Bowl was one of four sites that did not experience a major avalanche cycle during this time period. Their research identified an upper-level trough over the Pacific Northwest in the days leading to the event, which resulted in primarily zonal/southwesterly flow across most of the western United States, and a southward shift in the storm track. While this pattern is likely to result in heavy precipitation at many sites in the western U.S., it does not favor precipitation at Bridger Bowl. Birkeland and Mock (1996) previously identified this trend, and our findings further support it (Figures 7-9, Tables 3-5). This was indeed the outcome in February of 1986, with precipitation totals reaching 380% and 307% of average at Mammoth Mountain and Jackson Hole, respectively, but a more modest 178% of average at Bridger Bowl (Birkeland and Mock, 2001).

At both Jackson Hole and Mammoth Mountain, onset of avalanche activity began on February 13, and large direct-action avalanches failing at or near the old snow surface continued to occur through February 18. Both days recorded large deep persistent slab avalanches immediately following the storm, on February 24 and 25 at Jackson Hole, and February 21 at Mammoth Mountain (Figure 26).

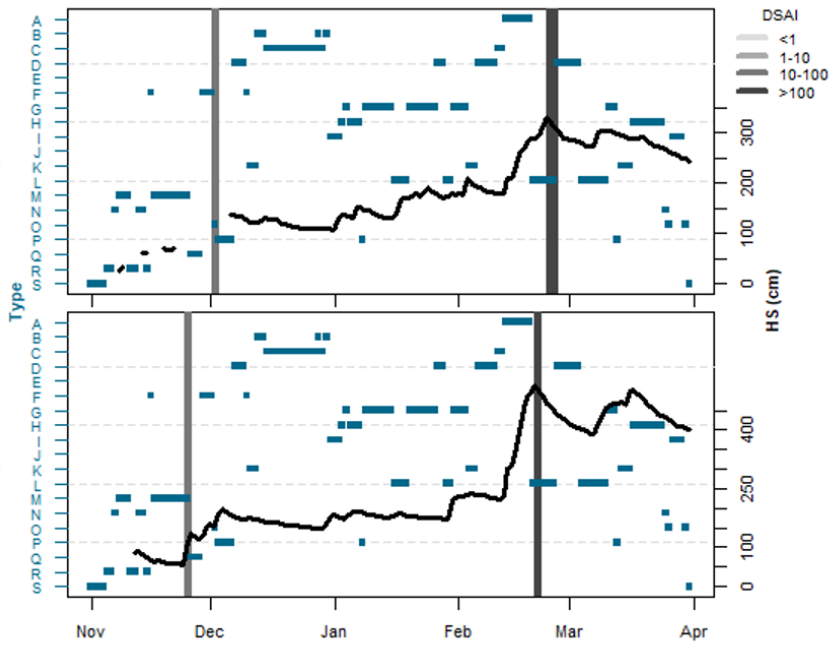

Figure 26: Seasonal plot of daily synoptic type classification (blue rectangles), accumulated snow depth (black line), and daily DSAI score (vertical bars) for the 1985-1986 season at Jackson Hole (top) and Mammoth Mountain (bottom). The vertical bars representing DSAI score are color-coded such that darker bars indicate a higher daily score. A similar plot for each season at each location may be found in Appendix D.

During the February 13-18 storm event, Jackson Hole received 211 mm SWE and Mammoth Mountain received 538 mm. Bridger Bowl only received 33 mm during that same 6-day period. Every day from February 13-18 was assigned to type A, which is characterized by a southern shift in the storm track with primarily zonal flow and an

omega block over western Alaska. Mock and Birkeland (2001) included a 500 mb composite map for February 13-21, 1986 that closely resembles type A as well as type L, which was assigned to the last three days of that time period (Figure 27). Both Jackson Hole and Mammoth Mountain record frequent and heavy precipitation during days which are designated type A (Figs. 8 and 9), while precipitation events are less frequent and relatively smaller in magnitude at Bridger Bowl (Figure 7). This geographic distribution of precipitation was manifested during February of 1986, and it eventually led to major avalanche cycles at Jackson Hole and Mammoth Mountain, while Bridger Bowl remained relatively stable.

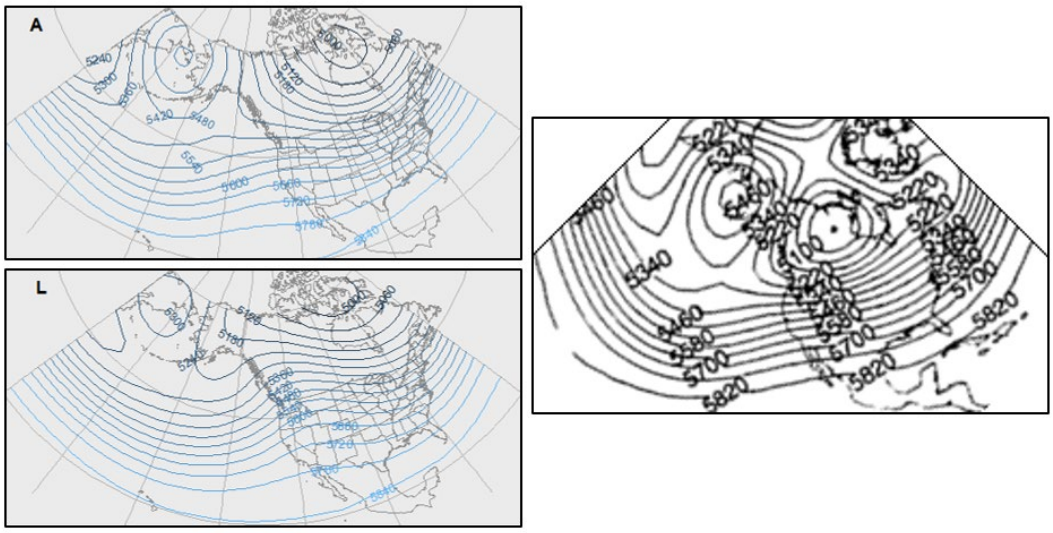

Figure 27: Six out of nine of the days from February 13-21, 1986 were assigned to synoptic type A (upper left). The remaining three days were assigned to type L (lower left). Both types closely resemble the composite map for that period (right), taken from Birkeland and Mock (2001) .

This work builds off of the findings of previous synoptic climatology studies that have investigated the link between the atmosphere and avalanche cycles. Hatchett et al. (2017) found that avalanche fatality rates increase during atmospheric river events

throughout the western U.S. They used 500 mb geopotential height maps to identify circulation patterns that facilitate inland vapor transport, which results in precipitation rates that exceed the threshold at which a snowpack becomes unstable. Birkeland et al. (2001) investigated the atmospheric conditions during the days with the most avalanche activity at four locations across the western U.S. They found increased avalanche activity to be closely tied to upper-level troughing, which facilitates moisture transport and heavy precipitation. Fitzharris (1987) performed a similar analysis in western Canada, focusing on major avalanche seasons, rather than major days. He found that major seasons had at least one month in the beginning of the winter with sustained anticyclonic blocking patterns and resulting cold, dry periods conducive to weak layer formation. In addition, he found each major season to exhibit a rapid change from blocking to zonal patterns, which resulted in heavy precipitation with immediate avalanching thereafter. He also noted different frequencies of certain synoptic types during major and minor seasons. We extended these and other studies (e.g. Martin and Germain, 2017; Schuenemann et al., 2009; Wise 2012) to find the synoptic drivers of deep persistent slab avalanches in the western U.S, and our results are consistent with prior work. At each location, there are certain synoptic types that are often warmer while others are colder, and certain types that more commonly record substantial precipitation while others do not. The frequency of occurrence of each of these types on a seasonal scale will in turn control snow stability. We have utilized these relatively simple concepts to identify the sequences that often lead to deep persistent slab avalanches.

This work also highlights the utility of SOM in the field of snow and avalanches. SOM have emerged as a key tool in the field of synoptic climatology (Sheridan and Lee, 2011; Hewitson and Crane, 2002; Reusch et al., 2005; Wise and Dannenberg, 2015), but their utility in understanding avalanches is just beginning to be explored. Shandro and Haegeli (2018) used SOM to characterize avalanche types in western Canada for over 14,000 avalanche advisories in order to better understand typical avalanche problems, which has provided forecasters with another tool to anticipate avalanche hazard for a given day. With this work we provide another example of the use of SOM in describing avalanche activity, and another tool to try to anticipate a difficult to predict event.

Limitations

The utility of this work is limited by the available data and by the nature of synoptic climatology. There is a large amount of subjectivity in the observations recorded in ski patrol avalanche records, which are maintained as an effective means to communicate between practitioners and incorporated in a multi-faceted approach towards stability assessment. This is particularly relevant in the size classification of the avalanche as well as the bed surface. Furthermore, the crown depth observations are simply ad-hoc estimations of crown depth, rather than precise measurements. We acknowledge the uncertainty in these measurements, and subsequently use the observations only in general terms to identify deep slab events. Furthermore, the index which we have implemented to describe individual events assigns a numeric index based on R-size, which is a reliable measurement in the data record. This index ranges on a

scale that is two orders of magnitude larger than the crown depth measurement, which reduces the error in the analysis associated with measurement uncertainty.

By its nature, synoptic climatological studies identify broad patterns over a continental scale. While this framework is quite useful in identifying large-scale patterns, it is somewhat limited in its ability to capture variability in smaller scale processes. This is highly relevant when considering mountain weather, which is equally dependent on processes operating on scales as small as 10s of meters. It is equally important to consider the limitations related to a mountain snowpack, which exhibits variability on a multitude of scales ranging from thousands of kilometers down to sub-millimeter.

Conclusions

This research builds on previous work to highlight connections between the upper atmosphere, meteorology, and snow metamorphism to improve our understanding of the processes controlling deep slab instabilities. We used state of the art methodology to classify 5,899 daily 500 mb geopotential height maps and generate a continuum of 20 general map patterns that captures major modes of variability over the Pacific, North America, and the West Atlantic. The classification scheme captures different phases of the Pacific-North American teleconnection, which is a major driver of regional scale precipitation patterns in the western U.S. In doing so, it also summarizes variability of semi-permanent pressure centers over the Aleutian Islands, USA, and Hudson Bay, Canada. The array illustrates a spectrum of synoptic types that transition from zonal to

blocking patterns, and it also captures the east-west variability of a blocking ridge that may occur over the Pacific or over continental North America.

The implications of these different synoptic types are summarized by plotting frequency distributions for daily maximum and minimum temperature as well as daily SWE totals. Different circulation patterns lead to very different meteorological outcomes, which have been described in terms of teleconnections, storm track direction, and meridional or zonal flow. This research supports previous work describing hydroclimatology and temperature variability in the western U.S., and builds on it by applying these concepts to deep slab avalanches.

We examined avalanche records at three different locations in the western U.S., and identified atmospheric patterns that tend to occur at higher rates during years with the most deep slab avalanche activity. Early season patterns tended to be associated with colder temperatures and low snowfall at the two intermountain sites, while the coastal site had some types that are associated with frequent precipitation and others that do not. All three locations had large counts of synoptic types with high SWE frequencies in the 72 hours leading to deep slab avalanches. This supports findings by previous work that identifies recent loading as a leading indicator of potential for deep persistent slab avalanches. Furthermore, the frequency distribution for the 72-hour period preceding deep persistent slab avalanches at each of the three study sites is unique and distinctly different from the overall distribution during the duration of the study period. This suggests that a vulnerable snowpack at each study site reacts to a unique set of atmospheric circulation patterns. This is very promising in terms of avalanche

forecasting, as these higher-risk circulation patterns may indicate increasing likelihood of deep persistent slab avalanches.

This work should improve the ability of practitioners to anticipate deep slab avalanche cycles by highlighting the atmospheric processes driving them. There is a large amount of uncertainty associated with weather and avalanche forecasts, and forecasters improve their accuracy by incorporating more pieces of information. This research can be used to understand the processes that form a snowpack conducive to deep slab avalanches, and it may be used as another tool to anticipate when a lurking persistent weak layer will become ripe for triggering large avalanches.

Acknowledgments

We wish to thank Ella Darham, Doug Richmond, and Pete Maleski of Bridger Bowl Ski Patrol for sharing weather and avalanche data and discussing its use and limitations. Ned Bair and Mammoth Mountain Ski Patrol provided records for Mammoth Mountain, and Chris McCollister, Bob Comey, and Patrick Wright of the Bridger-Teton National Forest Avalanche Center provided records for the Jackson area, which were maintained by Jackson Hole and Grand Targhee ski patrol. Cary Mock provided influential feedback for the atmospheric classification process. Funding was provided through two separate research grants from the American Avalanche Association. Time and effort by M.D Higgs was in part supported by Institutional Development Awards (IDeA) from the National Institute of General Medical Sciences of the National Institutes of Health under Awards P20GM103474, U54GM115371, 5P20GM104417, and

2U54GM104944-06. The content is solely the responsibility of the authors and does not necessarily represent the official views of the National Institutes of Health. NCEP Reanalysis data provided by the NOAA/OAR/ESRL PSD, Boulder, Colorado, USA, from their Web site at https://www.esrl.noaa.gov/psd/.

References

American Avalanche Association, 2016. Snow, Weather, and Avalanche Guidelines: Observation guidelines for avalanche programs in the United States (3rd ed). Victor, ID.

Atwater, M., 1954. Snow Avalanches. Scientific American, 190 (1), 26-31.

Barry, R., Chorley, R., 2003. Atmosphere, Weather and Climate. Eighth ed., Routledge. pp 112-122

Birkeland, K.W., and Landry, C.C., 2002. Power-laws and snow avalanches. Geophysical Research Letters, 29 (11).

.

Birkeland, K., Mock, C., and Shinker, J., 2001. Avalanche extremes and atmospheric circulation patterns. *Annals of Glaciology, 32,* 135-140.

Birkeland, K., and Mock, C., 2001. The major snow avalanche cycle of February 1986 in the Western United States. Natural Hazards, 24, 75-95.

Birkeland, K.W., and Mock, C., 1996. Atmospheric circulation patterns associated with heavy snowfall events, Bridger Bowl, Montana, U.S.A. Mountain Research and Developments, 16 (3) 281-286.

Conlan, M., Tracz, D., Jamieson, B., 2014. Measurements and weather observations at persistent deep slab avalanches. *Cold Regions Science and Technology*, 97, 104-112.

Dettinger, M., Caya, D., Diaz, H., Meko, D., 1998. North-South precipitation patterns in Western North America on interannual-to-decadal timescales. Journal of Climate, 11 (12), 3095-3111.

Davis, R.E., Elder, K., Howlett, D., Bouzaglou, E., 1999. Relating storm and weather factors to dry slab avalanche activity at Alta, Utah and Mammoth Mountain, California, using classification and regression trees. Cold Regions Science and Technology, 30, 79-89.

Esteban, P., Jones, P., Martín-Vide, J., Mases, M., 2005. Atmospheric circulation patterns related to heavy snowfall days in Andorra, Pyrenees. *International Journal of Climatology, 25,* 319-329.

Fitzharris, B.B., 1987. A climatology of major avalanche winters in Western Canada. *Atmosphere-Ocean,* 25 (2), 115-136.

Fitzharris, B.B., Bakkehøi, S., 1986. A synoptic climatology of major avalanche winters in Norway. *Journal of Climatology, 6,* 431-446.

Grundstein, A., 2003. A synoptic-scale climate analysis of anomalous snow water equivalent over the norther Great Plains of the USA. *International Journal of Climatology, 23,* 871-886.

Hammonds, K., Lieb-Lappen, R., Baker, I., Wang, X., 2015. Investigating the thermophysical properties of the ice-snow interface under a controlled temperature gradient Part I: Experiments and observations. Cold Regions Science and Technology, 120, 157-167

Hartley, S., Keables, M., 1998. Synoptic associations of winter climate and snowfall variability in New England, USA, 1950-1992. *International Journal of Climatology, 18,* 281-298.

Hatchett, B., Burak, S., Rutz, J., Oakley, N., Bair, E., Kaplan, M., 2017. Avalanche fatalities during atmospheric river events in the western United States. Journal of Hydrometeorology, 18, 1359-1374.

Hewitson, B.C., and Crane, R.G., 2002. Self-organizing maps: applications to synoptic climatology. *Climate Research, 22 (1)*, 13-26.

Jiang, N., Hay, J.E., Fisher, G.W., 2004. Classification of New Zealand synoptic weather types and relation to the Southern Oscillation Index. *Weather and Climate, 23,* 3-24.

Kalnay et al., 1996. The NCEP/NCAR 40-year reanalysis project, Bull. Amer. Meteor. Soc., 77, 437-470.

Kidson, J., 2000. An analysis of New Zealand synoptic types and their use in defining weather regimes. *International Journal of Climatology, 20,* 299-316.

Kohonen, T., 1998. The Self-organizing map. *Neurocomputing, 12,* 1-6.

LaChapelle, 1980. The fundamental processes in conventional avalanche forecasting. Journal of Glaciology, 26 (94), 75-84.

LaChapelle E., 1966. Avalanche forecasting- A modern synthesis. IAHS Publication 69: 350-356.

Marienthal, A., Hendrikx, J., Birkeland, K., Irvine, K., 2015. Meteorlogical variables to aid forecasting deep slab avalanches on persistent weak layers. *Cold Regions Science and Technology*, 120, 227-236.

Marienthal, A., Hendrikx, J., Chabot, D., Maleski, P., Birkeland, K., 2012. Depth Hoar, Avalanches, and Wet Slabs: A case study of the historic March 2012 wet slab avalanche cycle at Bridger Bowl, Montana. Proceedings of the International Snow Science Workshop, Anchorage, AK, USA.

Martin, J.P., Germain, D., 2017. Large-scale teleconnection patterns and synoptic climatology of major snow-avalanche winters in the Presidential Range (New Hampshire, USA). *International Journal of Climatology, 37,* 109-123.

McGinnis, D., 2000. Synoptic controls on upper Colorado River Basin snowfall. *International Journal of Climatology, 20,* 131-149.

Mock C., and Birkeland, K., 2000. Snow Avalanche Climatology of the Western United States Mountain Ranges. *Bulletin of the American Meteorological Society, 87 (10),* 2367-2392.

Mock, C., 1996. Climatic Controls and Spatial Variations of Precipitation in the Western United States. Journal of Climate, 9, 1111-1125.

Price, M.F., Byeres, A.C., Friend, D.A., Kohler, T., Price, L.W., 2013. Mountain Geography: Physical and human dimensions, University of California Press.

Reusch, David B., Alley, Richard B., Hewitson, Bruce C., 2005. Relative performance of self-organizing maps and principal component analysis in pattern extraction from synthetic climatological data. *Polar Geography,* 29:3, 188-212. DOI: 10.1080/789610199

Schuenemann, C., Cassano, J., Finnis, J., 2009. Synoptic forcing of precipitation over Greenalnd: Climatology for 1961-99. *Journal of Hydrometeorology*, 10, 60-78.

Schweizer, J., Camponovo, C., 2001. The skier's zone of influence in triggering slab avalanches. *Annals of Glaciology, 32,* 314-320.

Schweizer, J., Jamieson, B., Skjonsberg, D., 1998. Avalanche forecasting for transportation corridor and backcountry in Glacier National Park (BC, Canada). In: Hestnes, E. (Ed.), 25 Seasons of Snow Avalanche Research, Voss, Norway, 12 – 16 May 1998. NGI Publication, Norwegian Geotechnical Institute, Oslo, Norway, pp. 238 – 243.

Shandro, B., and Haegeli, P., 2018. Characterizing the nature and variability of avalanche hazard in western Canada. Natural Hazards and Earth System Sciences, 18, 1141-1158.

Sheridan, S.C., Lee., C.C., 2011. The self-organizing map in synoptic climatological research. *Progress in Physical Geography, 35 (1),* 109-119.

Thumlert, S., Jamieson, B., 2014. Stress measurements in the snow cover below localized dynamic loads. *Cold Regions Science and Technology, 106-107,* 28-35.

U.S. census Bureau, 2016. Cartographic Boundary Shapefiles. [Dataset]. Retrieved from www.census.gov/geo/maps-data/data/cbf/cbf_state.html.

USGS National Center for EROS, 2005. Grayscale North America Shaded Relief- 1-Kilometer Resolution. [Dataset]. Retrieved from http://nationalatlas.gov/atlasftp.html.

Wallace, J.M., and Gutzler, D.S., 1981. Teleconnections in the geopotential height field during the Northern Hemisphere winter. Monthly Weather Review, 109, 784-812.

Wehrens, R., and Buydens, L.M.C., 2007. Self- and Superorganizing maps in R: the kohonen package. *Journal of Statistical software, 21 (5).*

Wise, E.K., Dannenberg, M.P., 2014. Persistence of pressure patterns over North America and the North Pacific since AD 1500. *Nature Communications, 5,* 1-6.

Wise, E.K., 2012. Hydroclimatology of the US intermountain west. Progress in Physical Geography, 36 (4), 458-479. DOI: 10.1177/030913312446538.

Wise, E.K., 2010. Spatiotemporal variability of the precipitation dipole transition zone in the western United States. Geophysical Research Letters, 37 (7), L07706.

Yarnal, B. 1993. Synoptic Climatology in Environmental Analysis: A Primer. Bellhaven Press, London, UK. 195 pp.

Yokley, L., Hendrikx, J., Birkeland, K., Williams, K., Leonard, T., 2014. Role of synoptic atmospheric conditions in the formation and distribution of surface hoar. Proceedings of the 2014 International Snow Science Workshop, Banff, Alberta, CA.

CONCLUSIONS

Summary

The utility of self-organizing maps in synoptic climatology studies has only recently been established (e.g. Sheridan and Lee, 2011; Hewitson and Crane, 2002), and new applications are still being explored. To the best of my knowledge, the only other research to date that has used self-organizing maps to investigate avalanches is presented in Shandro and Haegeli (2018). However, their work did not apply SOM to classifying atmospheric circulation; rather, the SOM was used to summarize variability in avalanche types over western Canada. Our work compiled nearly 40 years of avalanche records from three locations across the western United States and used state of the art methodology to address an avalanche problem that is difficult for avalanche practitioners to predict. We described relationships between atmospheric circulation patterns and weather metrics at three locations, and used these relationships to connect atmospheric circulation to deep persistent slab avalanches. This research can aid in avalanche forecasting through an improved understanding of the processes leading to deep persistent avalanches on seasonal and daily time scales.

Upper-level Circulation and Surface Weather

We used 20 synoptic types to characterize the atmospheric circulation over the Pacific and North America for the winter months (November-March) in the Northern Hemisphere from 1979/80 through 2017/18. The map types summarize atmospheric

variability with patterns that range from direct zonal to enhanced meridional upper-level airflow. The classification captures a transition from positive to negative phases in the Pacific-North American (PNA) teleconnection (Wallace and Gutzler, 1981), and it generalizes changes in the strength and location of semi-permanent pressure centers over the Aleutian Islands, AK, USA and Hudson Bay, Canada. We found that certain meteorological responses to these different patterns are shared between all three study sites, while others are site-specific.

At all three sites, we find the coldest temperatures occur with an upper-level ridge over the Pacific and Gulf of Alaska and a trough over the western United States. This results in the southward migration of polar air masses, which causes temperatures to drop. Alternatively, higher temperatures will be recorded when a given site is situated under an upper-level ridge. Our synoptic typing scheme identified changes in magnitude and longitudinal location of such a ridge. We find the highest temperatures at Mammoth are typically recorded when this ridge is situated over the West Coast, which can coincide with cooler temperatures at Jackson and Bridger Bowl. Higher temperatures are recorded at the latter two sites when the ridge migrates eastward over the Rockies.

Due to the geographical distance between sites, the same pattern can have different responses at different sites. We found responses to vary by both latitude and longitude, which was previously described by Wise (2012). In addition to N-S and E-W orientation, we found a strong relationship between storm track, local topography, and precipitation totals at all three sites. At Bridger Bowl, the most productive storms approached from the Northwest. This is consistent with anecdotal observations from

practitioners in the area and with previous research (e.g. Birkeland and Mock, 1996; Birkeland et al., 2001). Jackson also benefits from the northwest storm track, but it also experiences high precipitation totals for storms that approach along the Snake River Plain directly out of the west. The most consistent precipitation at Mammoth occurred when storms approached directly out of the west or southwest.

Snowpack Response to Atmospheric Circulation

We identified key relationships between circulation patterns and deep persistent slab avalanches at each of the three study sites. At each site, there is a distinct difference in the distribution of the number of days assigned to each synoptic type during November through January of major and minor deep persistent slab avalanche seasons. Furthermore, all of these distributions differ from the overall frequency distribution for November through January during the duration of the study. This implies that there are distinct patterns that lead to deep persistent problems, and different patterns that result in a stable snowpack. At Bridger Bowl, there is a shift toward increased meridional circulation during major deep persistent slab seasons, which coincides with a sharp decrease in the patterns most commonly associated with substantial precipitation. The circulation patterns favor zonal flow with a northwest-southeast trajectory during most minor deep persistent slab seasons. There is an additional group of days which display an enhanced southwesterly flow pattern that are associated with mild temperatures. The Jackson area sees a spike in the number of days assigned to synoptic types that are characterized by a blocking ridge over the region during the beginning of the winter in major deep slab

seasons. The minor seasons have a larger number of days assigned to synoptic types that feature enhanced zonal flow, or where the ridge shifts westward over the Pacific, resulting in northwest flow over the area. Circulation patterns in the beginning of major deep persistent slab seasons at Mammoth are dominated by patterns which exhibit a blocking ridge over the West Coast, or zonal patterns with a northwest-southeast trajectory. The minor seasons see a slight increase in the number of days assigned to types characterized by enhanced zonal flow. However, since the majority of seasons at Mammoth do not see a deep persistent slab problem the frequency distribution for minor seasons more closely resembles the overall distribution for all seasons in the study period.

Each study site exhibits a unique set of synoptic types occurring frequently in the 72 hours prior to deep persistent slab activity. Furthermore, the frequency at which each of these high-risk types occurs during the 72-hour period is very different from the overall frequency during the duration of the study. This implies that there are specific circulation patterns that are associated with deep persistent slab avalanches, which can be a potentially valuable indicator when timing of these events is otherwise very difficult to predict.

Future Work

This research has identified key relationships between regional-scale circulation patterns and deep persistent avalanche cycles at three locations across the United States. This constitutes an additional tool that may be used by practitioners to improve avalanche forecasts, thereby reducing fatality rates and damage to infrastructure. However, the work

presented in this thesis covers a narrow scope in the field of snow and avalanches. The following list outlines several avenues for future work that can expand the scope of this study, further our understanding of the connections between atmosphere and snowpack, and lower avalanche fatality rates for backcountry users:

1. Future work can build on this research by applying the same framework to more sites. This research has demonstrated that synoptic controls on deep slab instabilities are site-specific, and they operate differently in different snow climates. In order to extend the benefits of this study to a large group of practitioners, it would be necessary to perform a similar investigation at any site where practitioners are forecasting avalanches. While the data compilation process will be time consuming at any new location, this study has provided a framework for analysis that can be easily adapted to any site. All of the analysis for this project was implemented in the free statistical software R (R core team, 2017). The script for each step of the analysis is included in Appendix C of this manuscript, including sections describing the requisite data structure and explanations of every function written for the analysis. Thus, it should be feasible for future researchers to adapt this study to any location for which similar data are available.

2. While this work has effectively identified general relationships between large-scale circulation patterns and deep persistent instabilities, it does not provide direct explanations of the processes driving the response in the snowpack. Future research could improve on this study by downscaling these synoptic patterns and exploring directly how a local snowpack responds to changes in atmospheric circulation. Recent studies have demonstrated the ability to couple numerical weather models with SNOWPACK (Bartlelt

and Lehning, 2002) to simulate snow stratigraphy over broad geographical extent (Van Peuresem, 2016; Bellaire and Jamieson, 2013). Future work could identify statistical associations between these synoptic types and numerical weather model output, which could be used to drive snow cover models. The snow cover model output could then be compared to manual observations (as in Van Peursem, 2016) to assess the accuracy of such a model chain and further explore the synoptic drivers of snow stratigraphy. Additionally, the NCEP/NCAR reanalysis data are available at intervals down to 6 hours. Using a higher resolution historical time series of synoptic types from a previous season, it should be possible to recreate a seasonal snowpack structure and compare it to manual snowpit profiles. This would further solidify the connection between the atmosphere and the mountain snowpack, and could be beneficial to operational avalanche forecasting.

3. The utility of self-organizing maps is just beginning to be explored in the field of snow and avalanches. Future work can build on this by characterizing snowpack stratigraphy and local weather measurements related to snow stability. Such work will improve our conceptual model of the relationships between weather and avalanches and may be a powerful tool in terms of improving our ability to describe the snowpack and forecast avalanches.

Self-organizing maps can be used to describe any multi-dimensional dataset. This can apply to the field of snow and avalanches beyond weather and snowpack observations. There is a growing body of work exploring decision making in backcountry terrain, and there is potential to incorporate SOM in such studies. One such application could be in characterizing demographics of backcountry users, and examining a response

(such as fatality rates) for each user type. Such a study could have the potential to identify strengths and weaknesses in the current avalanche education framework, thereby reducing fatality rates of backcountry users.

References

Bartelt, P., and Lehning, M., 2002. A physical SNOWPACK model for the Swiss avalanche warning: Part I: numerical model. Cold Regions Science and Technology, 35 (3), 123-145.

Bellaire, S., Jamieson, B., 2013. Forecasting the formation of critical snow layers using a coupled snowcover and weather model. Cold Regions Science and Technology, 94, 37-44.

Birkeland, K., Mock, C., and Shinker, J., 2001. Avalanche extremes and atmospheric circulation patterns. Annals of Glaciology, 32, 135-140.

Birkeland, K.W., and Mock, C., 1996. Atmospheric circulation patterns associated with heavy snowfall events, Bridger Bowl, Montana, U.S.A. Mountain Research and Developments, 16 (3) 281-286.

Hewitson, B.C., and Crane, R.G., 2002. Self-organizing maps: applications to synoptic climatology. Climate Research, 22 (1), 13-26.

R Core Team, 2017. R: A language and environment for statistical computing. R Foundation for Statistical Computing, Vienna, Austria. URL https://www.R-project.org/.

Shandro, B., and Haegeli, P., 2018. Characterizing the nature and variability of avalanche hazard in western Canada. Natural Hazards and Earth System Sciences, 18, 1141-1158.

Sheridan, S.C., Lee., C.C., 2011. The self-organizing map in synoptic climatological research. Progress in Physical Geography, 35 (1), 109-119.

Van Peursem, K., Hendrikx, J., Birkeland, K.W., Miller, D., Gibson, C., 2016. Validation of a coupled weather and snowpack model across western Montana. Proceedings of the 2016 International Snow Science Workshop, Breckenridge, CO.

Wise, E.K., 2012. Hydroclimatology of the US intermountain west. Progress in Physical Geography, 36 (4), 458-479. DOI: 10.1177/030913312446538.

REFERENCES CITED

Aguado, E. and Burt, J., 2015. Understanding Weather and Climate. Seventh ed., Pearson Education, Inc.

American Avalanche Association, 2016. Snow, Weather, and Avalanche Guidelines: Observation guidelines for avalanche programs in the United States (3rd ed). Victor, ID.

Armstrong, R.L., and Brun, E., 2008. Snow and Climate: Physical processes, surface energy exchange and modeling. Cambridge University Press. 256 pp.

Atwater, M., 1954. Snow Avalanches. Scientific American, 190 (1), 26-31.

Avanzi, F., Hirashima, H., Yamaguchi, S., Katsushima, T., De Michele, C., 2016. Observations of capillary barriers and preferential flow in layered snow during cold laboratory experiments. The Cryosphere, 10, 2013-2026.

Baggi, S., and Schweizer, J., 2009. Characteristics of wet-snow avalanche activity: 20 years of observations from a high alpine valley (Dischma, Switzerland). *Natural Hazards, 50,* 97-108.

Barry, R., Chorley, R., 2003. Atmosphere, Weather and Climate. Eighth ed., Routledge. pp 112-122.

Bartelt, P., and Lehning, M., 2002. A physical SNOWPACK model for the Swiss avalanche warning: Part I: numerical model. Cold Regions Science and Technology, 35 (3), 123-145.

Baur, F., Hess, P., Nagel, H., 1944. Calendar of European Grosswetterlagen 1881-1939; in German/ Bad Homburg v.d. H., 35 pp.

Bellaire, S., Jamieson, B., 2013. Forecasting the formation of critical snow layers using a coupled snowcover and weather model. Cold Regions Science and Technology, 94, 37-44.

Birkeland, K.W., Greene, E.M., Logan, S., 2017. In response to avalanche fatalities in the United States by Jekich et al. ([Epub ahead of print]) Wilderness and Environmental Medicine 18 (4).

Birkeland K.W., van Herwijnen A., Reuter B., Bergfeld B., 2019. Temporal changes in the mechanical properties of snow related to crack propagation after loading. *Cold Regions Science and Technology.* https://doi.org/10.1016/ j.coldregions.2018.11.007

Birkeland, K., van Herwijnen, A., Knoff, E., Staples, M., Bair, E., Simenhois, R., 2014. The role of slabs and weak layers in fracture arrest. *Proceedings of the 2014 International Snow Science Workshop*, Breckenridge, CO, USA.

Birkeland, K.W., and Landry, C.C., 2002. Power-laws and snow avalanches. Geophysical Research Letters, 29 (11).

Birkeland, K., Mock, C., and Shinker, J., 2001. Avalanche extremes and atmospheric circulation patterns. *Annals of Glaciology, 32,* 135-140.

Birkeland, K., and Mock, C., 2001. The major snow avalanche cycle of February 1986 in the Western United States. Natural Hazards, 24, 75-95.

Birkeland, K.W., and Mock, C., 1996. Atmospheric circulation patterns associated with heavy snowfall events, Bridger Bowl, Montana, U.S.A. Mountain Research and Developments, 16 (3) 281-286.

Colbeck, S.C., 1983 (a). Ice crystal morphology and growth rates at low supersaturations and high temperatures. *Journal of Applied Physics, 54 (5),* 2677-2682.

Colbeck, S.C., 1983 (b). Theory of metamorphism of dry snow. *Journal of Geophysical Research, 88 (C9),* 5475-5482.

Colorado Avalanche Information Center, 2019. Avalanche Accident Statistics. [Dataset]. Retrieved from https://avalanche.state.co.us/accidents/statistics-and-reporting.

Conlan, M., Tracz, D., Jamieson, B., 2014. Measurements and weather observations at persistent deep slab avalanches. *Cold Regions Science and Technology*, 97, 104-112.

Dettinger, M., Caya, D., Diaz, H., Meko, D., 1998. North-South precipitation patterns in Western North America on interannual-to-decadal timescales. Journal of Climate, 11 (12), 3095-3111.

Davis, R.E., Elder, K., Howlett, D., Bouzaglou, E., 1999. Relating storm and weather factors to dry slab avalanche activity at Alta, Utah and Mammoth Mountain, California, using classification and regression trees. Cold Regions Science and Technology, 30, 79-89.

Esteban, P., Jones, P., Martín-Vide, J., Mases, M., 2005. Atmospheric circulation patterns related to heavy snowfall days in Andorra, Pyrenees. *International Journal of Climatology, 25,* 319-329.

Fitzharris, B.B., 1987. A climatology of major avalanche winters in Western Canada. *Atmosphere-Ocean,* 25 (2), 115-136.

Fitzharris, B.B., Bakkehøi, S., 1986. A synoptic climatology of major avalanche winters in Norway. *Journal of Climatology, 6,* 431-446.

Gaume, J., Reuter, B., 2017. Assessing snow instability in skier-triggered snow slab avalanches by combining failure initiation and crack propagation. *Cold Regions Science and Technology*, 144, 6-15.

Gaume, J., van Herwijnen, A., Chambon, G., Wever, N., Schweizer, J., 2017. Snow fracture in relation to slab avalanche release: critical state for the onset of crack propagation. *The Cryosphere*, 11, 217-228.

Grundstein, A., 2003. A synoptic-scale climate analysis of anomalous snow water equivalent over the norther Great Plains of the USA. *International Journal of Climatology, 23,* 871-886.

Hammonds, K., Lieb-Lappen, R., Baker, I., Wang, X., 2015. Investigating the thermophysical properties of the ice-snow interface under a controlled temperature gradient Part I: Experiments and observations. Cold Regions Science and Technology, 120, 157-167

Hartley, S., Keables, M., 1998. Synoptic associations of winter climate and snowfall variability in New England, USA, 1950-1992. *International Journal of Climatology, 18,* 281-298.

Hatchett, B., Burak, S., Rutz, J., Oakley, N., Bair, E., Kaplan, M., 2017. Avalanche fatalities during atmospheric river events in the western United States. Journal of Hydrometeorology, 18, 1359-1374.

Hewitson, B.C., and Crane, R.G., 2002. Self-organizing maps: applications to synoptic climatology. *Climate Research, 22 (1)*, 13-26.

Hoy, A., Sepp, M., Matschullat, J., 2013. Atmospheric circulation variability in Europe and northern Asia (1901 to 2010). *Theoretical and Applied Climatology, 113 (1-2),* 105-106.

Jiang, N., Hay, J.E., Fisher, G.W., 2004. Classification of New Zealand synoptic weather types and relation to the Southern Oscillation Index. *Weather and Climate, 23,* 3-24.

Kalkstein, L., Tan, G., Skindlov, J., 1987. An evaluation of three clustering procedures for use in synoptic climatological classification. *Journal of Climate and Applied Meteorology, 26,* 717-730.

Kalnay et al., 1996. The NCEP/NCAR 40-year reanalysis project, Bull. Amer. Meteor. Soc., 77, 437-470.

Key, J., and Crane, R., 1986. A comparison of synoptic classification schemes based on 'objective' procedures. *Journal of Climatology, 6,* 375-388.

Keylock, C.J., 2003. The North Atlantic Oscillation and snow avalanching in Iceland. *Geophysical Research Letters, 30 (5).*

Kidson, J., 2000. An analysis of New Zealand synoptic types and their use in defining weather regimes. *International Journal of Climatology, 20,* 299-316.

Kohonen, T., 1998. The Self-organizing map. *Neurocomputing, 12,* 1-6.

LaChapelle, 1980. The fundamental processes in conventional avalanche forecasting. Journal of Glaciology, 26 (94), 75-84.

LaChapelle E., 1966. Avalanche forecasting- A modern synthesis. IAHS Publication 69: 350-356.

Lamb H., 1972 British Isles weather types and a register of the daily sequences of circulation patterns 1861-*1971 Geophysical Memo No. 116 (85)* HMSO, London.

Lang, R.M., Leo, B.R., Brown, R.L., 1984. Observations on the growth process and strength characteristics of surface hoar. Proceedings of the 1984 International Snow Science Workshop, Aspen, CO.

Marienthal, A., Hendrikx, J., Birkeland, K., Irvine, K., 2015. Meteorlogical variables to aid forecasting deep slab avalanches on persistent weak layers. *Cold Regions Science and Technology*, 120, 227-236.

Marienthal, A., Hendrikx, J., Chabot, D., Maleski, P., Birkeland, K., 2012. Depth Hoar, Avalanches, and Wet Slabs: A case study of the historic March 2012 wet slab avalanche cycle at Bridger Bowl, Montana. Proceedings of the International Snow Science Workshop, Anchorage, AK, USA.

Martin, J.P., Germain, D., 2017. Large-scale teleconnection patterns and synoptic climatology of major snow-avalanche winters in the Presidential Range (New Hampshire, USA). *International Journal of Climatology, 37,* 109-123.

McClung, D., and Schaerer, P., 2006. The Avalanche Handbook. 3rd ed. The Mountaineers Books.

McGinnis, D., 2000. Synoptic controls on upper Colorado River Basin snowfall. *International Journal of Climatology, 20,* 131-149.

Mock C., and Birkeland, K., 2000. Snow Avalanche Climatology of the Western United States Mountain Ranges. *Bulletin of the American Meteorological Society, 87 (10),* 2367-2392.

Mock, C., 1996. Climatic Controls and Spatial Variations of Precipitation in the Western United States. Journal of Climate, 9, 1111-1125.

National Research Council (U.S.). (1990). *Snow Avalanche Hazards and Mitigation in the United States. Washington, D.C.: National Academies Press*. Retrieved from http://search.ebscohost.com.proxybz.lib.montana.edu/login.aspx?direct=true&db=nlebk&AN=14505&site=ehost-live

Pietzsch, E.H., 2009. Water movement in a stratified and inclined snowpack: Implications for wet slab avalanches. MSc thesis, Montana State University, Bozeman, MT, USA.

Price, M.F., Byeres, A.C., Friend, D.A., Kohler, T., Price, L.W., 2013. Mountain Geography: Physical and human dimensions, University of California Press.

R Core Team, 2017. R: A language and environment for statistical computing. R Foundation for Statistical Computing, Vienna, Austria. URL https://www.R-project.org/.

Reusch, David B., Alley, Richard B., Hewitson, Bruce C., 2005. Relative performance of self-organizing maps and principal component analysis in pattern extraction from synthetic climatological data. *Polar Geography,* 29:3, 188-212. DOI: 10.1080/789610199

Reuter, B., and Schweizer, J., 2018. Describing snow instability by failure initiation, crack propagation, and slab tensile support. *Geophysical Research letters*, 45, 7019-7027. https://doi.org/10.1029/2018GL078069

Richman, M. 1981. Obliquely rotated principal components: An improved meteorological map typing technique? *Journal of Applied Meteorology, 20,* 1145-1159.

Savage, S., 2006. Deep slab avalanche hazard forecasting and mitigation: the south face at Big Sky ski area. Proceedings of the 2006 International Snow Science Workshop, Telluride, CO, pp. 483–490.

Schuenemann, C., Cassano, J., Finnis, J., 2009. Synoptic forcing of precipitation over Greenalnd: Climatology for 1961-99. *Journal of Hydrometeorology*, 10, 60-78.

Schweizer, J., Camponovo, C., 2001. The skier's zone of influence in triggering slab avalanches. *Annals of Glaciology, 32,* 314-320.

Schweizer, J., Jamieson, B., Skjonsberg, D., 1998. Avalanche forecasting for transportation corridor and backcountry in Glacier National Park (BC, Canada). In: Hestnes, E. (Ed.), 25 Seasons of Snow Avalanche Research, Voss, Norway, 12 – 16 May 1998. NGI Publication, Norwegian Geotechnical Institute, Oslo, Norway, pp. 238 – 243.

Schweizer, J., Reuter, B., van Herwijnen, A., Gaume, J., 2016. Avalanche release 101. Proceedings of the International Snow Science Workshop, Breckenridge, CO.

Shandro, B., and Haegeli, P., 2018. Characterizing the nature and variability of avalanche hazard in western Canada. Natural Hazards and Earth System Sciences, 18, 1141-1158.

Sheridan, S.C., Lee., C.C., 2011. The self-organizing map in synoptic climatological research. *Progress in Physical Geography, 35 (1),* 109-119.

Thumlert, S., Jamieson, B., 2014. Stress measurements in the snow cover below localized dynamic loads. *Cold Regions Science and Technology, 106-107,* 28-35.

U.S. census Bureau, 2016. Cartographic Boundary Shapefiles. [Dataset]. Retrieved from www.census.gov/geo/maps-data/data/cbf/cbf_state.html.

USGS National Center for EROS, 2005. Grayscale North America Shaded Relief- 1-Kilometer Resolution. [Dataset]. Retrieved from http://nationalatlas.gov/atlasftp.html.

Van Peursem, K., Hendrikx, J., Birkeland, K.W., Miller, D., Gibson, C., 2016. Validation of a coupled weather and snowpack model across western Montana. Proceedings of the 2016 International Snow Science Workshop, Breckenridge, CO.

Wallace, J.M., and Gutzler, D.S., 1981. Teleconnections in the geopotential height field during the Northern Hemisphere winter. Monthly Weather Review, 109, 784-812.

Wehrens, R., and Buydens, L.M.C., 2007. Self- and Superorganizing maps in R: the kohonen package. *Journal of Statistical software, 21 (5).*

Werner, P.C., and Gerstengarbe, F.W., 2010. Catalog of European Grosswetterlagen; in German, 7th edtion. PIK Report 119. 140 pp.

Wise, E.K., Dannenberg, M.P., 2014. Persistence of pressure patterns over North America and the North Pacific since AD 1500. *Nature Communications, 5,* 1-6.

Wise, E.K., 2012. Hydroclimatology of the US intermountain west. Progress in Physical Geography, 36 (4), 458-479. DOI: 10.1177/030913312446538.

Wise, E.K., 2010. Spatiotemporal variability of the precipitation dipole transition zone in the western United States. Geophysical Research Letters, 37 (7), L07706.

Yarnal, B. 1993. Synoptic Climatology in Environmental Analysis: A Primer. Bellhaven Press, London, UK. 195 pp.

Yokley, L., Hendrikx, J., Birkeland, K., Williams, K., Leonard, T., 2014. Role of synoptic atmospheric conditions in the formation and distribution of surface hoar. Proceedings of the 2014 International Snow Science Workshop, Banff, Alberta, CA.

APPENDICES

APPENDIX A

OPTIMIZATION PROCEDURE FOR SELF-ORGANIZING MAPS

The SOM algorithm requires the user to specify the number of nodes to be used, the rate at which the nodes are adjusted at each iteration (referred to as the "learning rate"), and the number of iterations to perform. Learning rate and number of iterations are adjusted to minimize the variability between map patterns represented by the same node, and to maximize variability between groups of maps represented by different nodes. The optimization procedure follows a two-step procedure. In the first step, the learning rate and the number of iterations is optimized for SOM configurations using 9, 12, 15, 20, 25, 35, and 56 nodes. For each number of nodes, changes in the output is assessed by comparing similarity of daily observations assigned to the same group and the difference between the nodes. Each node generated by the SOM is characterized by 1197 grid point values on the same 2.5^{o} x 2.5^{o} grid used by the NCEP/NCAR daily 500-mb geopotential height maps. Within-group variability is measured by calculating the root mean square error (RMSE) between each grid point of the node and its corresponding grid point for a given day, so each day has an associated RMSE value. These RMSE values are then averaged over all days in the record. Each learning rate- iteration- number of nodes configuration is run 10 times, and the average RMSE of the 10 runs summarizes the within- group variability for a specific configuration of the SOM. Between-group variability is measured by calculating a RMSE value for each combination of two nodes in the SOM, and averaging all of the RMSE values for each of the 10 runs for a given learning rate-iteration- number of nodes configuration. Finally, mean between-group RMSE values are averaged over the 10 runs for each configuration. The configurations tested are summarized in Table 1.

Table 1: Summary of SOM configurations tested during optimization.

Number of Nodes	Iterations	Learning Rate (initial, finish)
9	500, 1000, 5000, 10000	(.05, .01); (.03, .001)
12	500, 1000, 5000, 10000	(.05, .01); (.03, .001)
15	500, 1000, 5000, 10000	(.05, .01); (.03, .001)
20	500, 1000, 5000, 10000	(.05, .01); (.03, .001)
25	500, 1000, 5000, 10000	(.05, .01); (.03, .001)
35	500, 1000, 5000, 10000	(.05, .01); (.03, .001)
56	500, 1000, 5000, 10000	(.05, .01); (.03, .001)

Since the SOM does not assume independence among nodes, the between-group variability is less important than it would be in other classification methods such as principal components analysis and clustering. However, this research relies heavily on the assumption that observations within the same group are similar. Thus, the optimal configuration should minimize within-group variability and maximize between-group variability, but the within- group variability is much more important. For this reason, configurations may be compared to each other quantitatively with the following:

$$\boldsymbol{\alpha = \frac{w^2}{b}}$$

Where α is the optimization index, *w* is the within-group mean RMSE, and *b* is the between-group mean RMSE. For each number of nodes, the optimal combination of learning rate and number of iterations minimizes α.

In the second step, I assess the effect of changing the number of nodes while using the optimized learning rate/number of iterations configuration determined in step 1. Note that if the goal of SOM optimization is only to minimize α, one could simply set the number of nodes equal to the number of observations. This defeats the purpose of

implementing a classification scheme. Since the analysis is both more practical and easier to understand with fewer types retained, an optimal classification scheme needs to find a balance between interpretability and over-generalization. Milligan and Cooper (1989) discuss 30 procedures for identifying the number of clusters in a dataset. Most of these procedures are dependent on the method used to generate the clusters and cannot be applied to the SOM methodology. One procedure that may be used in this research is the scree test. This test involves plotting the cumulative variability explained in the dataset versus the number of clusters retained. The scree plot should display exponential decay, with an initial steep drop in variability as the number of clusters increases, followed by a slow taper as the number of clusters approaches the number of observations. The ideal number of clusters to retain is the point at which the slope transitions from steep to flat. In this analysis, the scree plot is implemented by plotting α on the y axis and the number of nodes on the x axis.

Plots of α versus number of iterations (Figure 1) and α versus learning rate (Figure 2) suggest that changes in the iteration-learning rate configuration have little effect on optimizing the alpha parameter.

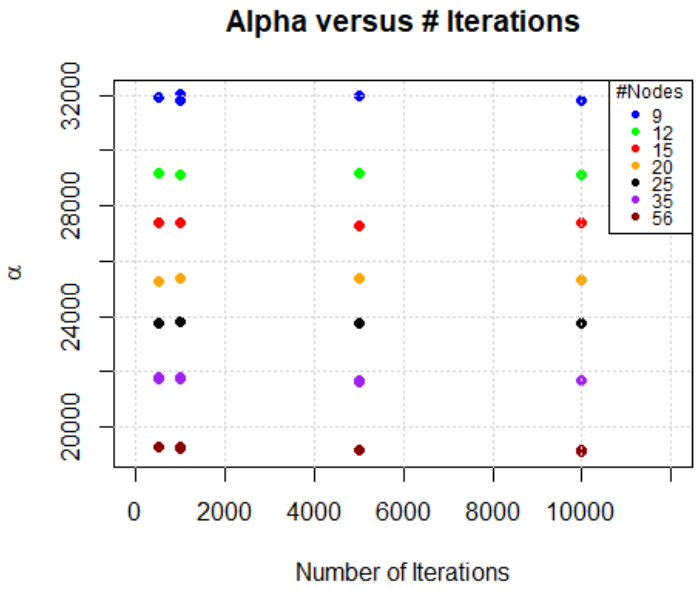

Figure 1: Scatter plot of α index versus number of iterations.

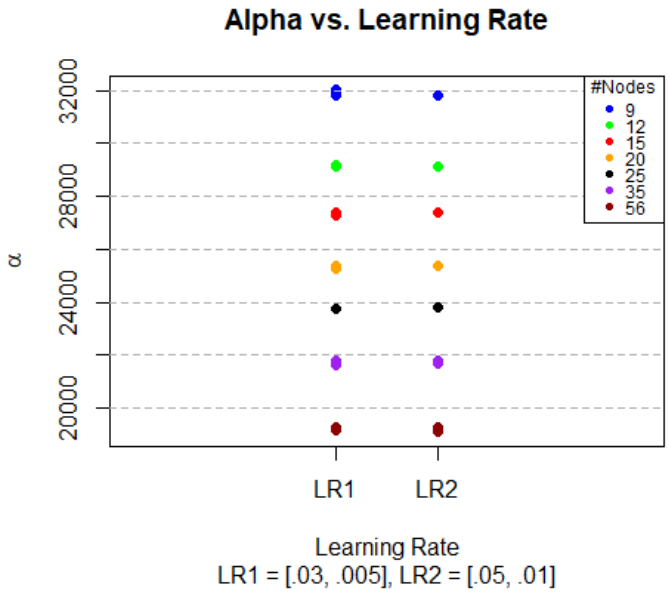

Figure 2: Scatterplot of α versus learning rate for two learning rates.

The scree plot of α versus number of nodes shows a large drop in the α index as number of nodes decreases, with a large decrease in the rate of change between 20 and 30 nodes

(Figure 3). Since the SOM arrays become more difficult as the number of nodes increases, this research will use a 20 node array.

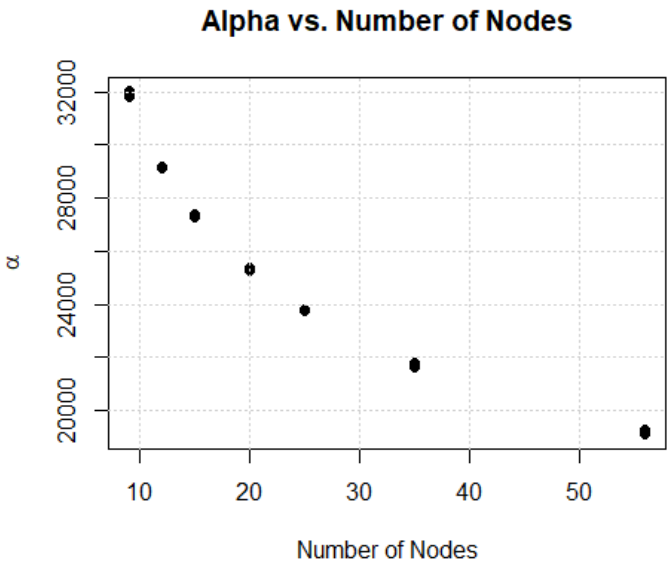

Figure 3: Scree plot of α value versus number of nodes.

APPENDIX B

NOTES ON APPARENT ERRORS AND CHANGES MADE TO WEATHER AND AVALANCHE RECORDS

This appendix summarizes apparent errors in the raw weather and avalanche records, and the changes made to address these errors.

Bridger Bowl

Table 1: Summary of errors and changes made to the weather record for Bridger Bowl

Date	Error	Action
19930317	Apparent typo. HS jumps from 73 to 94 to 71 in three consecutive days.	Change 19930317 ΔHS value from 94 to 74
19940116	Apparent typo. HS jumps from 54 to 76 to 63 in three days. NS value is 11 in.	Change 19940116 ΔHS value from 76 to 66.
19810317	Large discrepancy b/t NS and HS. HS record seems consistent.	None. Use ΔHS as planned.
Jan 2012, Nov/Dec 2015 & 2017	Max. temp = Min temp = -18 C. HS = 0, when adjacent days are well above zero.	All observations set to NA
Nov 2016	Max. temp = Min temp = -17.6 C. HS = 0	All observations set to NA
Any dates with missing value for previous day HS		Use NS value for ΔHS.

Table 2: Summary of errors and changes made to the avalanche record at Bridger Bowl

Date	Record	Error	Action
19991216		Depth recorded as “2/3/2007”	Depth changed to NA
22050214		Year recorded as 2205	Changed to 2005
20040101		Excel wasn’t recognizing as a date when transferred to r	Entered date manually
19990208,		One record was missing a date, but the record was in the middle of the day.	Entered date manually
20070224	12363	Size entered as “^2/2”	Changed to 2
2008/09 – 2012/13		Column with ‘Layer’ heading seems to be records of bed	The bed surface observation is taken

Date	Record	Error	Action
		surface. No values recorded in the bed surface column.	from the layer column.
2012: 12-04, 12-05, 12-07, 12-08, 12-09, 12-10, 12-11, 12-24, 12-28, 12-37 2013: 01-01, 01-04, 01-31, 02-13, 02-15, 03-07, 03-26		Size entered as “NR”	Changed to “NA”
19990226		Multiple sizes 30, 20, and 10. size 30 avalanches ran 70-100% of full track, size 20 were 60-90%, and size 10 was 30%. Interpreted as an input error.	Sizes changed to 3, 2, and 1, respectively.
19961127		Crown depth entered as “G”	Depth changed to NA. Bed surface changed to “G”
20051201	10643, 10644	Sizes for records 10643 and 10644 entered as “?”	Changed to NA.
14376	14376	Depth entered as 39116	Changed to NA
20060407, 20060409, 20070217	21945, 21962, 21963, 22612	Depths recorded as “1’”, “2’”, or “3’”.	Changed to 12, 24, 36 respectively.
20070224	22743	Depth recorded as “^7/10”.	Changed to NA
20080115	23354	Depth recorded as “17868”.	Changed to NA
20100320	26340	Depth recorded as “1O”	Changed to 10
20110101	26840-26843	Depth recorded as “18-24”	Changed to 21
20110113	26979	Depth recorded as “4—6”	Changed to 5
20130304		Depth recorded as “S”	Changed to NA
19990202	13563 and later	Depth records change from feet to inches. The change is inconsistent, and some	For depth = 1-3: If size >= 2, depths are inferred as feet, depth = 4-8: If size

Date	Record	Error	Action
		records are in feet while others are in inches.	>= 3, depths are inferred as feet. For depth = 9-11, if size is >= 4, depths are inferred as feet. All other depths are inferred as inches.
2013-2018	2799, 2800, 5266, 5404, 5439, 5440, 5446, 5447, 5448, 5449, 5450, 5451, 5452, 5466, 5448, 5556, 5558, 5591, 5592, 5594, 5596, 5598, 5599, 5600, 5623, 5633, 5634, 5635, 5753, 5756, 5757, 5758, 5759, 5760, 5761, 5762, 5809	Records are missing dates. Max crown depth for this period is 20”	Records are thrown out.
20140312	1496 - 1500	Depths recorded as “18-48”, “20-40”, and “18-24”.	Switched to average for each range.
20140319	1612	Depth recorded as “20-30”	Switched to 25.
20141201	1773	Depth recorded as “18-6”	Switched to 12.
20141202	1803-1805	Depth recorded as “24-6”	Switched to 15.
20150319	2709	Depth recorded as “O”	Switched to NA.
20131205	34	Surface recorded as “5”	Switched to NA.
20131215	256	Surface recorded as “TR”	Switched to NA.
20140112	853	Surface recorded as “1”	Switched to NA.
20120315	24544-24577	Year entered as 2017. Adjacent days are 20120314 and 20120316	Year switched to 2012

Jackson Hole

The data from the Teton AM weather record are more reliable than manual historical records (Chris McCollister, Pers. comm.). This dataset only contains temp and wind records. The only station that is used in both the AM and manual records is the mid-mountain station. For the Jackson Hole study site, I use the following weather records:

-Teton AM mid-mountain station for daily max/min temp from 19971219 on

-Historic manual mid-mountain Max/Min temp from 19791101 to 19971219

-Historic manual mid-mountain for HS, HN, and SWE24 for the entire record

Table 3: Summary of errors and changes made for the Teton AM weather record

Date	Record	Description	Adjustment
20100218	4648, 4649	Date was duplicated, max and min temp are identical	Erase record# 4648

Table 4: Summary of errors and changes made for the manual historical record.

Date	Record	Description	Adjustment
20061209, 20070313, 20071129, 20080112, 20091129, 20100209, 20101215, 20120123, 20141128	4123, 4124, 4218, 4219, 4266, 4267, 4311, 4312, 4572, 4573, 4645, 4646, 4741, 4742, 4932, 4933, 5332, 5333	Dates duplicated, all values identical.	Erase one record for each date
20130126	5088, 5099	Dates duplicated. All values identical except SWE, which differs by .01 inches for each observation	The difference in SWE is negligible. Observation 5088 is removed.

Date	Record	Description	Adjustment
20080117	4318	Date is duplicated, but one record does not have any measurements.	Remove record 4318
20131204	5177	Temperatures recorded as -458	Changed to "NA"

Table 5: Summary of errors and changes made to the avalanche record at Jackson.

Date	Record	Description	Adjustment
Unknown	29569 - 29582	No date included	Removed events from record.
19811230	3563	Location recorded as "AreaArea"	Changed location to "Area"
20030323	16074	Location recorded as "`"	Changed location to "BC", based on a previous entry of the same slide path in the dataset.
19801203	2971-2983, 2986-2993, 3011, 3012, 3016-3019, 3033, 3036, 3038, 3106, 3107, 3114, 3115, 3207, 3208, 3328, 3329-3334, 3394-3404, 3439-3459, 3477, 3553-3558, 3694, 3695, 3974-3984, 4963, 4964, 5372-5374, 5850, 5856-5861, 6267, 6268, 6273, 8238, 3206, 3380-3390, 3414, 3425-3438, 3544, 3548-3552, 3559, 3663, 3693, 3815-3822, 4642, 5169, 5170, 5370, 5371, 58418, 5849, 5853, 5854, 5876, 5958, 6264-6266, 3001, 3034, 3035, 3204, 3205, 3378, 3379, 3424, 3547, 4024-4026, 5368, 5369, 5875, 5878, 3419, 3420, 3421, 3422, 3810-3814, 3338-3343, 3466-3469, 3025, 3209-3211, 3225, 3823-3825, 6269, 6311, 3323-3327, 3372-3376, 3108, 3109, 3213, 3406, 3478, 3985, 3986, 4643, 4965, 5788,	Crown depth rercorded as 0.	Crown depth changed to "NA"

Date	Record	Description	Adjustment
	6073, 6270, 6306, 6307, 7299, 3105, 3203, 3692, 3807, 3808, 3809, 4023, 3688, 3700, 3701, 3990, 3024, 3026, 3040, 3321, 3322, 3470, 3471, 3927, 3939, 6272, 5846, 5847, 5877, 3545, 3741, 3037, 3409, 3472, 3991, 3212, 3335, 3336, 3337, 3377, 5874, 6310, 7772		

Mammoth Mountain

New snow is measured in the mornings between 0600 and 1000 PST at Mammoth Mountain. This presents a disagreement between weather data and the NCEP/NCAR data, since the daily reanalysis data are averaged from 0000-2400 UTC (1600-1600 PST) at 6-hour intervals. This means that while three of the five measurements used to replicate the atmospheric condition for a given 24-hour period of new snow align with the measurement period, two are associated with the next day's date. The reanalysis data may be downloaded for to fit the measurements better at this location, but that would create the same discrepancy at the other two study sites. One alternative would be to generate a separate classification scheme to use for Mammoth, but this would add to uncertainty in comparisons between study sites. Instead, we acknowledge this offset in measurements as a source of uncertainty, and proceed with the analysis using the same classification scheme for all three study sites.

Table 6: Summary of apparent errors and changes made to the weather record at Mammoth Mountain.

Date	Record	Notes	Changes
19871213, 19910117, 19910328, 19961228, 20060429, 20090129, 20091123, 20110609, 20131210, 20140114	911, 1523, 1593, 2713, 4676, 5237, 5391, 5814, 6269, 6306	Max temp lower than min temp	Both temperatures set to NA
77 entries throughout record		Max temp = min temp (both = 0ºF	none
20131224	5198, 5199	Dates duplicated. All zero values for record 5198	Delete record 5198
20770208	4184, 4185	Dates duplicated. Record 4184 has HS and HN values that do not add up based on previous day's HS. Temperatures for 4184 are also significantly colder than adjacent days, while 4185 seems to agree fairly well with adjacent days.	Delete record 4184
19841108-19841117, 19841204, 19851111, 19870104, 19870214, 19871105, 19871210, 19881109, 19881114, 19881122, 19901120, 20001226, 20010217,	765-774, 791, 919, 1124, 1165, 1215, 1250, 1371, 1376, 1384, 1684, 3233, 3286, 3675, 4257, 4258, 4274, 4340, 4518, 4529, 4964, 5015, 5071, 5126, 5181, 5182, 5184, 5279	Max and min temp both recorded as zero.	All values set to NA.

Date	Record	Notes	Changes
20031215, 20071122, 20071123, 20071209, 20020080213, 20090311, 20090322, 20120303, 20121123, 20130118, 20130314, 20131208, 20131209, 20131211, 20140316.			
19841204, 19850219, 20001226, 20010217, 20031215, 20071224, 20080215, 20090129, 20090322, 20120331	791, 868, 3233, 3286, 3675, 4289, 4342, 4477, 4529, 4992	HS drops to zero, returns to previous day's value on the following day.	HS set to NA
19890311, 19940201, 20010224, 20021229	1493, 2211, 1108, 3293, 3538	HS drops to single digits, returns to previous day's value on the following day	HS set to NA
20081127	4414	HN is 2", SWE says 15 in. Manual record says 3" HN, .26" SWE	SWE changed to .26

There are 4716 events where depth is less than or equal to 6 (roughly 9.3% of the entire record). However, unlike the Bridger Bowl data, there is no clear transition from recording depths in feet to inches or vice versa. Additionally, there is no clear signal based on R-size whether these events should be reclassified as in the Bridger data. As a result, all depth values are assumed to be in inches.

Table 7: Summary of apparent errors and changes made to the avalanche record at Mammoth Mountain.

Date	**Record**	**Notes**	**Changes**
1982-2006	18418 events	Size recorded as "0"	Size changed to NA

APPENDIX C

R SCRIPT FOR FUNCTIONS USED IN THE ANALYSIS

This appendix contains the functions written to run this analysis. The functions require specific format of weather and avalanche records. Weather tables must be saved as an .Rdata object with the name "<sitename>_wx". A list of the names for each column is given in Table 1. These names must be matched exactly in order to run any of the functions included in this appendix.

Table 1: List of column names and corresponding data types required as inputs for the functions used in the analysis.

Column Heading	Data Type
date	Numeric, format: "YYYYMMDD"
maxT_C	Numeric
maxT_C	Numeric
minT_F	Numeric
minT_C	Numeric
HS_cm	Numeric
HS_in	Numeric
NS_cm	Numeric
NS_in	Numeric
SWE_cm	Numeric
SWE_in	Numeric
rain_cm	Numeric
rain_in	Numeric
rho	Numeric

Avalanche tables must be saved as "<sitename>.avy", with the column names and data types summarized in Table 2 below.

Table 2: List of column headings and data types required as avalanche inputs for functions used in the analysis.

Column Heading	Data Type
date	Numeric, format: "YYYYMMDD"
pathname	character string
type	character string
trigger	character string
size	numeric, min 0 max 5
depth	numeric
surface	character string
comments	character string

The script also requires a table of all of the dates in the record period, which must be stored as a data.frame object with numeric columns titled “date”, “month”, “year”, and “day”. The date is formatted “YYYYMMDD”, month is “MM”, year is “YYYY”, and day is “DD”. All values must be numeric.

The SOM object is the output from the supersom() function in the kohonen package (Wehrens and Buydens, 2007). Data input for the SOM comes from the NCEP/NCAR reanalysis in the form of an .ncdf4 file, with a slice for each day. These data need to be reformatted into a matrix with each row representing one day and each column representing one gridpoint value from the reanalysis.

The code for the functions used in this analysis is included below. Commented script describes the functions, including the arguments and outputs for each function. This is not meant to serve as a standalone script, rather it is included to provide further insight on how the analysis was run and to make it possible to reproduce.

Functions for Classifying Deep Slabs and Generating Heat Maps

```
#Function to calculate 3-day storm snow
#inputs:
#   site.name: name of study site (character, needs to match naming scheme of _wx
files)
#outputs:
#   NS72: vector, 3-day storm snow total (cm) for each day
#   SWE72: vector, 3-day SWE total (cm) for each day

stormCm72 <- function(site.name){
  station <- get(paste(site.name, "_wx", sep = ""))
  ns24 <- station[,"NS_cm"]
  swe24 <- station[,"SWE_cm"]
  SWE72 <- NS72 <- rep(0, nrow(station))
  md <- as.numeric(substr(station$date,5,8))
  date <- station$date
```

```
  for(d in 1:nrow(station)){
    NS72[d] <-
      ifelse(md[d] == 1101, ns24[d],
             ifelse(md[d] == 1102,
                    sum(c(na.omit(ns24[d]), na.omit(ns24[d-1]))),
                    sum(c(na.omit(ns24[d]), na.omit(ns24[d-1]), na.omit(ns24[d-2]))
                    )
             )
      )
    SWE72[d] <-
      ifelse(md[d] == 1101, swe24[d],
             ifelse(md[d] == 1102,
                    sum(na.omit(c(swe24[d], swe24[d-1]))),
                    sum(na.omit(c(swe24[d], swe24[d-1], swe24[d-2])))
             )
      )
  }
  NS72[is.na(ns24)] <- NA
  SWE72[is.na(swe24)] <- NA
  attributes(stormCm72) <- list("NS72" = data.frame(date,NS72), "SWE72" =
data.frame(date,SWE72))
}

#Algorithm to identify DS events, adjusting windslab cutoff
#Algorithm to identify DS events
#inputs:
# site.name = character, name used in table convention (e.g. "bridger" for
bridger_wx)
# cIndex = C-multiplier determined by Cmult function.
#outputs:
# summary: data.frame of deep slab avalanches identified with the algorithm. Values
#   include date, depth, and daily count.
# rejects: vector of integers. These are index numbers for the .stormtot table for
#   observations which had crown depth > 3ft but were rejected either by NS totals
or daily average
#           crown depth
DSsort <- function(site.name, cIndex){
  avy <- get(paste(site.name, ".avy", sep = ""))
  station <- get(paste(site.name, "_wx", sep = ""))
  ns72 <- stormCm72(site.name = site.name)$NS72
  date <- station$date
  stormtot <- merge(ns72, avy, all = TRUE, by = "date")
  avy.month <- as.numeric(substr(stormtot$date,5,6))

  # crown > 3 ft, ns <= 3 ft
  c3 <- which(stormtot[,"depth"]>=3 & stormtot[,"NS72"]<= 91.44)

  # bed = G, crown >= 3 ft
  ground <- which(stormtot[,"surface"] == "G" & stormtot[,"depth"]>=3)

  #All avalanches FMA, with Crown > 3ft & NS72 < 3ft, or bed = G
  c3ground <- stormtot[union(c3, ground),]
```

```
  #All avalanches where type = HS, bed = O, crown >= 3ft, size >= 4
  HSold <- which(is.na(stormtot$NS72) == TRUE & stormtot$surface == "O" &
stormtot$size >= 4 & stormtot$type == "HS" & stormtot$depth >= 3)

  #daily max/mean avy depth
  max.ds <- aggregate(stormtot[c3,"depth"] ~ stormtot[c3,"date"], FUN=max)
  names(max.ds) <- c("date", "max_depth")
  mean.ds <- aggregate(stormtot[c3,"depth"] ~ stormtot[c3,"date"], FUN=mean)
  names(mean.ds) <- c("date", "mean_depth")
  c3mean <- na.omit(merge(stormtot[c3, c("date", "depth")], mean.ds, by = "date",
all = TRUE))

  #crown depth >= 150% of daily mean
  c3150 <- c3mean[which(c3mean[,"depth"] >= 1.5*c3mean[,"mean_depth"]),]
  c3retain <- c3[which(c3mean[,"depth"] >= 1.5*c3mean[,"mean_depth"])]
  c3150reject <- c3[which(c3mean[,"depth"] < 1.5*c3mean[,"mean_depth"])]

  #crown depth <= 3* NS72
  ns300 <- which(stormtot$depth >= cIndex*(stormtot$NS72)/(12*2.54) &
stormtot$depth >= 3)

  #combine bed = ground, crown >150% of daily mean, crown > 300% NS72
  ds <- sort(unique(c(ground, c3retain, ns300, HSold)))
  loose <- which(stormtot[, "type"] %in% c("L", "WL"))
  ds <- ds[!(ds %in% loose)]
  ds.count <- data.frame(table(stormtot[ds, "date"]))
  names(ds.count) <- c("date", "count")
  max.ds<-aggregate(stormtot[ds,"depth"] ~ stormtot[ds, "date"],FUN=max)
  names(max.ds)<-c("date","max_depth")
  ds.sum <- merge(max.ds, ds.count, by="date")

  #identify big avalanches that were rejected
  rejects <- c3[!(c3 %in% c(ground, c3retain, ns300))]
  attributes(DSsort) <- list("summary" = ds.sum,
                             "DS" = ds ,
                             "rejects" = rejects,
                             "stormtot" = stormtot,
                             "DS.tab" = stormtot[ds,])
}
#histogram of ws multipliers
#Arguments
# site.name: character, name used in table convention (e.g. "bridger" for
bridger_wx)
# main: name for plot titles
# plot.yax: “y” or “n”. Should the y-axis ticks and labels be plotted?
# plot.xlab: “y” or “n”. Should x-axis title be plotted?
# cIndex: argument passed to DSsum function
#Returns a histogram of C-index for each avalanche for the specified site
Cmult <- function(site.name, main, plot.yax = "y", plot.xlab = "y", cIndex){

  stormtot <- DSsum(site.name = site.name, cIndex = cIndex)$full
```

```
storm <- stormtot[which(stormtot$NS72 >= 15),]
loose <- which(storm$type %in% c("WL", "L", "L ", "WL "))
slab <- storm[- loose,]
wMult <- slab$depth/(slab$NS72/(2.54*12))
sumTable <- data.frame(slab[,c("date", "depth", "type")], wMult)
quantVec <- quantile(wMult,
                     probs = c(.25, .5, .75, .85, .9, .95, .97, .99),
                     na.rm = TRUE)
quantTab <- cbind(c(.25, .5, .75, .85, .9, .95, .97, .99), quantVec)

hist(sumTable$wMult,
     xlab = ifelse(plot.xlab == "y", "C-Multiplier", ""),
     ylab = "",
     main = main,
     breaks = seq(from = 0, to = 20, by = .25),
     ylim = c(0, 4000),
     yaxt = ifelse(plot.yax == "y", "s", "n"),
     col = "gray87",
     border = "gray37",
     font.lab = 2,
     fg = "gray57"
     )
mtext(ifelse(plot.yax == "y", "Frequency", ""),
      side = 2,
      line = 2,
      font = 2,
      cex = .75
      )
abline(h = seq(from = 0, to = 4000, by = 500),
       col = "gray89")
par(new = TRUE)
hist(sumTable$wMult,
     xlab = ifelse(plot.xlab == "y", "C-Multiplier", ""),
     ylab = "",
     main = main,
     breaks = seq(from = 0, to = 20, by = .25),
     ylim = c(0, 4000),
     yaxt = ifelse(plot.yax == "y", "s", "n"),
     col = "gray87",
     border = "gray37",
     font.lab = 2,
     fg = "gray57"
)
axis(1,
     at = 1:20,
     labels = rep("", 20),
     col = "gray37"
     )
abline(v = cIndex,
       lty = "dashed",
       col = "gray69")
```

```
  box(which = "plot", col = "gray37")
  attributes(Cmult) <- list("summary" = sumTable)

  attributes(Cmult) <- list("cValues" = wMult,
                            "quantiles" = quantTab,
                            "maxC" = max(wMult, na.rm = TRUE))
}
#Algorithm to identify DS events
#inputs:
# site.name = character, name used in table convention (e.g. "bridger" for
bridger_wx)
# cIndex = C-multiplier determined by Cmult function.
#outputs:
# summary: data.frame of deep slab avalanches identified with the algorithm. Values
include
#           date, depth, and daily count.
# rejects: vector of integers. These are index numbers for the .stormtot table for
#      observations which had crown depth > 3ft but were rejected either by NS
       totals or
#      daily average crown depth
DSsort <- function(site.name, cIndex){
  avy <- get(paste(site.name, ".avy", sep = ""))
  station <- get(paste(site.name, "_wx", sep = ""))
  ns72 <- stormCm72(site.name = site.name)$NS72
  date <- station$date
  stormtot <- merge(ns72, avy, all = TRUE, by = "date")
  avy.month <- as.numeric(substr(stormtot$date,5,6))

  # crown > 3 ft, ns <= 3 ft, feb-mar constraint is removed
  #c3 <- which(stormtot[,"depth"]>=3 & stormtot[,"NS72"]<= 91.44 & avy.month %in%
c(2,3,4))
  c3 <- which(stormtot[,"depth"]>=3 & stormtot[,"NS72"]<= 91.44)

  # bed = G, crown >= 3 ft, feb-mar constraint is removed
  #ground <- which(stormtot[,"surface"] == "G" & avy.month %in% c(2,3,4) &
stormtot[,"depth"]>=3)
  ground <- which(stormtot[,"surface"] == "G" & stormtot[,"depth"]>=3)

  #All avalanches FMA, with Crown > 3ft & NS72 < 3ft, or bed = G
  c3ground <- stormtot[union(c3, ground),]

  #All avalanches where type = HS, bed = O, crown >= 3ft, size >= 4
  HSold <- which(is.na(stormtot$NS72) == TRUE & stormtot$surface == "O" &
stormtot$size >= 4 & stormtot$type == "HS" & stormtot$depth >= 3)

  #daily max/mean avy depth
  max.ds <- aggregate(stormtot[c3,"depth"] ~ stormtot[c3,"date"], FUN=max)
  names(max.ds) <- c("date", "max_depth")
  mean.ds <- aggregate(stormtot[c3,"depth"] ~ stormtot[c3,"date"], FUN=mean)
  names(mean.ds) <- c("date", "mean_depth")
  c3mean <- na.omit(merge(stormtot[c3, c("date", "depth")], mean.ds, by = "date",
all = TRUE))
```

```
  #crown depth >= 150% of daily mean
  c3150 <- c3mean[which(c3mean[,"depth"] >= 1.5*c3mean[,"mean_depth"]),]
  c3retain <- c3[which(c3mean[,"depth"] >= 1.5*c3mean[,"mean_depth"])]
  c3150reject <- c3[which(c3mean[,"depth"] < 1.5*c3mean[,"mean_depth"])]

  #crown depth <= c* NS72
  ns300 <- which(stormtot$depth >= cIndex*(stormtot$NS72)/(12*2.54) &
stormtot$depth >= 3)

  #combine bed = ground, crown >150% of daily mean, crown > c*NS72
  ds <- sort(unique(c(ground, c3retain, ns300, HSold)))
  loose <- which(stormtot[, "type"] %in% c("L", "WL"))
  ds <- ds[!(ds %in% loose)]
  ds.count <- data.frame(table(stormtot[ds, "date"]))
  names(ds.count) <- c("date", "count")
  max.ds<-aggregate(stormtot[ds,"depth"] ~ stormtot[ds, "date"],FUN=max)
  names(max.ds)<-c("date","max_depth")
  ds.sum <- merge(max.ds, ds.count, by="date")

  #identify big avalanches that were rejected
  rejects <- c3[!(c3 %in% c(ground, c3retain, ns300))]
  attributes(DSsort) <- list("summary" = ds.sum,
                             "DS" = ds ,
                             "rejects" = rejects,
                             "stormtot" = stormtot,
                             "DS.tab" = stormtot[ds,])
}
#Function to examine rejected large avalanches
#inputs:
# site.name = character, name used in table convention (e.g. "bridger" for
bridger_wx)
#outpus:
# rejected: data.frame of rejected avalanches, all attributes
# full: complete avalanche record for the specified site
DSsum <- function(site.name){

  avy <- get(paste(site.name, ".avy", sep = ""))
  ns72 <- stormCm72(site.name = site.name)$NS72
  stormtot <- merge(ns72, avy, all = TRUE, by = "date")

  rejects <- DSsort(site.name = site.name)$rejects
  record <- stormtot[rejects,]
  ds <- stormtot[DSsort(site.name = site.name)$DS,]
  attributes(DSsum) <- list("rejected" = record,"DS" =  ds,"full" = stormtot)
}

#Function to examine rejected large avalanches
#inputs:
# site.name = character, name used in table convention (e.g. "bridger" for
bridger_wx)
#outpus:
```

```
# rejected: data.frame of rejected avalanches, all attributes
# full: complete avalanche record for the specified site
DSsum <- function(site.name, cIndex){

  avy <- get(paste(site.name, ".avy", sep = ""))
  ns72 <- stormCm72(site.name = site.name)$NS72
  stormtot <- merge(ns72, avy, all = TRUE, by = "date")

  rejects <- DSsort(site.name = site.name, cIndex = cIndex)$rejects
  record <- stormtot[rejects,]
  ds <- stormtot[DSsort(site.name = site.name, cIndex = cIndex)$DS,]
  attributes(DSsum) <- list("rejected" = record,"DS" =  ds,"full" = stormtot)
}

#function to count number of times each node was recorded within 72 hours of DS avy
#inputs:
# site.name = character string, name used in table convention (e.g. "bridger" for
bridger_wx)
# SOM = object, the SOM used for synoptic classification
#outpus:
# node.<0-3>: table of counts each node was observed at 0,1,2, and 3 days prior to
DS
# node.72: cumulative 3-day count of each synoptic type for each avalanche
DS72 <- function(site.name, SOM, cIndex){

  node.days <- SOM$unit.classif
  station <- get(paste(site.name, "_wx", sep = ""))
  date <- data.frame("date" = station$date)
  ds.sum <- DSsort(site.name = site.name, cIndex = cIndex)$summary
  ds.vec <- merge(ds.sum, date, by = "date", all.y = TRUE)

#identify days of deep slabs, 24, 48, and 72 hours prior to deep slabs
  ds.days <- which(ds.vec$count>0)
  ds72 <- sort(unique(c(ds.days, ds.days-1, ds.days-2, ds.days-3)))
  node.0 <- node.days[ds.days]
  node.1 <- node.days[ds.days-1]
  node.2 <- node.days[ds.days-2]
  node.3 <- node.days[ds.days-3]
  node72 <- node.days[ds72]

#count number of times each node was recorded within 72 hours of DS
  node0.count <- tabulate(node.0, nbins = length(unique(node.days)))
  node1.count <- tabulate(node.1, nbins = length(unique(node.days)))
  node2.count <- tabulate(node.2, nbins = length(unique(node.days)))
  node3.count <- tabulate(node.3, nbins = length(unique(node.days)))
  node72.count <- tabulate(node72, nbins = length(unique(node.days)))

  attributes(DS72) <- list("node.0" = node0.count,
                           "node.1" = node1.count,
                           "node.2" = node2.count,
                           "node.3" = node3.count,
                           "node72" = node72.count)
```

```
}

#Function to generate 72-hour cumulative count heat maps
#inputs:
# site.name = character, name used in table convention (e.g. "bridger" for
bridger_wx)
# main = character, title for plots
# SOM = object of class som, from SOM output used in analysis
# zlim = upper limit (maximum counts per node) to use for color scale gradient.
#outputs:
# plots a heat map of number of times each class was counted within 72 hours of DS
DS72heat <- function(site.name, main, SOM, zlim = 45, cIndex){

  counts <- DS72(site.name = site.name, SOM = SOM, cIndex = cIndex)$node72
  cbhr <- function(n, alpha = 1){rainbow(n, end = 4/6, alpha = alpha)[n:1]}

  plot(SOM,type="property",
       property=counts,
       palette.name=cbhr,
       shape="straight",
       main= main,
       zlim = c(0, zlim)
       )
}

#Function to generate 72-hour heat maps for wet slab events
# Arguments:
#   site.name: character string. name of site to be plotted (<site.name>.avy)
#   main: character string. Name of location to be included in title of plots
#   SOM: object. som object used for synoptic classification
#   zlim: numeric. upper limit (maximum counts per node) to use for color scale
gradient.
#   cIndex: passed to DSsort function
# Outputs:
#   A heatmap of counts for number of times each synoptic type occurred within 72
hours
#   of wet slab events
#   node.<0-3>: table of counts each node was observed at 0,1,2, and 3 days prior
to DS
#   node.72: cumulative 3-day count of each synoptic type for each avalanche

WS72heat <- function(site.name, main, SOM, zlim = 5, cIndex){

  node.days <- SOM$unit.classif
  station <- get(paste(site.name, "_wx", sep = ""))
  avy <- get(paste(site.name, ".avy", sep = ""))
  date <- data.frame("date" = station$date)
  ns72 <- stormCm72(site.name = site.name)$NS72
  stormtot <- merge(ns72, avy, all = TRUE, by = "date")
  events <- stormtot[DSsort(site.name = site.name, cIndex = cIndex)$DS,]
  ws <- events[which(events$type == "WS"),"date"]
  ws.count <- data.frame(table(ws))
```

```
  names(ws.count) <- c("date", "count")
  ws.count$date <- as.numeric(as.character(ws.count$date))
  ws.vec <- merge(ws.count, date, by = "date", all.y = TRUE)

  #identify days of deep slabs, 24, 48, and 72 hours prior to wet slabs
  ws.days <- which(ws.vec$count > 0)
  ws72 <- sort(unique(c(ws.days, ws.days-1, ws.days-2, ws.days-3)))
  node.0 <- node.days[ws.days]
  node.1 <- node.days[ws.days-1]
  node.2 <- node.days[ws.days-2]
  node.3 <- node.days[ws.days-3]
  node72 <- node.days[ws72]

  #count number of times each node was recorded within 72 hours of DS
  node0.count <- tabulate(node.0, nbins = length(unique(node.days)))
  node1.count <- tabulate(node.1, nbins = length(unique(node.days)))
  node2.count <- tabulate(node.2, nbins = length(unique(node.days)))
  node3.count <- tabulate(node.3, nbins = length(unique(node.days)))
  node72.count <- tabulate(node72, nbins = length(unique(node.days)))

  cbhr <- function(n, alpha = 1){rainbow(n, end = 4/6, alpha = alpha)[n:1]}

  plot(SOM,type="property",
       property=node72.count,
       palette.name=cbhr,
       shape="straight",
       main= main,
       zlim = c(0, zlim)
  )

  DSevents <- DSsort(site.name, cIndex = cIndex)$DS
  WS <- DSevents[which(stormtot[DSevents, "type"] == "WS")]
  WStable <- stormtot[WS,]

  attributes(WS72heat) <- list("node.0" = node0.count,
                               "node.1" = node1.count,
                               "node.2" = node2.count,
                               "node.3" = node3.count,
                               "node72" = node72.count,
                               "WSdays" = date[ws.days,"date"],
                               "WStable" = WStable)
}

#Heat maps for dry deep slab events
# Arguments:
#   site.name: character string. name of site to be plotted (<site.name>.avy)
#   main: character string. Name of location to be included in title of plots
#   SOM: object. som object used for synoptic classification
#   zlim: numeric. upper limit (maximum counts per node) to use for color scale
gradient.
#   default is 50
#   cIndex: passed to DSsort function
```

```
# Outputs:
#   A heatmap of ncounts for number of times each synoptic type occurred within 72
hours of dry
#     slab events
#   node.<0-3>: table of counts each node was observed at 0,1,2, and 3 days prior
to DS
#   node.72: cumulative 3-day count of each synoptic type for each avalanche
dry72heat <- function (site.name, main, SOM, zlim = 50, cIndex){

  node.days <- SOM$unit.classif
  station <- get(paste(site.name, "_wx", sep = ""))
  avy <- get(paste(site.name, ".avy", sep = ""))
  date <- data.frame("date" = station$date)
  ns72 <- stormCm72(site.name = site.name)$NS72
  stormtot <- merge(ns72, avy, all = TRUE, by = "date")
  events <- stormtot[DSsort(site.name = site.name, cIndex = cIndex)$DS,]
  ws <- events[which(events$type == "WS"),"date"]
  dry <- events[-which(events$type == "WS"), "date"]

  dry.count <- data.frame(table(dry))
  names(dry.count) <- c("date", "count")
  dry.count$date <- as.numeric(as.character(dry.count$date))
  dry.vec <- merge(dry.count, date, by = "date", all.y = TRUE)

  #identify days of deep slabs, 24, 48, and 72 hours prior to wet slabs
  dry.days <- which(dry.vec$count > 0)
  dry72 <- sort(unique(c(dry.days, dry.days-1, dry.days-2, dry.days-3)))
  node.0 <- node.days[dry.days]
  node.1 <- node.days[dry.days-1]
  node.2 <- node.days[dry.days-2]
  node.3 <- node.days[dry.days-3]
  node72 <- node.days[dry72]

  #count number of times each node was recorded within 72 hours of DS
  node0.count <- tabulate(node.0, nbins = length(unique(node.days)))
  node1.count <- tabulate(node.1, nbins = length(unique(node.days)))
  node2.count <- tabulate(node.2, nbins = length(unique(node.days)))
  node3.count <- tabulate(node.3, nbins = length(unique(node.days)))
  node72.count <- tabulate(node72, nbins = length(unique(node.days)))

  cbhr <- function(n, alpha = 1){rainbow(n, end = 4/6, alpha = alpha)[n:1]}

  plot(SOM,type="property",
       property=node72.count,
       palette.name=cbhr,
       shape="straight",
       main= main,
       zlim = c(0, zlim)
  )

  DSevents <- DSsort(site.name, cIndex = cIndex)$DS
  dry <- DSevents[-which(stormtot[DSevents, "type"] == "WS")]
```

```
  drytable <- stormtot[dry,]

  attributes(WS72heat) <- list("node.0" = node0.count,
                               "node.1" = node1.count,
                               "node.2" = node2.count,
                               "node.3" = node3.count,
                               "node72" = node72.count,
                               "days" = date[dry.days,"date"],
                               "table" = drytable)
}
#function to plot storm snow for a given year
WXseason <- function(site.name, main, plot.season){

  station <- get(paste(site.name, "_wx", sep = ""))

  date <- station$date
  year <- as.numeric(substr(station$date,1,4))
  month <- as.numeric(substr(station$date,5,6))
  season <- rep(0, nrow(dates))
  for (obs in 1:length(date)){
    season[obs] <-
      ifelse(month[obs] %in% c(11,12),
             year[obs],
             year[obs] - 1)
  }

  plot(station[season == plot.season, "HS_cm"],
       main = paste("HS - ", main, plot.season, sep = " "),
       xaxt = "n",
       xlab = "",
       ylab = "HS (cm)",
       type = "l")
}
```

Functions to Calculate Deep Slab Activity Index and Generate Plots

```
#Function to calculate AAI after Schweizer et al. 2018
#Arguments:
# site.name: character, name used in table convention (e.g. "bridger" for
bridger_wx)
# sub: subtitle included in plots
# hiquant: percentile used to identify major seasons
# loquant: quantity used as threshold to identify minor seasons
# missing: character, vector of missing seasons
# cIndex: passed to DSsum
# plot.yax, plot.xax: “y” or “n”. should y- and x- axes have ticks and labels
plotted?
# return.plot: “y” or “n” should the data be plotted?
# add.lines: “y” or “n”. Should the time series be plotted as a line plot?
# plot.xlab, plot.ylab: “y” or “n”. Should the x- and y- axis titles be plotted?
calcDSAI <- function(site.name,
                     sub,
```

```
                    hiquant = .9,
                    loquant = 0.1,
                    missing = c(),
                    cIndex,
                    plot.yax = "y",
                    plot.xax = "y",
                    return.plot = "y",
                    add.lines = "n",
                    plot.xlab = "y",
                    plot.ylab = "y"){

  avyRecord <-   avy <- get(paste(site.name, ".avy", sep = ""))
  dsRecord <- DSsum(site.name = site.name, cIndex = cIndex)$DS

  size <- dsRecord$size
  Di <- 10^(size-3)
  #tMult <- rep(0, length(Di))

  # for(i in 1:length(tMult)){
  #    tMult[i] <-
  #    ifelse(dsRecord[i, "trigger"] %in% c("N ", "N"),
  #           1,
  #           ifelse(dsRecord[i, "trigger"] == "AS",
  #                  .5,
  #                  .2))
  #  }

  DSAI.table <- data.frame(
    dsRecord[,"date"],
   # "DSAI" = Di*tMult,
   "DSAI" = Di,
    dsRecord[,c("NS72", "depth", "size", "surface" ,"trigger","pathname", "type")])
  names(DSAI.table) <- c("date", "DSAI", "NS72", "depth", "size", "surface"
,"trigger","pathname", "type")
  DSAI.month <- as.numeric(substr(DSAI.table$date, 5, 6))
  DSAI.year <- as.numeric(substr(DSAI.table$date, 1, 4))
  DSAI.season <- rep(0, nrow(DSAI.table))
  for (obs in 1:length(DSAI.year)){
    DSAI.season[obs] <-
      ifelse(DSAI.month[obs] %in% c(11,12),
             DSAI.year[obs],
             DSAI.year[obs] - 1)
  }
  DSAI.table <- data.frame("season" = DSAI.season, DSAI.table)
  DSAI.table <- DSAI.table[DSAI.table$season >= 1979,]
  DSAI.season <- DSAI.season[DSAI.season >= 1979]
  DSAI.ag <- aggregate(DSAI.table$DSAI ~ DSAI.season, FUN = sum)
  names(DSAI.ag) <- c("season", "DSAI")
  avy.years <- as.numeric(substr(avyRecord$date, 1, 4))
  avy.season <- avy.years - 1
  recordLength <- data.frame("season" = min(avy.season):max(avy.season))
  DSAI.full <- merge(recordLength, DSAI.ag, by = "season", all.x = TRUE)
```

```
  DSAI.full <- DSAI.full[DSAI.full$season >= 1979, ]
  DSAI.full[is.na(DSAI.full$DSAI), "DSAI"] <- 0

#make some plots


  #plot(Di,
  #    main = "DSAI, scaled and unscaled",
  #    sub = sub,
  #    ylab = "DSAI",
  #    xlab = "Observation")
  #points(Di*tMult, col = "green")
  #points(Di, col = "green")
  #legend("topright",
  #      legend = c("unscaled", "scaled"),
  #      col = c("black", "green"),
  #      pch = 1)

# plot(tMult,
#       main = "t- multiplier for trigger type",
#       sub = sub,
#       xlab = "Observation")

  missing.points <- which(DSAI.full$season %in% missing)
  if (length(missing) == 0) {DSAI.points <- DSAI.full} else {DSAI.points <-
DSAI.full[ -(missing.points), ]}

  hicuts <-quantile(DSAI.points$DSAI, hiquant, type = 1)
  locuts <- loquant
  major <- which(DSAI.points$DSAI >= .9*hicuts)
  minor <- which(DSAI.points$DSAI <= locuts)
  cols <- rep("gray69", length(DSAI.points$DSAI))
  cols[major] <- "black"
  cols[minor] <- "black"

  if(return.plot == "y"){
  plot(DSAI.points,
         type = "n",
         main = sub,
         xlab = "",
         ylab = "",
         xlim = c(1979,2017),
         ylim = c(0,650),
         yaxt = ifelse(plot.yax == "y", "s", "n"),
         xaxt = ifelse(plot.xax == "y", "s", "n"))

  grid()

    if(add.lines == "y") {lines(DSAI.points)}

  points(DSAI.points,
     pch = 16,
```

```
     col = cols)
  mtext(ifelse(plot.ylab == "y", "Seasonal DSAI", ""),
        side = 2,
        line = 2.5,
        font = 2,
        cex = .75
        )
  mtext(ifelse(plot.xlab == "y", "Year", ""),
        side = 1,
        line = 2.5,
        font = 2,
        cex = .75
  )
  abline(h = c(hicuts,locuts),
         lty = "dashed",
         col = "gray47")
  }
  #hist(DSAI.full$DSAI,
  #     breaks = trunc(max(DSAI.full$DSAI)),
  #     main = "DSAI Occurrences",
  #     xlab = "DSAI",
  #     ylab = "Counts")

  wet.days <- unique(DSAI.table[which(DSAI.table$type == "WS"),"date"])
  dry.days <- unique(DSAI.table[which(DSAI.table$type %in% c("HS", "SS", "C", NA)),
"date"])

  attributes(calcDSAI) <- list("Di" = Di,
                               #"tMult" = tMult,
                               "DSAI" = DSAI.full,
                               "DSAI.table" = DSAI.table,
                               "cut" = c(hicuts, locuts),
                               "wet.days" = wet.days,
                               "dry.days" = dry.days)

}

#Generate heat maps for the specified season
#inputs:
# site.name: character, <site.name>_wx
# SOM: character, name of SOM
# DSseason: numeric, year of interest
# main: character, name of ski area to be shown on plots
#outputs:
# heat map of # of days per node
# season: numeric, season specified
# table: numeric, vector of counts per node (as indexed in the vector)
yearHeat <- function(site.name, SOM, DSseason, main, zscale){

  node.days <- SOM$unit.classif
  station <- get(paste(site.name, "_wx", sep = ""))
```

```
  date <- station$date
  year <- as.numeric(substr(station$date,1,4))
  month <- as.numeric(substr(station$date,5,6))
  season <- rep(0, nrow(dates))
  for (obs in 1:length(date)){
    season[obs] <-
      ifelse(month[obs] %in% c(11,12),
             year[obs],
             year[obs] - 1)
  }
  dates <- data.frame(date, year, month, "node" = node.days, "season" = season)
  ndj.dates <- dates[dates$month %in% c(11,12,1),]
  ndj.sum <- aggregate(ndj.dates$node,
                       by = list(ndj.dates$node, ndj.dates$season),
                       FUN = length,
                       drop = FALSE)
  names(ndj.sum) <- c("syn_type", "season", "NDJ_count")
  ndj.sum$NDJ_count[ndj.sum$NDJ_count %in% NA] <- 0

  counts <- ndj.sum[ndj.sum$season == DSseason, "NDJ_count"]
  frequency <- counts/(sum(counts))
  cbhr <- function(n, alpha = 1){rainbow(n, end = 4/6, alpha = alpha)[n:1]}

  plot(SOM,type="property",
       property=counts,
       palette.name=cbhr,
       shape ="straight",
       main = paste("NDJ Frequency", DSseason),
       sub = "Frequency",
       zlim = c(0,zscale),
       ncolors = 6,
       heatkey = TRUE

  )

  attributes(yearHeat) <- list("season" = DSseason, "table" = counts, "freq" =
frequency)
}

#Generate plots for quantiles
# all arguments passed to calcDSAI function
dsHeatquant <- function(site.name, main, cIndex){

  DSAI <- calcDSAI(site.name = site.name, sub = main, cIndex = cIndex)$DSAI

  node.days <- SOM$unit.classif
  station <- get(paste(site.name, "_wx", sep = ""))

  date <- station$date
  year <- as.numeric(substr(station$date,1,4))
  month <- as.numeric(substr(station$date,5,6))
  season <- rep(0, nrow(dates))
```

```
for (obs in 1:length(date)){
  season[obs] <-
    ifelse(month[obs] %in% c(11,12),
           year[obs],
           year[obs] - 1)
}
dates <- data.frame(date, year, month, "node" = node.days, "season" = season)
ndj.dates <- dates[dates$month %in% c(11,12,1),]

ndj.sum <- aggregate(ndj.dates$node,
                     by = list(ndj.dates$node, ndj.dates$season),
                     FUN = length,
                     drop = FALSE)
names(ndj.sum) <- c("syn_type", "season", "NDJ_count")
ndj.sum$NDJ_count[ndj.sum$NDJ_count %in% NA] <- 0

Q90 <- which(DSAI$DSAI >= quantile(DSAI$DSAI, .90))
years90 <- DSAI[Q90,"season"]
counts90 <- ndj.sum[(ndj.sum$season %in% years90), ]
heat90 <- aggregate(counts90$NDJ_count~counts90$syn_type , FUN = sum)[,2]
Q75 <- which(DSAI$DSAI >= quantile(DSAI$DSAI, .75))
years75 <- DSAI[Q75,"season"]
counts75 <- ndj.sum[(ndj.sum$season %in% years75), ]
heat75 <- aggregate(counts75$NDJ_count~counts75$syn_type , FUN = sum)[,2]
Q50l <- which(DSAI$DSAI <= quantile(DSAI$DSAI, .5))
years50 <- DSAI[Q50l,"season"]
counts50 <- ndj.sum[(ndj.sum$season %in% years50), ]
heat50 <- aggregate(counts50$NDJ_count~counts50$syn_type , FUN = sum)[,2]
Q25l <- which(DSAI$DSAI <= quantile(DSAI$DSAI, .25))
years25 <- DSAI[Q25l,"season"]
counts25 <- ndj.sum[(ndj.sum$season %in% years25), ]
heat25 <- aggregate(counts25$NDJ_count~counts25$syn_type , FUN = sum)[,2]

plot(SOM,type="property",
     property= heat90,
     palette.name=cbhr,
     shape ="straight",
     main = paste(main,"-NDJ", ">90%"))
plot(SOM,type="property",
     property= heat75,
     palette.name=cbhr,
     shape ="straight",
     main = paste(main,"-NDJ", ">75%"))
plot(SOM,type="property",
     property= heat50,
     palette.name=cbhr,
     shape ="straight",
     main = paste(main,"-NDJ", "<50%"))
plot(SOM,type="property",
     property= heat25,
     palette.name=cbhr,
     shape ="straight",
```

```
       main = paste(main,"-NDJ", "<25%"))

  attributes(dsHeatquant) <- list("counts90" = counts90, "counts75" = counts75,
"counts50" = counts50, "counts25" = counts25,
                                  "years90" = years90, "years75" = years75,
"years50" = years50, "years25" = years25)
}

#Function to plot heat maps for a bunch of similar years
anQuant <- function(site.name, main, quantile){
a <- dsHeatquant(site.name = site.name, main = main)
years <- a[[paste("years", quantile, sep = "")]]
for(y in years[years >= 1979]){
  yearHeat(site.name = site.name,
           SOM = test.som,
           DSseason = y,
           main = main)}
}

#Function to generate table of counts of type for NDJ of each year
ndjYear <- function (site.name, SOM){
  node.days <- SOM$unit.classif
  station <- get(paste(site.name, "_wx", sep = ""))

  date <- station$date
  year <- as.numeric(substr(station$date,1,4))
  month <- as.numeric(substr(station$date,5,6))
  season <- rep(0, nrow(dates))
  for (obs in 1:length(date)){
    season[obs] <-
      ifelse(month[obs] %in% c(11,12),
             year[obs],
             year[obs] - 1)
  }
  dates <- data.frame(date, year, month, "node" = node.days, "season" = season)
  ndj.dates <- dates[dates$month %in% c(11,12,1),]

  ndj.sum <- aggregate(ndj.dates$node,
                       by = list(ndj.dates$node, ndj.dates$season),
                       FUN = length,
                       drop = FALSE)
  names(ndj.sum) <- c("syn_type", "season", "NDJ_count")
  ndj.sum$NDJ_count[ndj.sum$NDJ_count %in% NA] <- 0

  ndj.mat <- matrix(ndj.sum$NDJ_count,
                    ncol = length(unique(node.days)),
                    byrow = TRUE)

  list("ndj.sum" = ndj.sum,
       "ndj.mat" = ndj.mat)
}
```

```
#function to generate line plots for a specified set of years
linesQuant <- function(site.name, SOM, main, quantile, cIndex = cIndex){
  a <- dsHeatquant(site.name = site.name, main = main, cIndex = cIndex)
  years <- a[[paste("years", quantile, sep = "")]]
  years <- years[years >= 1979]
  ndj.sum <- ndjYear(site.name = site.name, SOM = SOM)$ndj.sum

  b <- ndj.sum[ndj.sum$season == years[1],]
  plot(x = b$syn_type,
       y = b$NDJ_count,
       main = paste(main, quantile, "% Quantile"),
       type = "n",
       xlab = "Class",
       ylab = "Count",
       ylim = c(0,30))

  abline(v = 1:20,
         h = seq(from = 0, to = 30, by = 5),
         lty = "dashed",
         col = "gray87")

  legend("topright",
         legend = years,
         col = 1:length(years),
         lty = 1,
         cex = .75)

  for(y in years){
    l <- ndj.sum[ndj.sum$season == y, "NDJ_count"]
    lines(l, col = which(years == y))

  }
}
#function to create spaghetti plots and heat maps specifying category by DSAI
# arguments:
# site.name: character, <site.name>_wx
# SOM: character, name of SOM
# main: name to be used in plot titles
# greater: Logical. Default is true, which plots the years greater than the
specified
#          threshold.
# cIndex, hiquant, loquant: passed to calcDSAI function
# outputs:
# years: vector of years identified based on DSAI threshold
# spaghetti plot of counts for each synoptic type during each specified year
# heatmaps for each individual year identified based on DSAI threshold.
catLines <- function(site.name, SOM, main, greater = TRUE, cIndex, hiquant, loquant
= .1){

  site.DSAI <- calcDSAI(site.name = site.name, sub = main, cIndex = cIndex, hiquant
= hiquant, loquant = loquant)
  a <- site.DSAI$DSAI
```

```
cutoff <- ifelse(greater == TRUE, site.DSAI$cut[1], site.DSAI$cut[2])
abline(v = cutoff,
       col = "red",
       lty = "dashed")


  if (greater == TRUE) {years <- a[a$DSAI >= .9*cutoff, "season"]}
  if (greater == FALSE) {years <- a[a$DSAI <= cutoff, "season"]}


ndj.sum <- ndjYear(site.name = site.name, SOM = SOM)$ndj.sum

title.ind <- ifelse(greater == TRUE,
                    ">",
                    "<")

b <- ndj.sum[ndj.sum$season == years[1],]

plot(x = b$syn_type,
     y = b$NDJ_count,
     main = paste(main, "DSAI", title.ind, cutoff),
     type = "n",
     xlab = "Class",
     ylab = "Count",
     ylim = c(0,30))

abline(v = 1:20,
       h = seq(from = 0, to = 30, by = 5),
       lty = "dashed",
       col = "gray87")

legend("topright",
       legend = years,
       col = 1:length(years),
       lty = 1,
       cex = .75)

for(y in years){
  l <- ndj.sum[ndj.sum$season == y, "NDJ_count"]
  lines(l, col = which(years == y))
}

for (y in years){
  heat <- ndj.sum[ndj.sum$season == y, "NDJ_count"]
  cbhr <- function(n, alpha = 1){
    rainbow(n, end = 4/6, alpha = alpha)[n:1]}

  plot(SOM,type="property",
       property= heat,
       palette.name=cbhr,
       shape ="straight",
       main = paste("NDJ", y))
```

```
  }
  attributes(catLines) <- list("years" = years)

}
#function to plot difference between frequency distributions
# for major, minor, and all seasons. This also performs the Chi-sq
# goodness of fit test.
#
freqBar <- function(site.name, main, SOM, major, minor){

  data<- ndjYear(site.name = site.name, SOM = SOM)$ndj.mat
  seasFull <- 1979:2017
  seasMaj <- which(seasFull %in% major)
  seasMin <- which(seasFull %in% minor)

  majTot <- colSums(data[seasMaj, ])
  minTot <- colSums(data[seasMin, ])
  fullTot <- colSums(data)

  majFreq <- majTot/sum(majTot)
  minFreq <- minTot/sum(minTot)
  fullFreq <- fullTot/sum(fullTot)

  nRows <- SOM$grid$ydim
  nCols <- SOM$grid$xdim
  nNodes <- nRows*nCols

  graphics.off()
  par(mfrow = c(3,1))
  layout.mat <- matrix(1:nNodes,
                       ncol = nCols,
                       byrow = TRUE)[nRows:1,]

  majFreqDiff <- (majFreq - fullFreq)[as.vector(t(layout.mat))]
  minFreqDiff <- (minFreq - fullFreq)[as.vector(t(layout.mat))]
  majminDiff <- (majFreq - minFreq)[as.vector(t(layout.mat))]

  barplot(majFreqDiff,
          names.arg = LETTERS[1:nNodes],
          main = paste("Major vs. All"),
          ylab = "",
          xlab = "",
          ylim = c(-.05, .05),
          yaxp = c(-.05,.05, 2),
          cex.names = .85,
          col = ifelse(majFreqDiff > 0, "gray37", "gray57"),
          border = FALSE)

  barplot(minFreqDiff,
          names.arg = LETTERS[1:nNodes],
          main = paste("Minor vs. All"),
          ylab = "",
```

```
          xlab = "",
          ylim = c(-.05, .05),
          yaxp = c(-.05,.05, 2),
          cex.names = .85,
          col = ifelse(minFreqDiff > 0, "gray37", "gray57"),
          border = FALSE)
  mtext("Difference in Frequency",
        side = 2,
        line = 2.5,
        font = 2,
        cex = 1
        )
  barplot(majminDiff,
          names.arg = LETTERS[1:nNodes],
          main = paste("Major vs. Minor"),
          ylab = "",
          xlab = "",
          ylim = c(-.05, .05),
          yaxp = c(-.05,.05, 2),
          cex.names = .85,
          col = ifelse(majminDiff > 0, "gray37", "gray57"),
          border = FALSE)
  mtext("Synoptic Type",
        side = 1,
        line = 2.5,
        font = 2,
        cex = 1
      )

  testMaj <- majTot[as.vector(t(layout.mat))]
  testMin <- minTot[as.vector(t(layout.mat))]
  testFull <- fullFreq[as.vector(t(layout.mat))]
  chiMaj <- chisq.test(x = testMaj,
                       p = testFull)
  chiMin <- chisq.test(x = testMin,
                       p = testFull)

  attributes(freqBar) <- list("major" = majFreq,
                              "minor" = minFreq,
                              "full" = fullFreq,
                              "counts" = data,
                              "tests" = list("Major" = chiMaj,
                                             "Minor" = chiMin))
}

#Function to create a plot of daily DSAI score w/synoptic type for each season
#Arguments:
# site.name: character. name of site (e.g. “bridger” for bridger.avy)
# main: character. title for plots
# plot.season: numeric. which season to be plotted (e.g. 1979 for the 1979/80
season).
# missing: numeric. vector of seasons missing from dataset.
```

```
# cIndex: passed to calcDSAI function.
# SOM: character. name of som object used for classification.
# HSlim: maximum value for HS on plots.
DSAIplot <- function(site.name, main, plot.season, missing = c(), cIndex, SOM,
HSlim){

  DSAI <- calcDSAI(site.name = site.name, sub = main, missing = missing, cIndex =
cIndex, return.plot = "n")
  daily <- DSAI$DSAI.table
  daySum <- aggregate(daily$DSAI~daily$date, FUN = sum)
  names(daySum) <- c("date", "DSAI")
  DStab <- merge(daySum, dates, by = "date", all.y = TRUE)
  date <- dates$date

  year <- as.numeric(substr(dates$date,1,4))
  month <- as.numeric(substr(dates$date,5,6))
  season <- rep(0, nrow(dates))
  for (obs in 1:length(date)){
    season[obs] <-
      ifelse(month[obs] %in% c(11,12),
             year[obs],
             year[obs] - 1)
  }

  nRows <- SOM$grid$ydim
  nCols <- SOM$grid$xdim
  nNodes <- nRows*nCols

  layout.mat <- matrix(1:nNodes,
                       ncol = nCols,
                       byrow = TRUE)[nRows:1,]
  node.y <- as.vector(t(layout.mat))
  letLab <- LETTERS[1:nNodes]

  plot.dates <- dates[season %in% plot.season, ]
  nodes <- plot.dates$node
  plot.date <- plot.dates$date
  monthday <- as.numeric(substr(plot.date, 5, 8))

  station <- get(paste(site.name, "_wx", sep = ""))
  wx <- station[which(season %in% plot.season),]
  plot.DSAI <- DStab[which(season %in% plot.season), "DSAI"]
  plot.DSAI[is.na(plot.DSAI)] <- 0

  bar.cols <- rep(NA, length(plot.DSAI))
  for (day in 1:length(bar.cols)){

    if(plot.DSAI[day] < 1 ) {bar.cols[day] <- "gray87"}
    if(plot.DSAI[day] >= 1 ) {bar.cols[day] <- "gray67"}
    if(plot.DSAI[day] >= 10 ) {bar.cols[day] <- "gray47"}
    if(plot.DSAI[day] >= 100 ) {bar.cols[day] <- "gray27"}
  }
```

```
  DSAI.omit <- plot.DSAI[plot.DSAI > 0]
  if(sum(DSAI.omit) > 0){
    line.cols <- rep(0, length(DSAI.omit))
    for(day in 1:length(line.cols)){
      if(DSAI.omit[day] < 1 ) {line.cols[day] <- "gray87"}
      if(DSAI.omit[day] >= 1 ) {line.cols[day] <- "gray67"}
      if(DSAI.omit[day] >= 10 ) {line.cols[day] <- "gray47"}
      if(DSAI.omit[day] >= 100 ) {line.cols[day] <- "gray27"}
    }
  }

  par(mar = c(3, 3, 3, 6), xpd = FALSE)
  plot(x = 1: length(plot.date),
       y = factor(nodes, levels = rev(node.y)),
       yaxt = "n",
       xaxt = "n",
       xlab = "",
       ylab = "",
       type = "n",
       main = paste(main, plot.season, sep = "")
       )
  abline(h = seq(from = 1, to = 17, by = 4),
         lty = "dashed",
         col = "gray87")
  abline(v = which(plot.DSAI >0),
         lwd = 3.5,
         col = line.cols
         )
  points(x = 1: length(plot.date),
         y = factor(nodes, levels = rev(node.y)),
         ylim = c(1, 20),
         pch = 15,
         cex = .75,
         col = "deepskyblue4")
  axis(side = 2,
       labels = rev(letLab),
       at = 1:20,
       cex.axis = .65,
       las = 1,
       col.axis = "deepskyblue4",
       col.ticks = "deepskyblue4")
  axis(side = 1,
       at = c(which(monthday %in% c(1101, 1201, 0101, 0201, 0301)), which(monthday
== 0331) + 1),
       labels = c("Nov", "Dec", "Jan", "Feb", "Mar", "Apr"),
       cex.axis = .75,
       padj = -.5
  )
  mtext(side = 2,
        line = 2,
        text = "Type",
```

```
        cex = .8,
        font = 2,
        col = "deepskyblue4")
  mtext(side = 1,
        line = 2,
        text = "",
        cex = .8,
        font = 2)
  par(new = TRUE)
  plot(wx$HS_cm,
       type = "l",
       axes = FALSE,
       ylim = c(0, 1.5*HSlim),
       xlim = c(0, nrow(wx)),
       lwd = 2,
       xlab = "",
       ylab = "")
  axis(side = 4,
       at = seq(0, HSlim, 50),
       ylab = "HS (cm)",
       cex.axis = .75,
       padj = -.5
  )
  mtext(text ="HS (cm)",
        side = 4,
        line = 2,
        font = 2,
        adj = .333,
        cex = .8
  )
par(xpd = TRUE)
legend( x = 160,
        y = 1.6*HSlim,
        col = c("gray87", "gray67", "gray47", "gray27"),
        lwd = 3,
        legend = c("<1", "1-10", "10-100", ">100"),
        cex = .7,
        title = "DSAI",
        bty = "n"
        )
}
```

Functions for Plotting Weather Metrics for each Synoptic Type

```
#plot a histogram of max/min temp for each node
# arguments:
#      site.name: character, <site.name>_wx
#      SOM: supersom object used in the classification
#      node: Number of node for which to plot the histograms
# outputs:
#      histograms of daily max/min temp for the specified synoptic type
```

```
classTempHist <- function(site.name, SOM, node){
  station <- get(paste(site.name, "_wx", sep = ""))
  node.days <- SOM$unit.classif

  record <- which(node.days == node)
  maxT <- station[record,"maxT_C"]
  minT <- station[record, "minT_C"]
  precip <- station[record, "SWE_cm"]

  minHist <- hist(minT,
      xlim = c(-40,40),
      breaks = 80,
      plot = FALSE)
  col.min <- cut(minHist$breaks, c(-Inf, 0, Inf))
  maxHist <- hist(maxT,
      xlim = c(-40,40),
      breaks = 80,
      plot = FALSE)
  col.max <- cut(maxHist$breaks, c(-Inf, 0, Inf))
  par(mfrow = c(2,1))
  hist(minT,
       xlim = c(-40,40),
       breaks = 80,
       col = c("deepskyblue3", "firebrick")[col.min],
       border = c("deepskyblue3", "firebrick")[col.min],
       main = "Min T (C)")
  abline(v = 0,
         lty = "dashed",
         col = "gray16")
  hist(maxT,
       xlim = c(-40,40),
       breaks = 80,
       col = c("deepskyblue3", "firebrick")[col.max],
       border = c("deepskyblue3", "firebrick")[col.max],
       main = "Max T (C)")
  abline(v = 0,
         lty = "dashed",
         col = "gray16")

}

#plot histograms of max temp for SOM array
# need to run for loop immediately below this function
# Agruments:
#      site.name: character, <site.name>_wx
#      SOM: supersom object used in the classification
#      node: Number of node for which to plot the histograms
#      plot.x, plot.y: “y” or “n” should x- and y- axis ticks be plotted?
maxTempHist <- function(site.name, SOM, node, plot.y = "yes", plot.x = "yes"){
  station <- get(paste(site.name, "_wx", sep = ""))
  node.days <- SOM$unit.classif
```

```
  record <- which(node.days == node)
  maxT <- station[record,"maxT_C"]

  maxHist <- hist(maxT,
                  xlim = c(-40, 40),
                  breaks = 80,
                  plot = FALSE)
  col.max <- cut(maxHist$breaks, c(-Inf, 0, Inf))

  hist(maxT,
       xlim = c(-40,40),
       ylim = c(0,35),
       breaks = 80,
       col = c("deepskyblue3", "firebrick")[col.max],
       border = c("deepskyblue3", "firebrick")[col.max],
       main = "",
       xlab = "",
       ylab = "",
       xaxt = "n",
       yaxt = "n",
       fg = "gray37")
  if(plot.x == "yes"){
  axis(side = 1,
       at = c(-40,0,40),
       mgp = c(3, .5, 0),
       fg = "gray37",
       col.axis = "gray37",
       col.lab = "gray37"
  )}
  if(plot.y == "yes"){
  axis(side = 2,
       at = 30,
       mgp = c(3, .5, 0),
       fg = "gray37",
       col.axis = "gray37",
       col.lab = "gray37"
       )}
  abline(v = 0,
         lty = "dashed",
         col = "gray37")

  box(fg = "gray37")
}

node.layout <- matrix(1:20, nrow = 5, byrow = TRUE)[5:1,]
layout(node.layout)
par(mar = c(1.5, 1.5, 0, 0.1))
for( i in 1:length(unique(node.days))){
maxTempHist(site.name = "jackson",
            SOM = som.90,
            node = i,
            plot.x = ifelse(i %in% 1:4, "yes", "no"),
```

```
            plot.y = ifelse(i %in% c(1,5,9,13,17), "yes", "no"))
}
#plot histograms of min temp for SOM array
# need to run for loop immediately below this function
# Arguments:
#      site.name: character, <site.name>_wx
#      SOM: supersom object used in the classification
#      node: Number of node for which to plot the histograms
#      plot.x, plot.y: “y” or “n” should x- and y- axis ticks be plotted?

minTempHist <- function(site.name, SOM, node, plot.y = "yes", plot.x = "yes"){
  station <- get(paste(site.name, "_wx", sep = ""))
  node.days <- SOM$unit.classif

  record <- which(node.days == node)
  minT <- station[record,"minT_C"]

  minHist <- hist(minT,
                  xlim = c(-40,40),
                  breaks = 80,
                  plot = FALSE)
  col.min <- cut(minHist$breaks, c(-Inf, 0, Inf))

  hist(minT,
       xlim = c(-40,40),
       ylim = c(0,35),
       breaks = 80,
       col = c("deepskyblue3", "firebrick")[col.min],
       border = c("deepskyblue3", "firebrick")[col.min],
       main = "",
       xlab = "",
       ylab = "",
       xaxt = "n",
       yaxt = "n",
       fg = "gray37"
       )
  abline(v = 0,
         lty = "dashed",
         col = "gray27")
  if(plot.x == "yes") {
  axis(side = 1,
       at = c(-40,0,40),
       mgp = c(3, .5, 0),
       fg = "gray37",
       col.axis = "gray37",
       col.lab = "gray37"
  )}

  if(plot.y == "yes"){
  axis(side = 2,
       at = 30,
       mgp = c(3, .5, 0),
```

```
      fg = "gray37",
      col.axis = "gray37",
      col.lab = "gray37"
  )}

  box(fg = "gray37")
}

node.layout <- matrix(1:20, nrow = 5, byrow = TRUE)[5:1,]
layout(node.layout)
par(mar = c(1.5, 1.5, 0, 0.1))
for( i in 1:length(unique(node.days))){
minTempHist(site.name = "jackson",
            SOM = som.90,
            node = i,
            plot.x = ifelse(i %in% 1:4, "yes", "no"),
            plot.y = ifelse(i %in% c(1,5,9,13,17), "yes", "no"))
}
#plot histograms of SWE for SOM array
# need to run for loop immediately below this function
# arguments:
#      site.name: character, <site.name>_wx
#      SOM: supersom object used in the classification
#      node: Number of node for which to plot the histograms
#      xlim, ylim, xlab: passed to hist() function
#      swebreaks: breaks to be used in the histogram, which will depend on the
range of
#      precipitation events.
#      plot.x, plot.y: “yes” or “no”. should x- and y- axis ticks be plotted?
sweHist <- function(site.name, SOM, node, xlim, ylim, xlab, swebreaks, plot.y =
"yes", plot.x = "yes"){
  station <- get(paste(site.name, "_wx", sep = ""))
  node.days <- SOM$unit.classif

  record <- which(node.days == node)
  swe <- station[record,"SWE_cm"]
  swe<- swe[which(swe>0)]

  sweHist <- hist(swe,
                  breaks = swebreaks,
                  plot = FALSE
                  )
  col.swe <- cut(sweHist$breaks, c(0, 1, 2.5, 4.999, Inf))

  hist(swe,
       xlim = xlim,
       ylim = ylim,
       breaks = swebreaks,
       col = c("green", "green4", "blue","deeppink3")[col.swe],
       border = c("green", "green4", "blue", "deeppink3")[col.swe],
       main = "",
       xlab = "",
```

```
      ylab = "",
      axes = FALSE
      )
  if(plot.x == "yes"){
  axis(1,
      at = xlab,
      labels = xlab*10,
      mgp = c(3, .5, 0)
      )}
  if(plot.y == "yes"){
  axis(2,
      at = ylim-5,
      mgp = c(3, .5, 0)
      )}
  box()
}

node.layout <- matrix(1:20, nrow = 5, byrow = TRUE)[5:1,]
layout(node.layout)
par(mai = c(0,0,0,0))
for(i in 1:length(unique(som.90$unit.classif))){

  sweHist(site.name = "bridger", SOM = som.90, node = i, ylim = c(0,20))
}

#generate plot of maxT and swe for each class
par(mai = c(0,0,0,0) + .2)
for(i in 1:length(unique(node.days))){
  tiff(filename = paste("bs_maxT_", i, ".tif", sep = ""))
  maxTempHist(site.name = "bigsky", SOM = test.som, node = i)
  dev.off()
  tiff(filename = paste("bs_swe_", i, ".tif", sep = ""))
  sweHist(site.name = "bigsky", SOM = test.som, node = i, ylim = c(0,15))
  dev.off()
}

#funtion to return table of quantiles for SWE for specified site
sweQuantile <- function(site.name, SOM){
  station <- get(paste(site.name, "_wx", sep = ""))
  node.days <- SOM$unit.classif
  nNodes <- length(unique(node.days))
  nRows <- SOM$grid$ydim
  nCols <- SOM$grid$xdim
  swe <- station[,"SWE_cm"]*10
  maxT <- station[ , "maxT_C"]
  minT <- station[ , "minT_C"]

  quantMat <- matrix(nrow = nNodes, ncol = 4)
  minMat <- maxMat <- matrix(nrow = nNodes, ncol = 3)

  for (node in 1:nNodes){
  type <- which(node.days == node)
```

```
  precip <- swe[type]
  precipEvents <- precip[which(precip >0)]
  maxTemp <- maxT[type]
  minTemp <- minT[type]

  SWEquants <- quantile(na.omit(precipEvents), c(.5, .75, .9))
  zeros <- length(which(precip == 0))
  zero.prop <- zeros/length(na.omit(precip))

  MaxTempQuants <- quantile(na.omit(maxTemp), c(.25, .5, .75))
  MinTempQuants <- quantile(na.omit(minTemp), c(.25, .5, .75))

  maxMat[node, ] <- MaxTempQuants
  minMat[node, ] <- MinTempQuants

  quantMat[node, 1:3] <- SWEquants
  quantMat[node, 4] <- (1-zero.prop)*100
  }


  layout.mat <- matrix(1:nNodes,
                       ncol = nCols,
                       byrow = TRUE)[nRows:1,]

  quantMat <- quantMat[as.vector(t(layout.mat)), ]
  minMat <- minMat[as.vector(t(layout.mat)), ]
  maxMat <- maxMat[as.vector(t(layout.mat)), ]

  colnames(quantMat) <- c("50", "75", "90", "% > 0")
  colnames(minMat) <- colnames(maxMat) <- c("25", "50", "75")
  rownames(quantMat) <- rownames(minMat) <- rownames(maxMat) <- LETTERS[1:nNodes]

  attributes(sweQuantile) <- list("sweMat" = t(quantMat),
                                  "maxMat" = t(maxMat),
                                  "minMat" = t(minMat),
                                  "full" = rbind(t(quantMat), t(maxMat),
t(minMat)))
    }
```

APPENDIX D

SEASONAL TIME SERIES OF DSAI SCORES AND DAILY SYNOPTIC TYPE

The plots on the following pages show annual time series of daily synoptic type, total snow depth in cm (HS), and daily DSAI score. The daily synoptic type is marked by a blue box corresponding with a scale on the y-axis on the left side of the plot. HS is shown as a line corresponding with the scale on the y-axis on the right-hand side of the plot. Daily DSAI score is shown with vertical bars for days when DSAI > 0. The bars are color-coded based on daily DSAI score at intervals of 1, 10, and 100.

Bridger Bowl

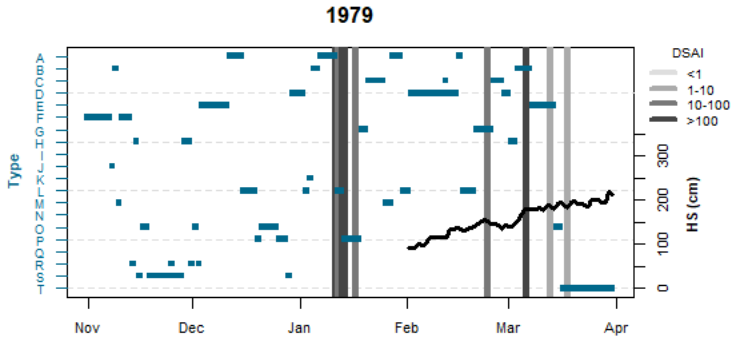

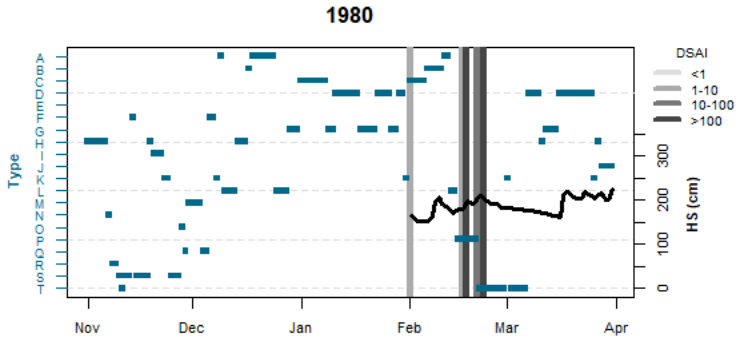

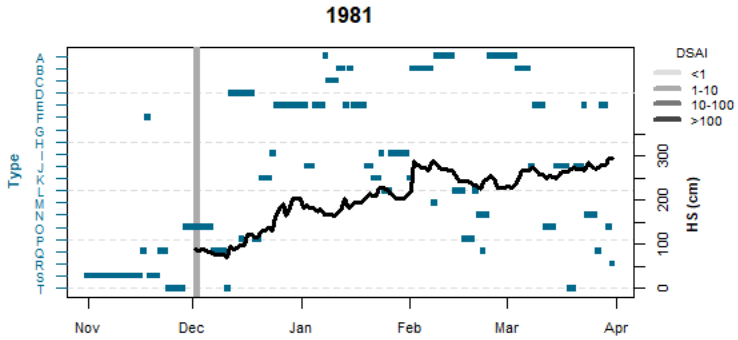

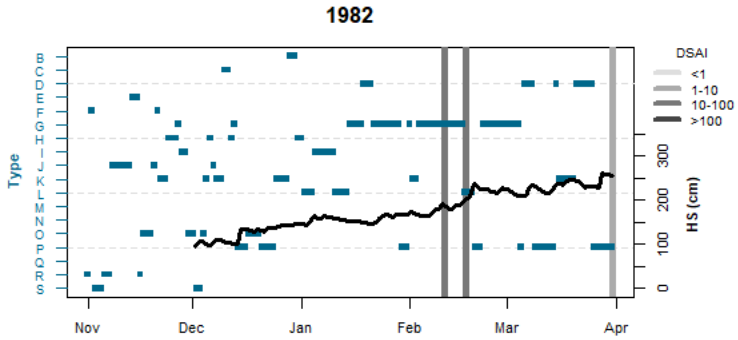

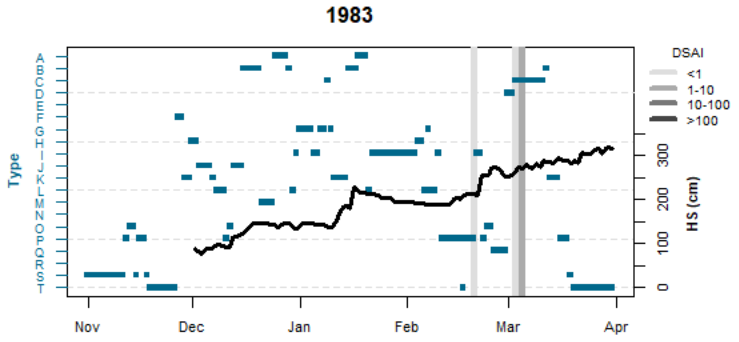
1983
Type
DSAI
<1
1-10
10-100
>100
HS (cm)
0
100
200
300
Nov
Dec
Jan
Feb
Mar
Apr

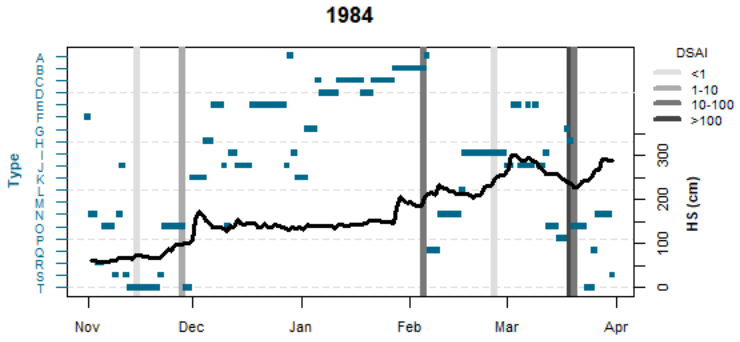
1984
Type
DSAI
<1
1-10
10-100
>100
HS (cm)
0
100
200
300
Nov
Dec
Jan
Feb
Mar
Apr

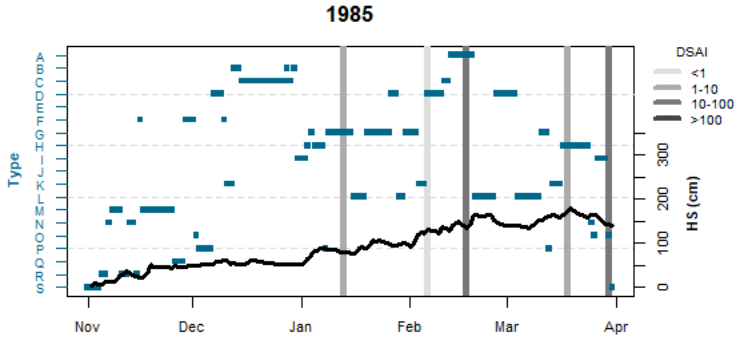
1985
Type
DSAI
<1
1-10
10-100
>100
HS (cm)
0
100
200
300
Nov
Dec
Jan
Feb
Mar
Apr

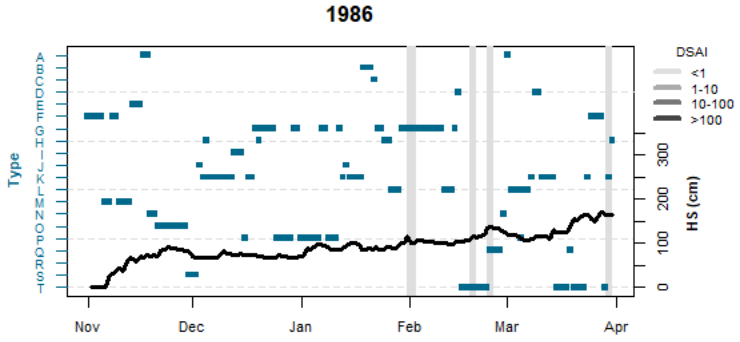
1986
Type
DSAI
<1
1-10
10-100
>100
HS (cm)
0
100
200
300
Nov
Dec
Jan
Feb
Mar
Apr

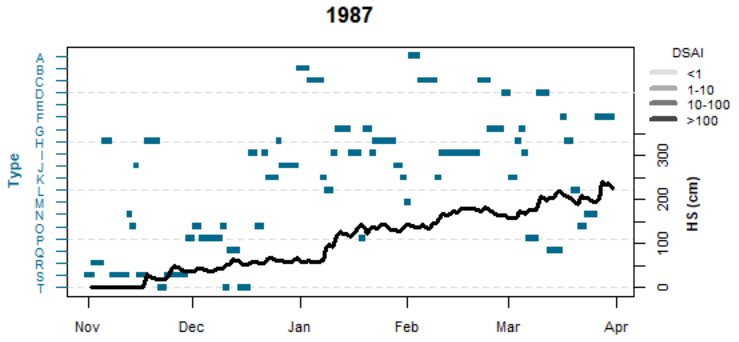
1987
Type
DSAI
<1
1-10
10-100
>100
HS (cm)
0
100
200
300
Nov
Dec
Jan
Feb
Mar
Apr

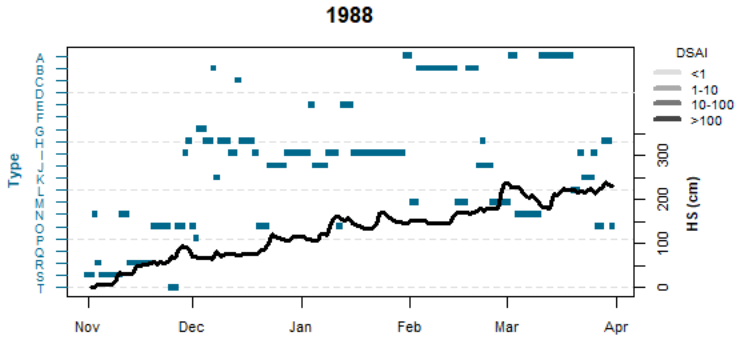
1988
Type
DSAI
<1
1-10
10-100
>100
HS (cm)
0
100
200
300
Nov
Dec
Jan
Feb
Mar
Apr

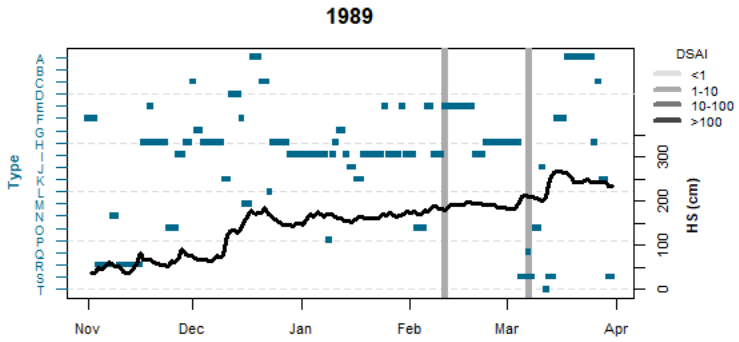
1989
Type
DSAI
<1
1-10
10-100
>100
HS (cm)
0
100
200
300
Nov
Dec
Jan
Feb
Mar
Apr

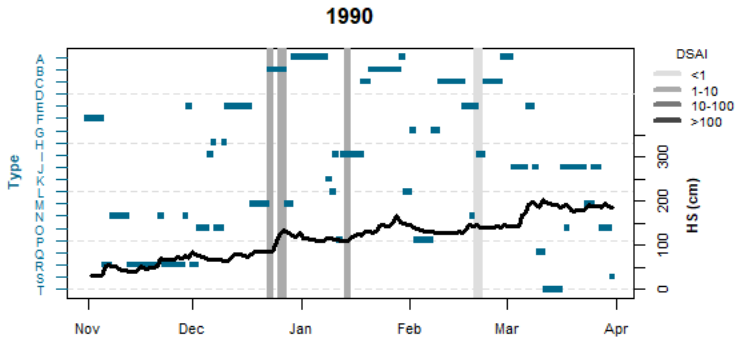
1990
Type
DSAI
<1
1-10
10-100
>100
HS (cm)
0
100
200
300
Nov
Dec
Jan
Feb
Mar
Apr

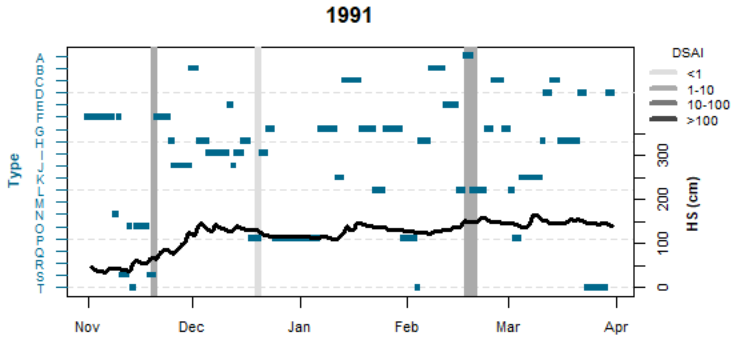
1991
Type
DSAI
<1
1-10
10-100
>100
HS (cm)
0
100
200
300
Nov
Dec
Jan
Feb
Mar
Apr

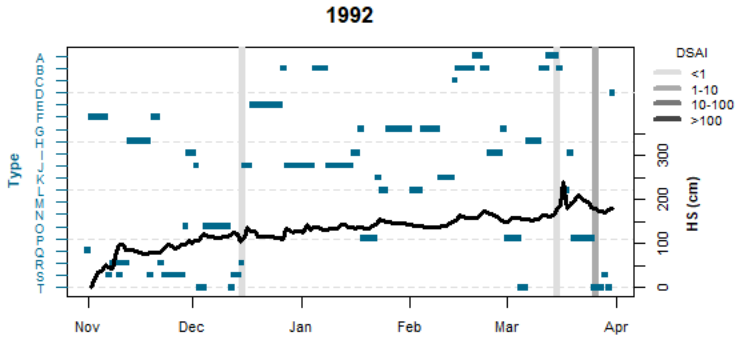
1992
Type
DSAI
<1
1-10
10-100
>100
HS (cm)
0
100
200
300
Nov
Dec
Jan
Feb
Mar
Apr

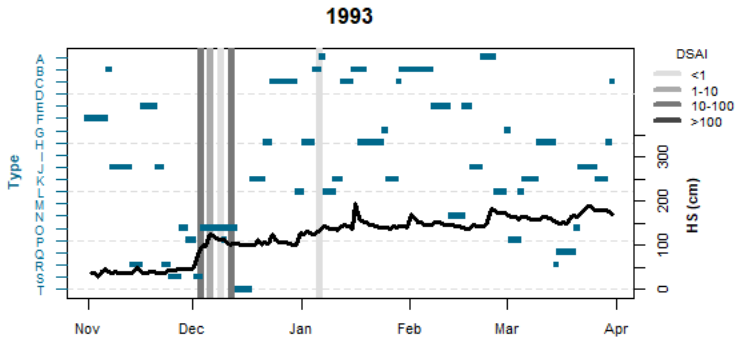
1993
Type
DSAI
<1
1-10
10-100
>100
HS (cm)
0
100
200
300
Nov
Dec
Jan
Feb
Mar
Apr

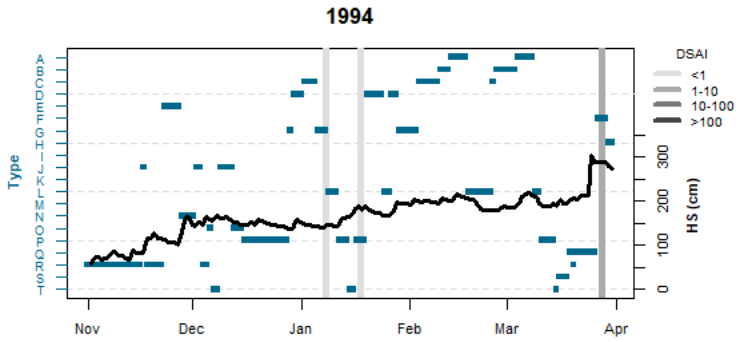
1994
Type
DSAI
<1
1-10
10-100
>100
HS (cm)
0
100
200
300
Nov
Dec
Jan
Feb
Mar
Apr

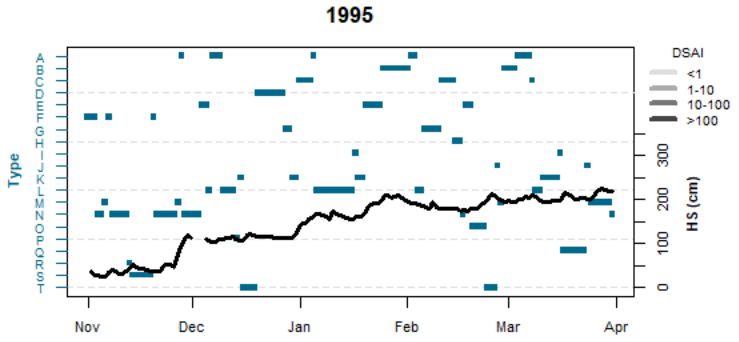
1995
Type
DSAI
<1
1-10
10-100
>100
HS (cm)
0
100
200
300
Nov
Dec
Jan
Feb
Mar
Apr

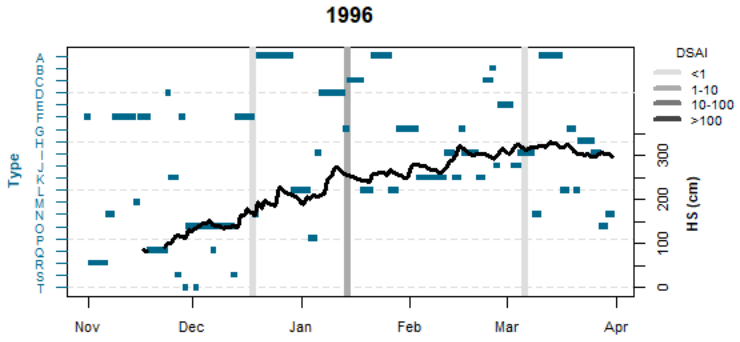
1996
Type
DSAI
<1
1-10
10-100
>100
HS (cm)
0
100
200
300
Nov
Dec
Jan
Feb
Mar
Apr

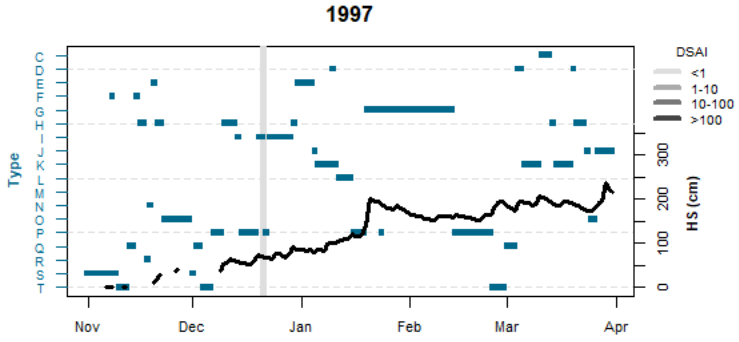
1997
Type
DSAI
<1
1-10
10-100
>100
HS (cm)
0
100
200
300
Nov
Dec
Jan
Feb
Mar
Apr

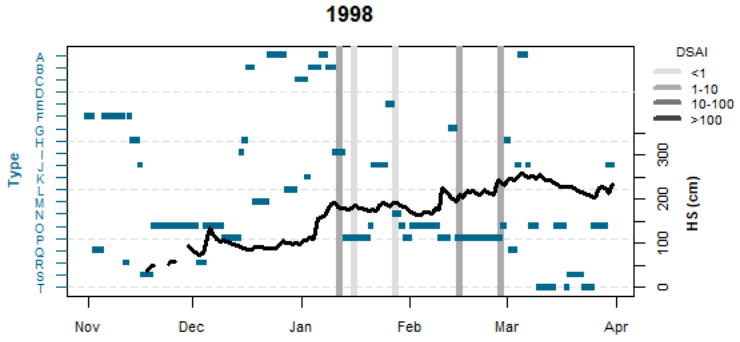
1998
Type
DSAI
<1
1-10
10-100
>100
HS (cm)
0
100
200
300
Nov
Dec
Jan
Feb
Mar
Apr

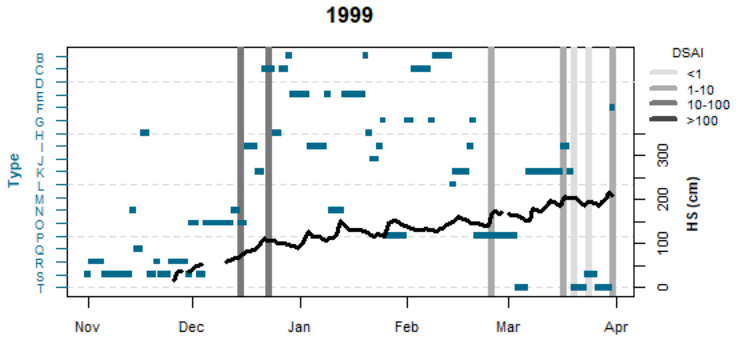
1999
Type
DSAI
<1
1-10
10-100
>100
HS (cm)
0
100
200
300
Nov
Dec
Jan
Feb
Mar
Apr

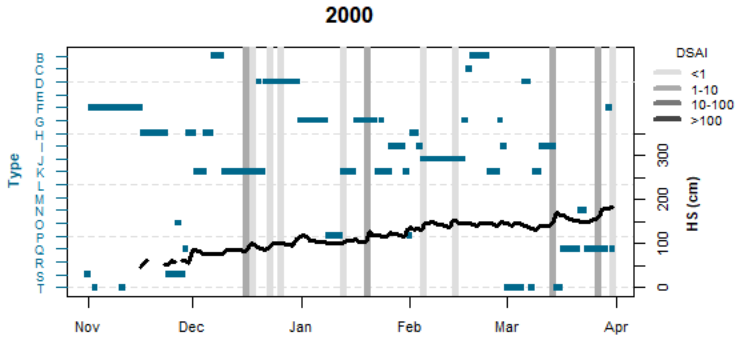
2000
Type
DSAI
<1
1-10
10-100
>100
HS (cm)
0
100
200
300
Nov
Dec
Jan
Feb
Mar
Apr

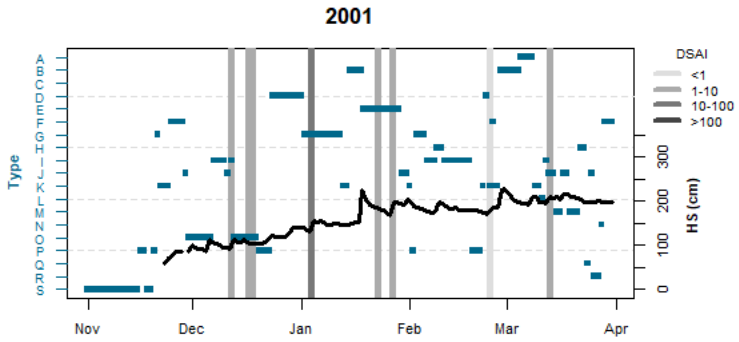
2001
Type
DSAI
<1
1-10
10-100
>100
HS (cm)
0
100
200
300
Nov
Dec
Jan
Feb
Mar
Apr

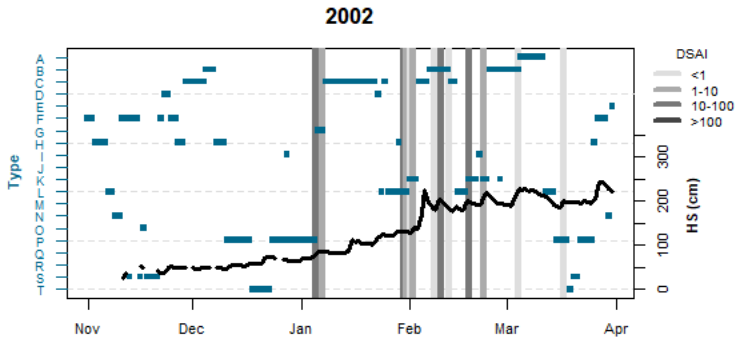
2002
Type
DSAI
<1
1-10
10-100
>100
HS (cm)
0
100
200
300
Nov
Dec
Jan
Feb
Mar
Apr

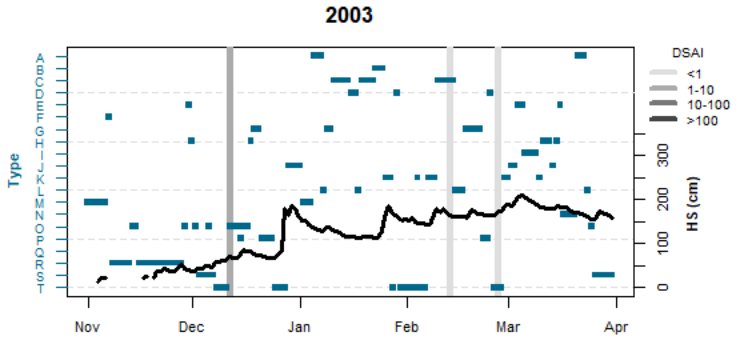
2003
Type
DSAI
<1
1-10
10-100
>100
HS (cm)
0
100
200
300
Nov
Dec
Jan
Feb
Mar
Apr

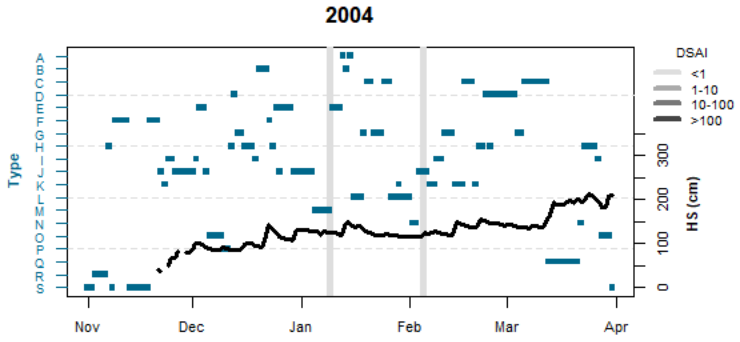
2004
Type
DSAI
<1
1-10
10-100
>100
HS (cm)
0
100
200
300
Nov
Dec
Jan
Feb
Mar
Apr

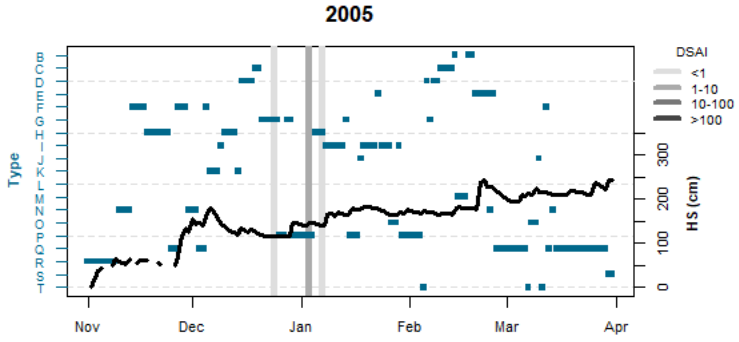
2005
Type
DSAI
<1
1-10
10-100
>100
HS (cm)
0
100
200
300
Nov
Dec
Jan
Feb
Mar
Apr

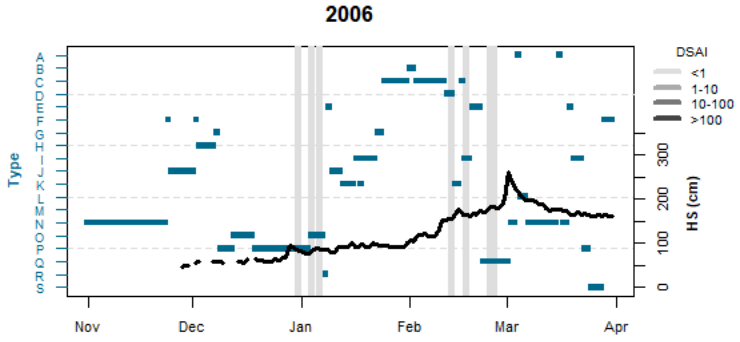
2006
Type
DSAI
<1
1-10
10-100
>100
HS (cm)
0
100
200
300
Nov
Dec
Jan
Feb
Mar
Apr

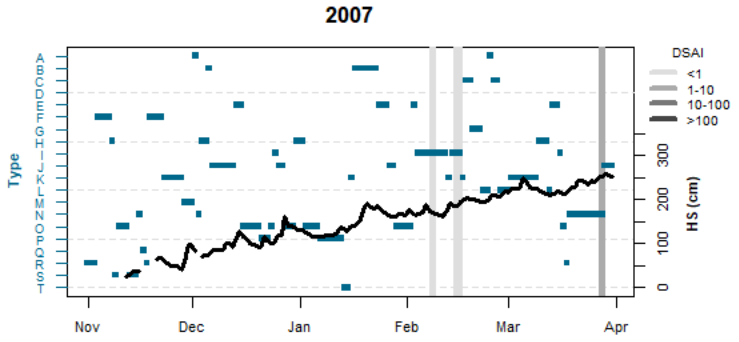
2007
Type
DSAI
<1
1-10
10-100
>100
HS (cm)
0
100
200
300
Nov
Dec
Jan
Feb
Mar
Apr

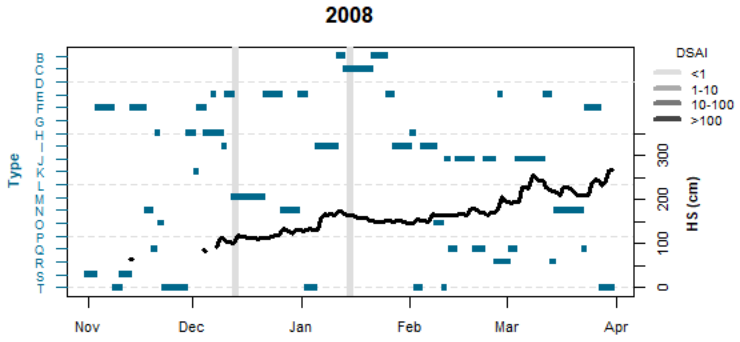
2008
Type
DSAI
<1
1-10
10-100
>100
HS (cm)
0
100
200
300
Nov
Dec
Jan
Feb
Mar
Apr

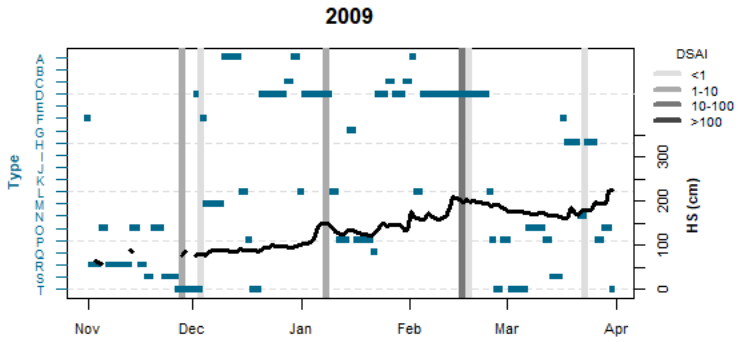
2009
Type
DSAI
<1
1-10
10-100
>100
HS (cm)
0
100
200
300
Nov
Dec
Jan
Feb
Mar
Apr

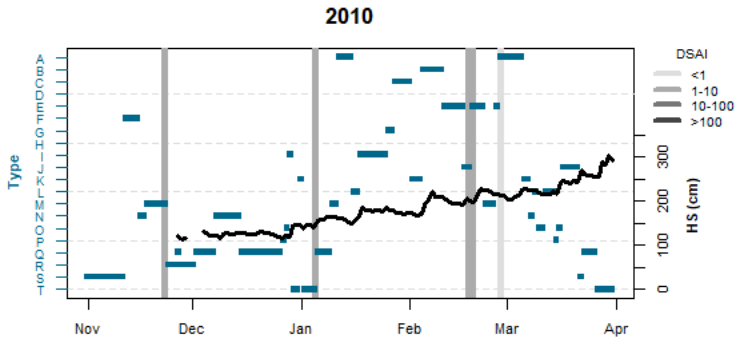
2010
Type
DSAI
<1
1-10
10-100
>100
HS (cm)
0
100
200
300
Nov
Dec
Jan
Feb
Mar
Apr

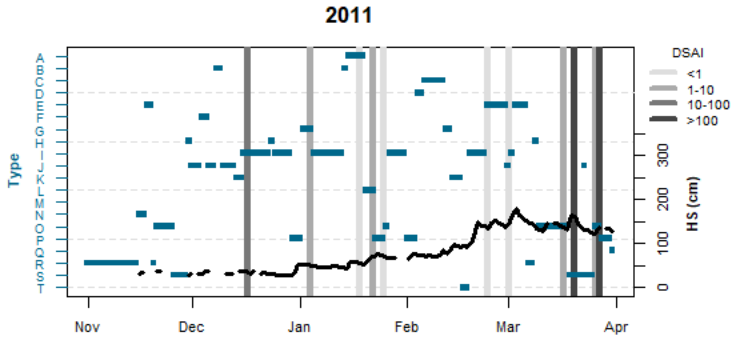
2011
Type
DSAI
<1
1-10
10-100
>100
HS (cm)
0
100
200
300
Nov
Dec
Jan
Feb
Mar
Apr

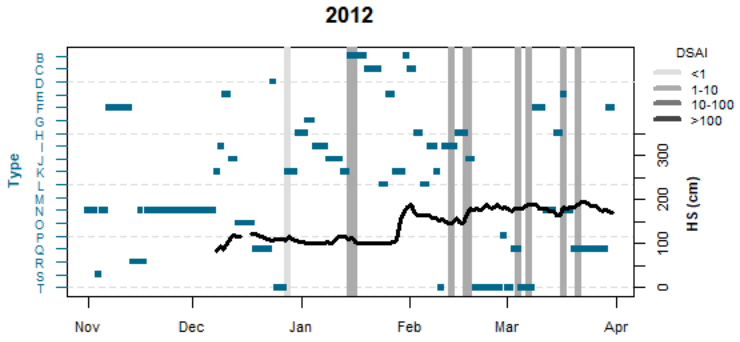
2012
Type
DSAI
<1
1-10
10-100
>100
HS (cm)
0
100
200
300
Nov
Dec
Jan
Feb
Mar
Apr

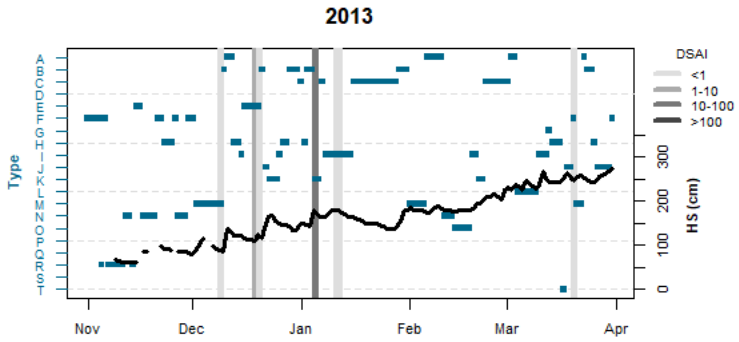
2013
Type
DSAI
<1
1-10
10-100
>100
HS (cm)
0
100
200
300
Nov
Dec
Jan
Feb
Mar
Apr

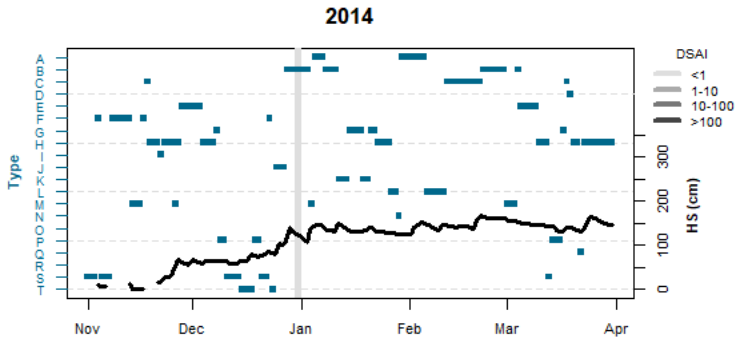
2014
Type
DSAI
<1
1-10
10-100
>100
HS (cm)
0
100
200
300
Nov
Dec
Jan
Feb
Mar
Apr

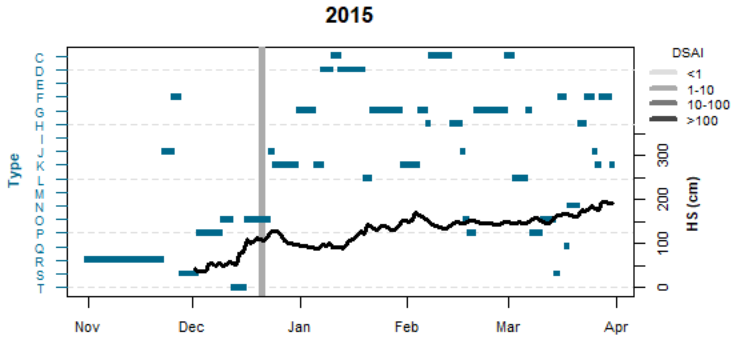
2015
Type
HS (cm)
DSAI
<1
1-10
10-100
>100
Nov
Dec
Jan
Feb
Mar
Apr

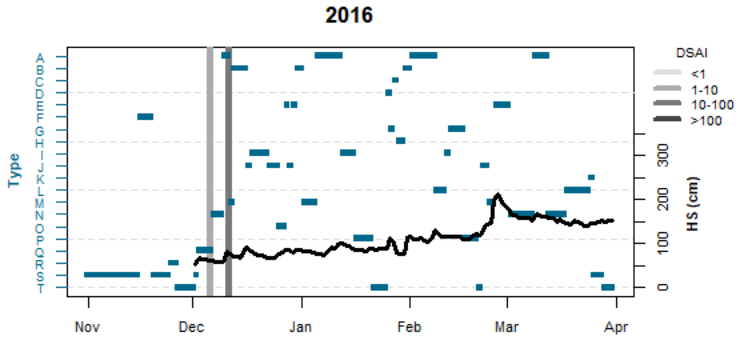
2016
Type
HS (cm)
DSAI
<1
1-10
10-100
>100
Nov
Dec
Jan
Feb
Mar
Apr

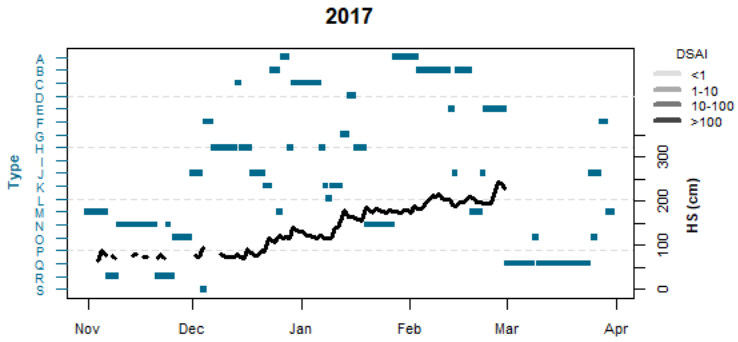
2017
Type
HS (cm)
DSAI
<1
1-10
10-100
>100
Nov
Dec
Jan
Feb
Mar
Apr

Jackson Hole

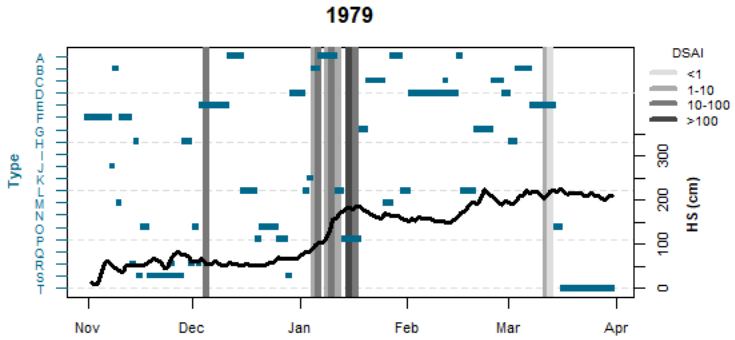

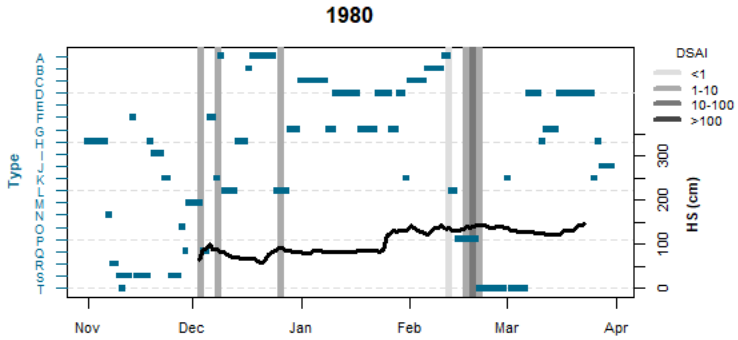

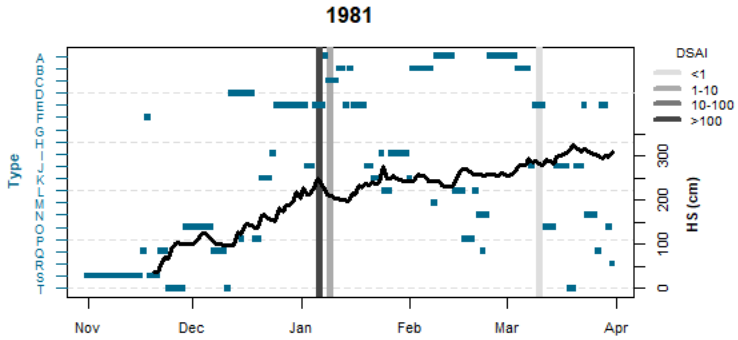

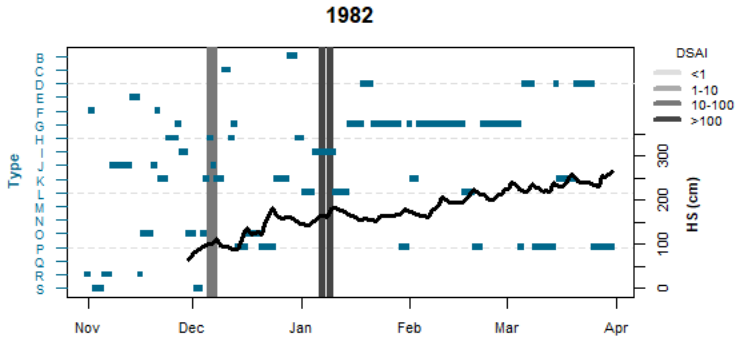

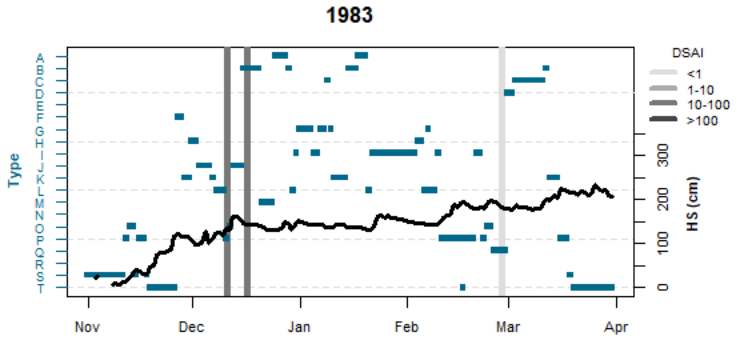
1983
Type
DSAI
<1
1-10
10-100
>100
HS (cm)
0
100
200
300
Nov
Dec
Jan
Feb
Mar
Apr

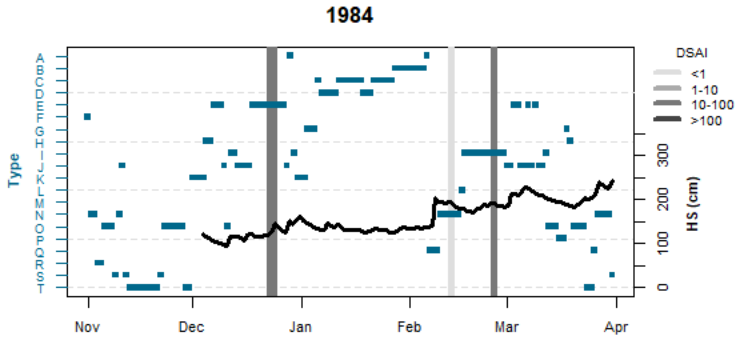
1984
Type
DSAI
<1
1-10
10-100
>100
HS (cm)
0
100
200
300
Nov
Dec
Jan
Feb
Mar
Apr

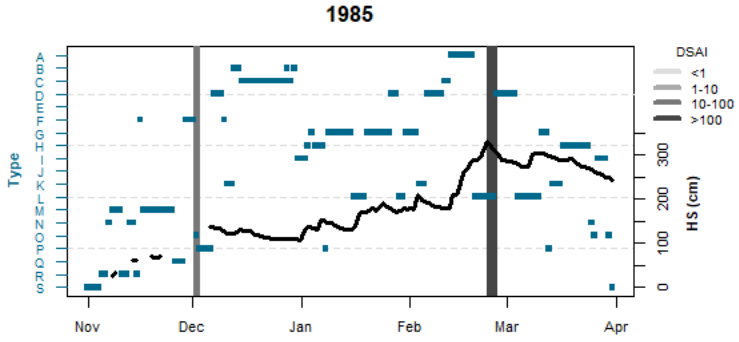
1985
Type
DSAI
<1
1-10
10-100
>100
HS (cm)
0
100
200
300
Nov
Dec
Jan
Feb
Mar
Apr

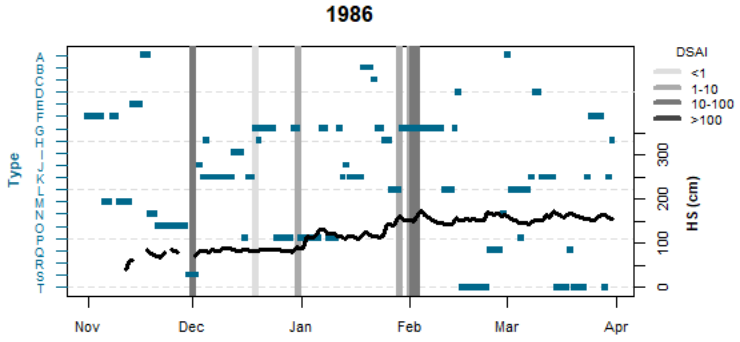
1986
Type
DSAI
<1
1-10
10-100
>100
HS (cm)
0
100
200
300
Nov
Dec
Jan
Feb
Mar
Apr

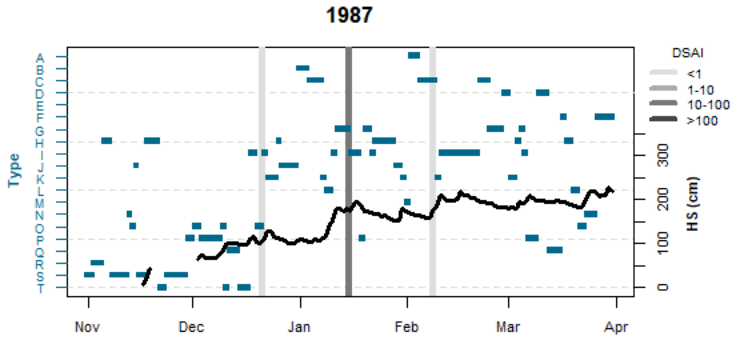
1987
Type
DSAI
<1
1-10
10-100
>100
HS (cm)
0
100
200
300
Nov
Dec
Jan
Feb
Mar
Apr

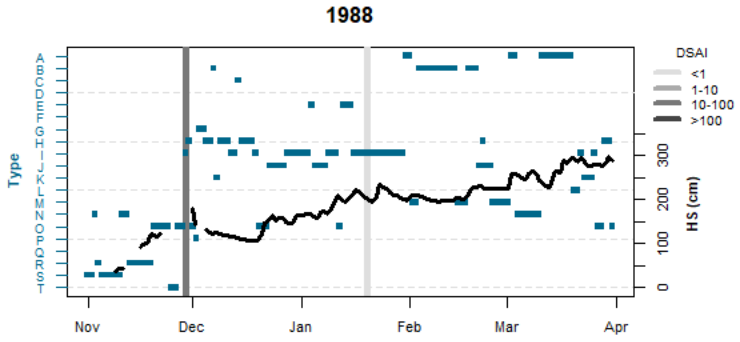
1988
Type
DSAI
<1
1-10
10-100
>100
HS (cm)
0
100
200
300
Nov
Dec
Jan
Feb
Mar
Apr

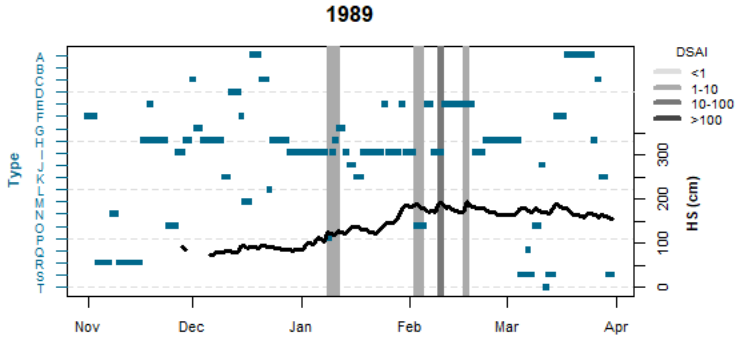
1989
Type
DSAI
<1
1-10
10-100
>100
HS (cm)
0
100
200
300
Nov
Dec
Jan
Feb
Mar
Apr

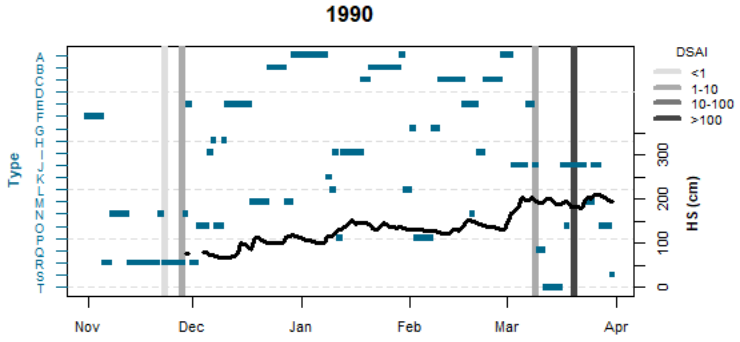
1990
Type
DSAI
<1
1-10
10-100
>100
HS (cm)
0
100
200
300
Nov
Dec
Jan
Feb
Mar
Apr

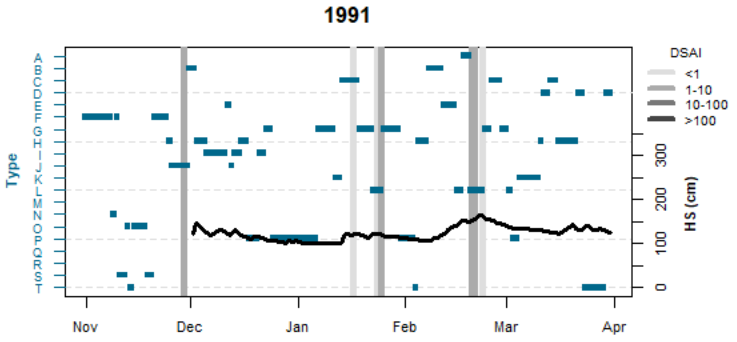
1991
Type
HS (cm)
DSAI
<1
1-10
10-100
>100
Nov
Dec
Jan
Feb
Mar
Apr

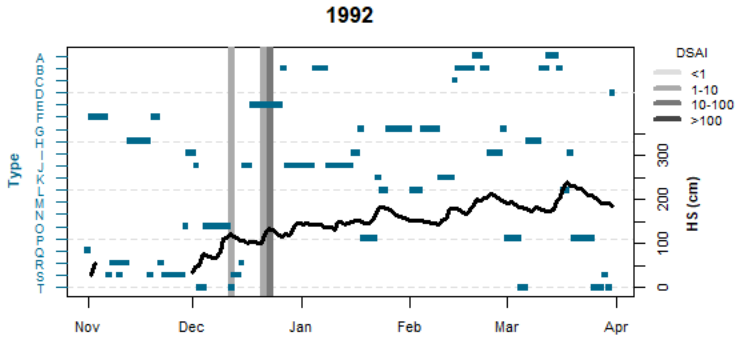
1992
Type
HS (cm)
DSAI
<1
1-10
10-100
>100
Nov
Dec
Jan
Feb
Mar
Apr

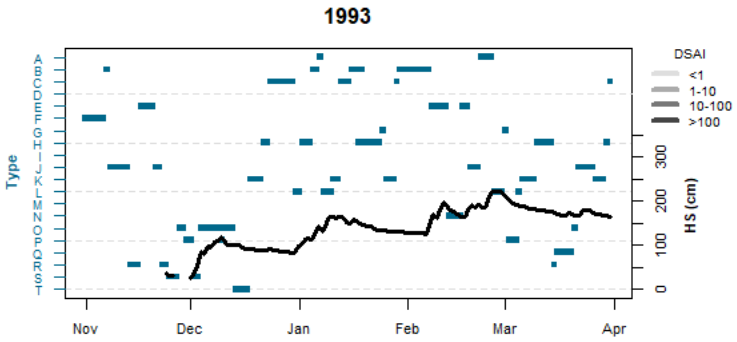
1993
Type
HS (cm)
DSAI
<1
1-10
10-100
>100
Nov
Dec
Jan
Feb
Mar
Apr

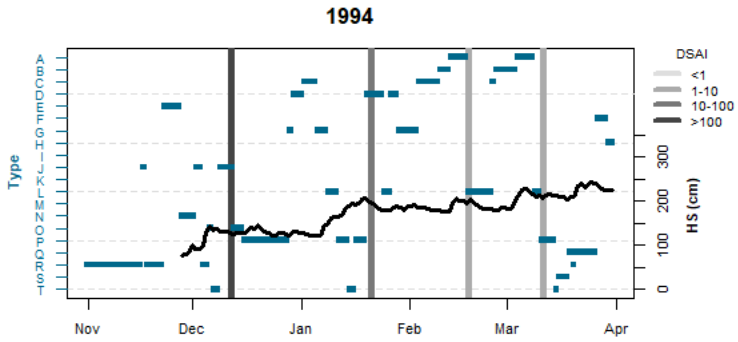
1994
Type
HS (cm)
DSAI
<1
1-10
10-100
>100
Nov
Dec
Jan
Feb
Mar
Apr

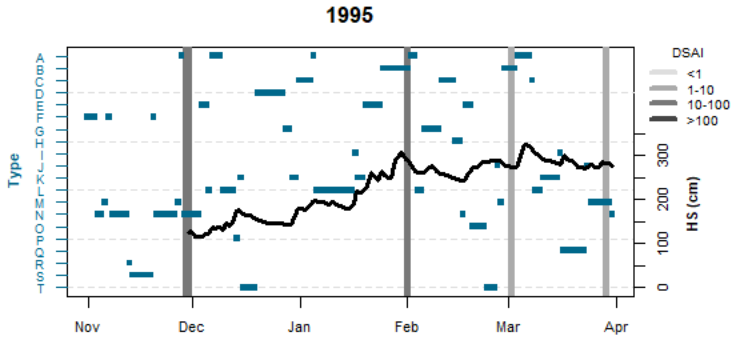
1995
Type
DSAI
<1
1-10
10-100
>100
HS (cm)
0
100
200
300
Nov
Dec
Jan
Feb
Mar
Apr

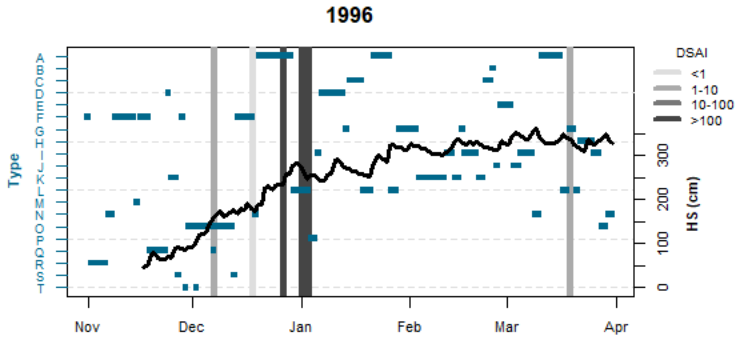
1996
Type
DSAI
<1
1-10
10-100
>100
HS (cm)
0
100
200
300
Nov
Dec
Jan
Feb
Mar
Apr

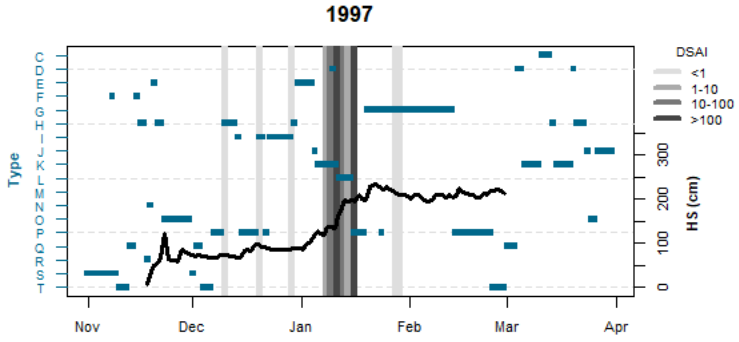
1997
Type
DSAI
<1
1-10
10-100
>100
HS (cm)
0
100
200
300
Nov
Dec
Jan
Feb
Mar
Apr

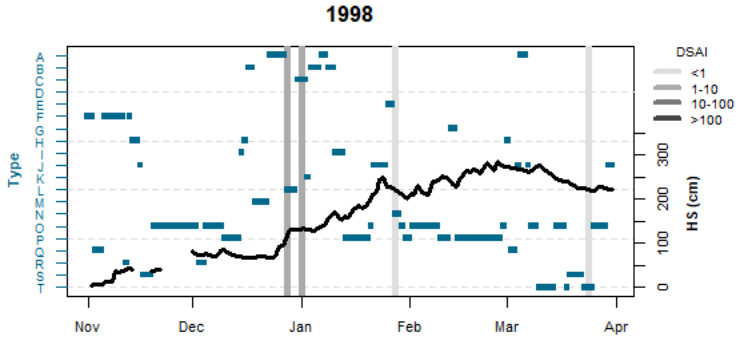
1998
Type
DSAI
<1
1-10
10-100
>100
HS (cm)
0
100
200
300
Nov
Dec
Jan
Feb
Mar
Apr

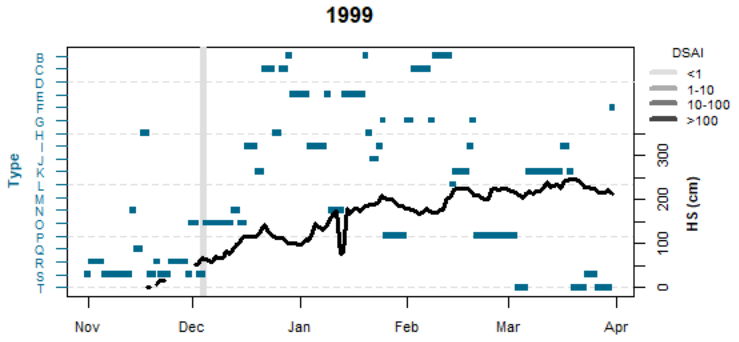
1999
Type
DSAI
<1
1-10
10-100
>100
HS (cm)
0
100
200
300
Nov
Dec
Jan
Feb
Mar
Apr

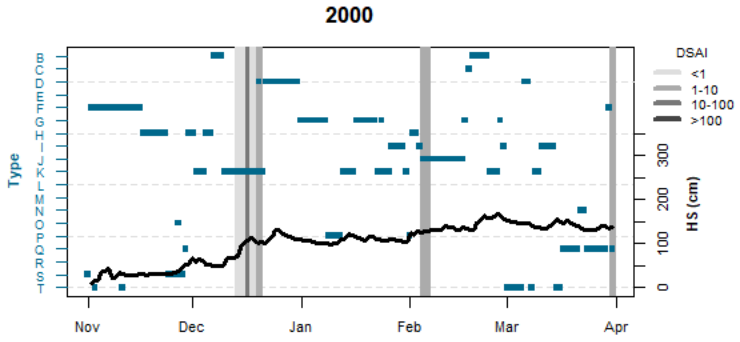
2000
Type
DSAI
<1
1-10
10-100
>100
HS (cm)
0
100
200
300
Nov
Dec
Jan
Feb
Mar
Apr

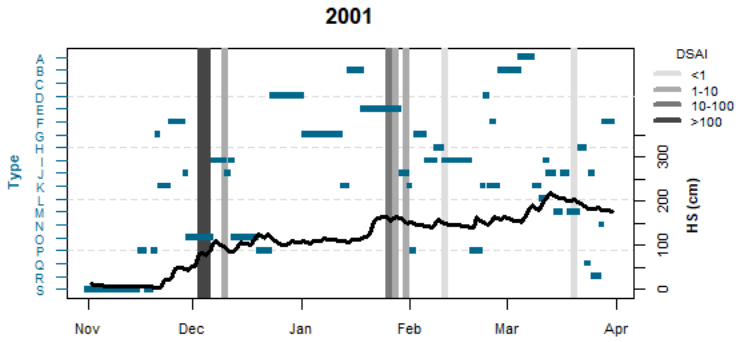
2001
Type
DSAI
<1
1-10
10-100
>100
HS (cm)
0
100
200
300
Nov
Dec
Jan
Feb
Mar
Apr

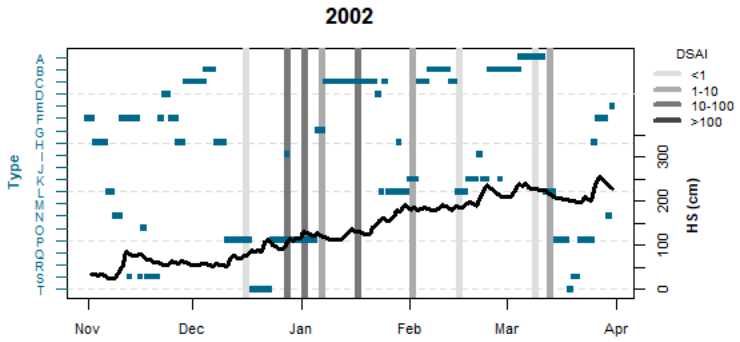
2002
Type
DSAI
<1
1-10
10-100
>100
HS (cm)
0
100
200
300
Nov
Dec
Jan
Feb
Mar
Apr

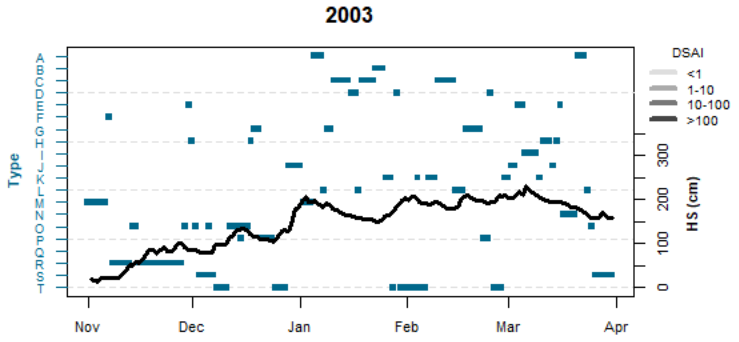
2003
Type
DSAI
<1
1-10
10-100
>100
HS (cm)
0
100
200
300
Nov
Dec
Jan
Feb
Mar
Apr

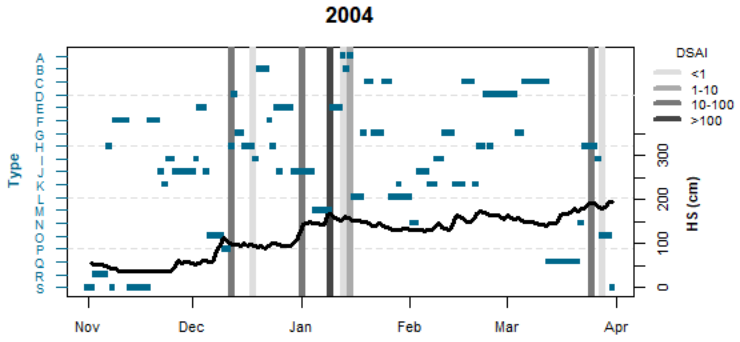
2004
Type
DSAI
<1
1-10
10-100
>100
HS (cm)
0
100
200
300
Nov
Dec
Jan
Feb
Mar
Apr

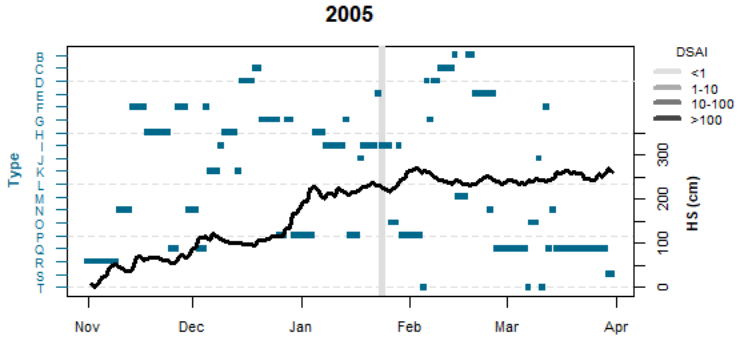
2005
Type
DSAI
<1
1-10
10-100
>100
HS (cm)
0
100
200
300
Nov
Dec
Jan
Feb
Mar
Apr

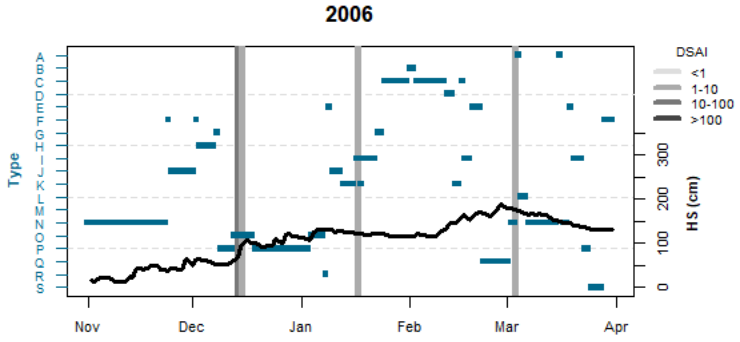
2006
Type
DSAI
<1
1-10
10-100
>100
HS (cm)
0
100
200
300
Nov
Dec
Jan
Feb
Mar
Apr

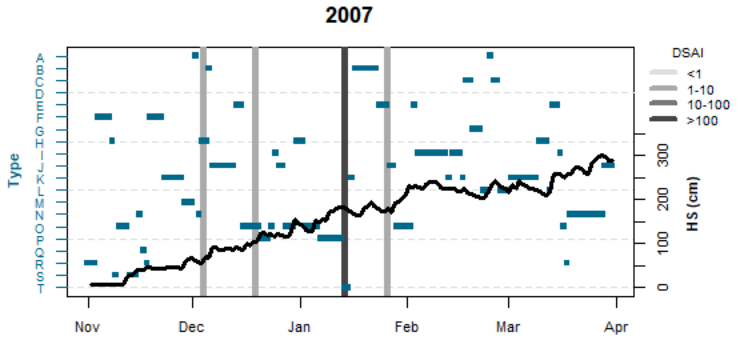
2007
Type
DSAI
<1
1-10
10-100
>100
HS (cm)
0
100
200
300
Nov
Dec
Jan
Feb
Mar
Apr

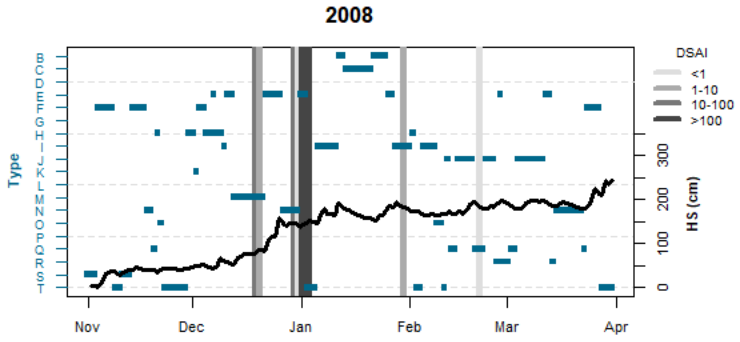
2008
Type
DSAI
<1
1-10
10-100
>100
HS (cm)
0
100
200
300
Nov
Dec
Jan
Feb
Mar
Apr

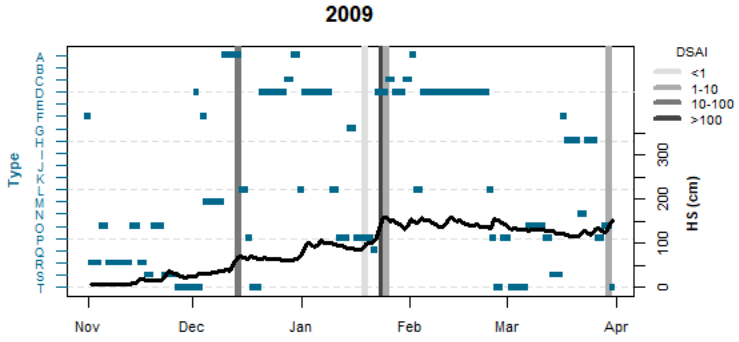
2009
Type
DSAI
<1
1-10
10-100
>100
HS (cm)
0
100
200
300
Nov
Dec
Jan
Feb
Mar
Apr

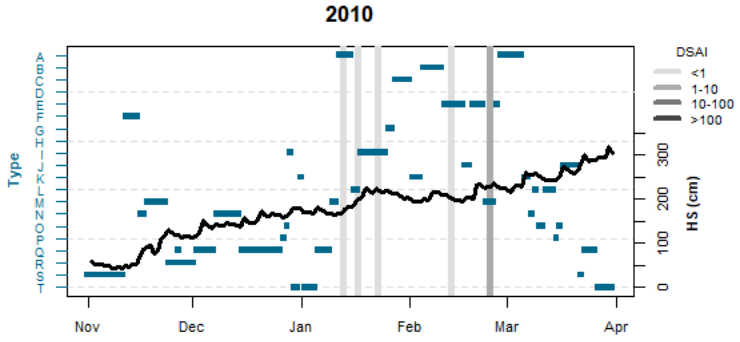
2010
Type
DSAI
<1
1-10
10-100
>100
HS (cm)
0
100
200
300
Nov
Dec
Jan
Feb
Mar
Apr

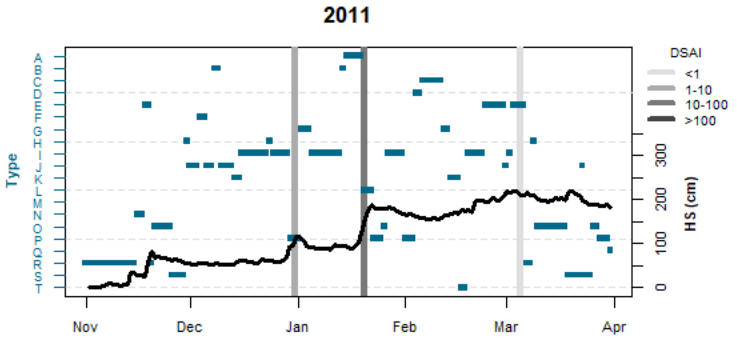
2011
Type
DSAI
<1
1-10
10-100
>100
HS (cm)
0
100
200
300
Nov
Dec
Jan
Feb
Mar
Apr

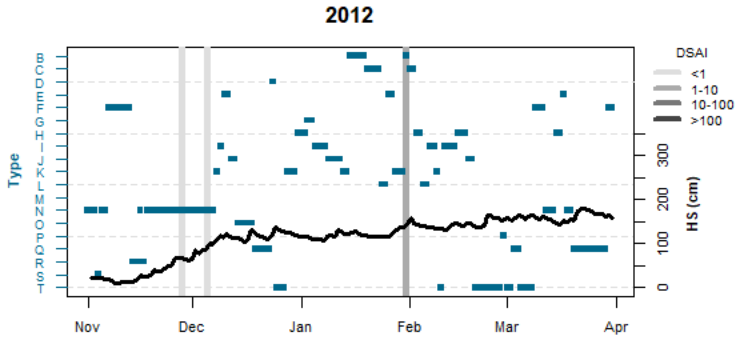
2012
Type
DSAI
<1
1-10
10-100
>100
HS (cm)
0
100
200
300
Nov
Dec
Jan
Feb
Mar
Apr

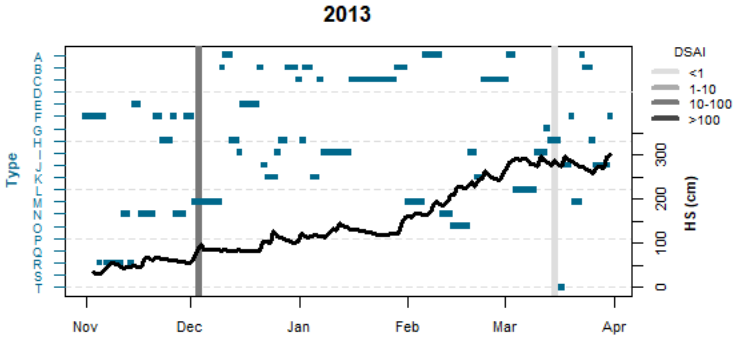
2013
Type
DSAI
<1
1-10
10-100
>100
HS (cm)
0
100
200
300
Nov
Dec
Jan
Feb
Mar
Apr

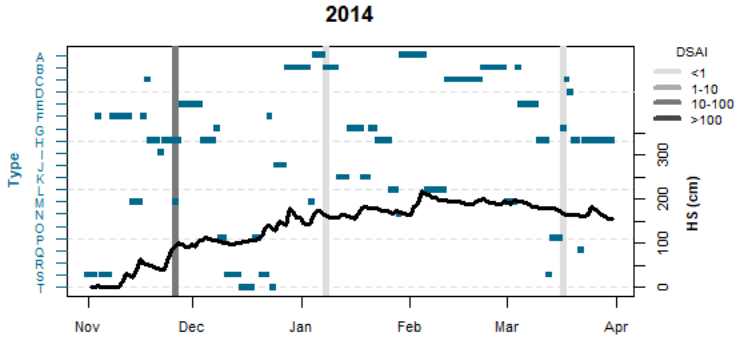
2014
Type
DSAI
<1
1-10
10-100
>100
HS (cm)
0
100
200
300
Nov
Dec
Jan
Feb
Mar
Apr

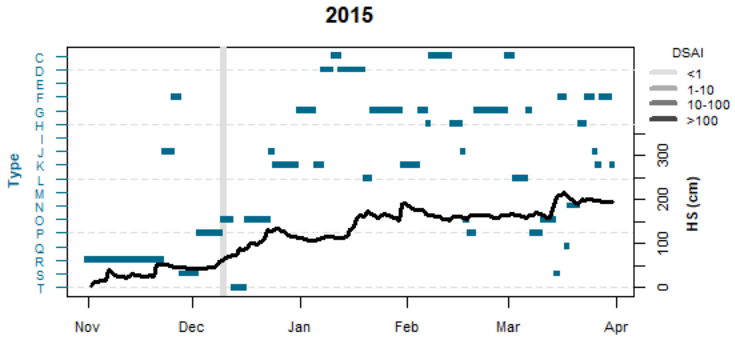
2015
Type
HS (cm)
DSAI
<1
1-10
10-100
>100
Nov
Dec
Jan
Feb
Mar
Apr

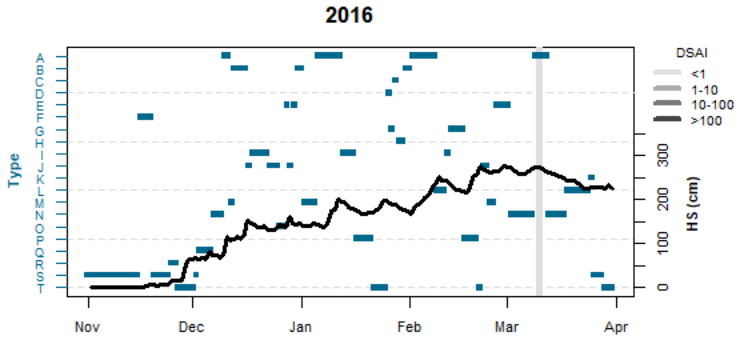
2016
Type
HS (cm)
DSAI
<1
1-10
10-100
>100
Nov
Dec
Jan
Feb
Mar
Apr

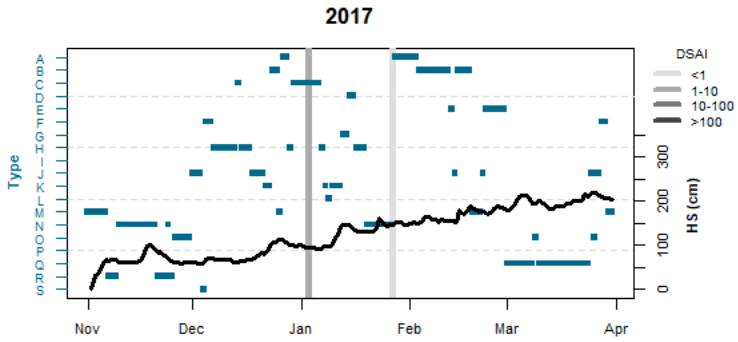
2017
Type
HS (cm)
DSAI
<1
1-10
10-100
>100
Nov
Dec
Jan
Feb
Mar
Apr

Mammoth Mountain

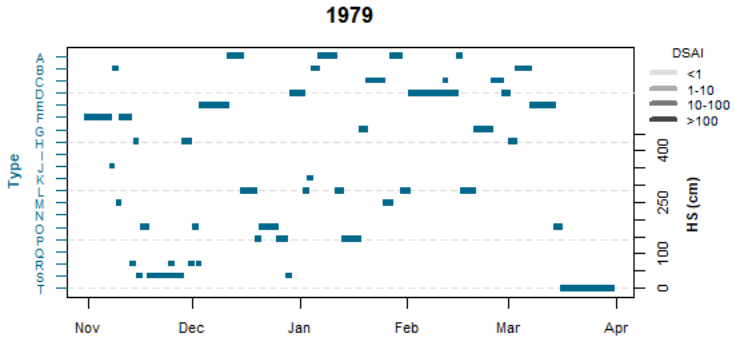

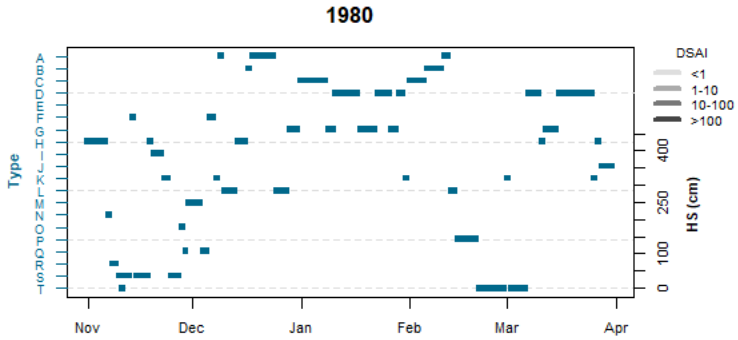

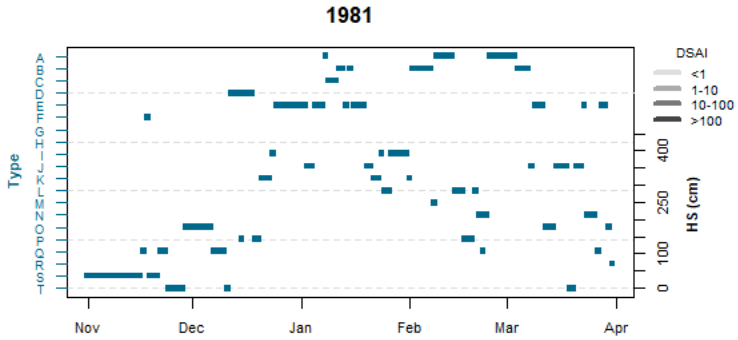

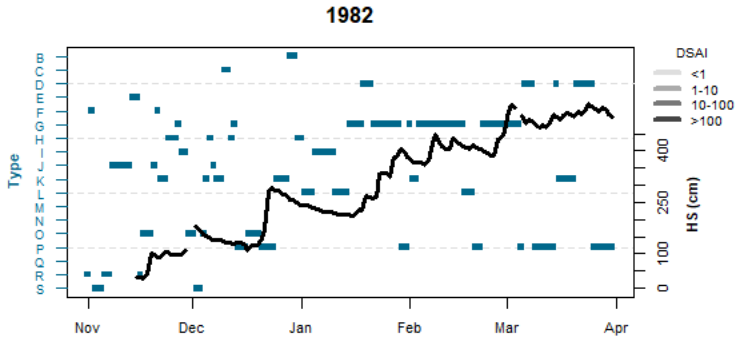

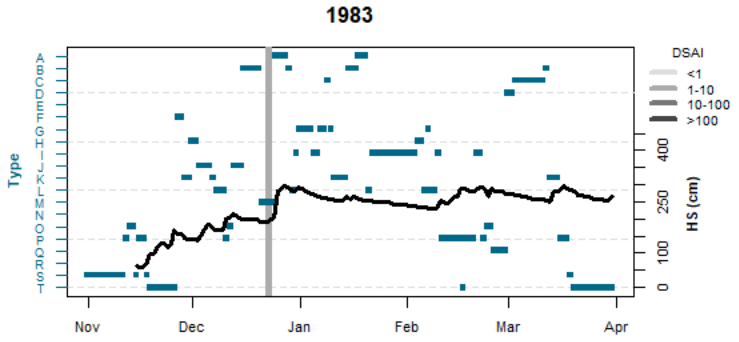
1983
Type
DSAI
<1
1-10
10-100
>100
HS (cm)
0
100
250
400
Nov
Dec
Jan
Feb
Mar
Apr

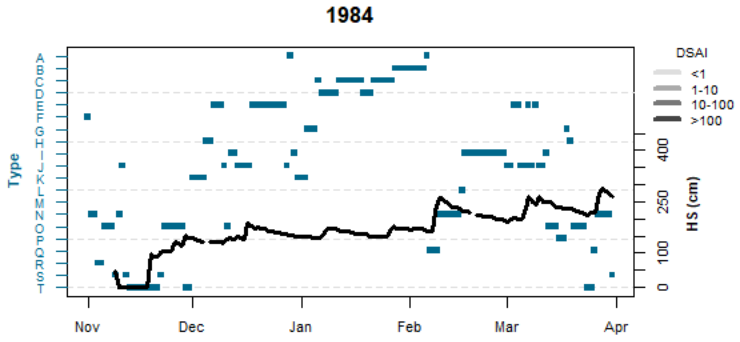
1984
Type
DSAI
<1
1-10
10-100
>100
HS (cm)
0
100
250
400
Nov
Dec
Jan
Feb
Mar
Apr

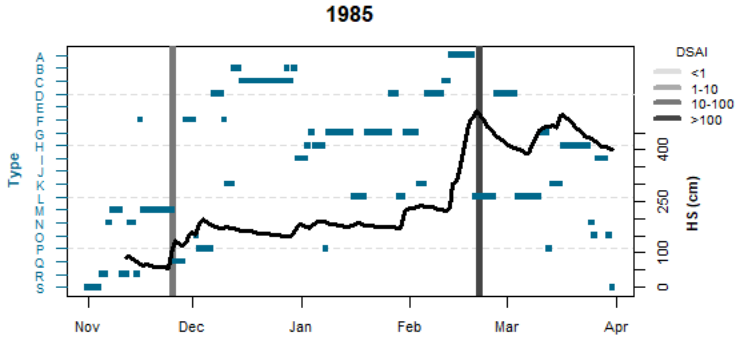
1985
Type
DSAI
<1
1-10
10-100
>100
HS (cm)
0
100
250
400
Nov
Dec
Jan
Feb
Mar
Apr

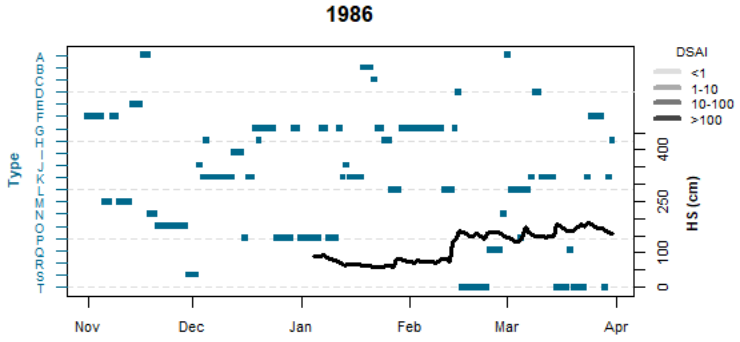
1986
Type
DSAI
<1
1-10
10-100
>100
HS (cm)
0
100
250
400
Nov
Dec
Jan
Feb
Mar
Apr

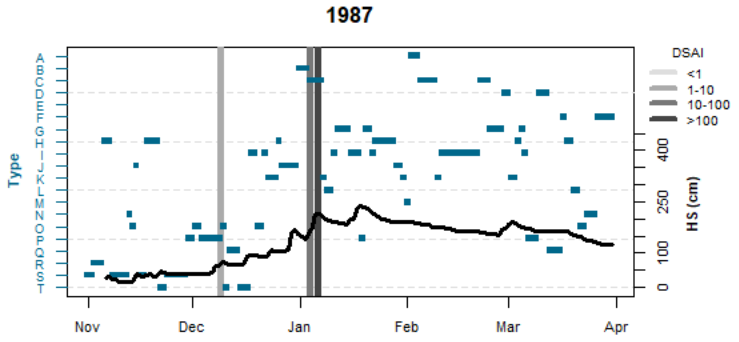
1987
Type
HS (cm)
DSAI
<1
1-10
10-100
>100
Nov
Dec
Jan
Feb
Mar
Apr

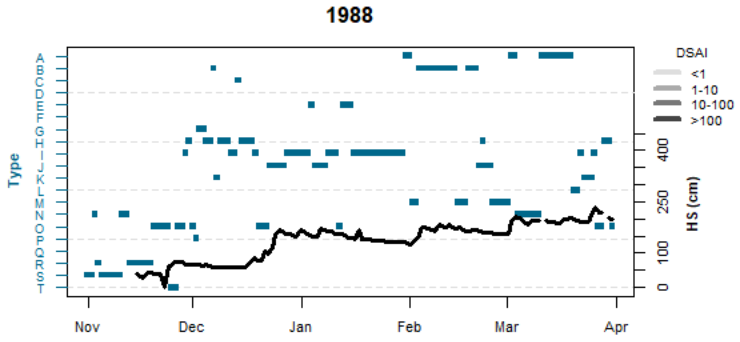
1988
Type
HS (cm)
DSAI
<1
1-10
10-100
>100
Nov
Dec
Jan
Feb
Mar
Apr

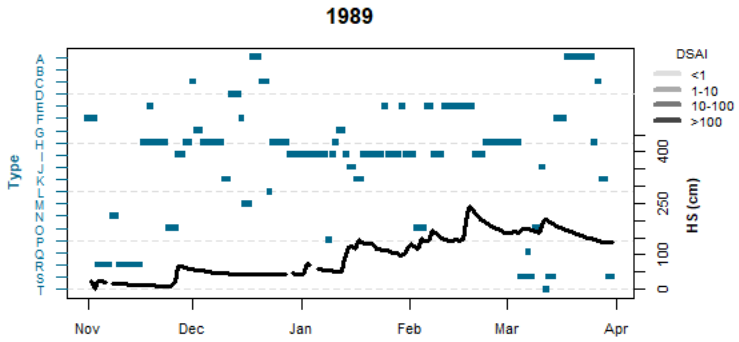
1989
Type
HS (cm)
DSAI
<1
1-10
10-100
>100
Nov
Dec
Jan
Feb
Mar
Apr

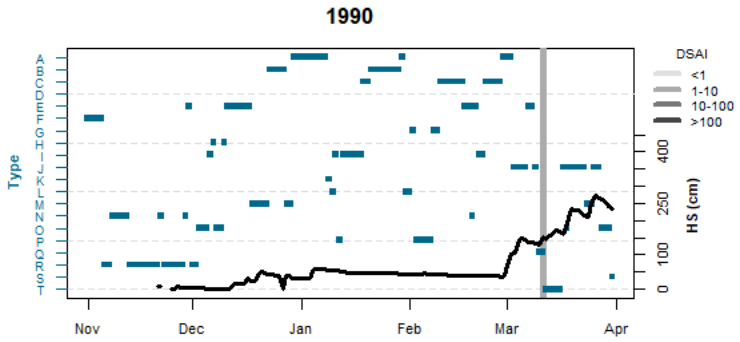
1990
Type
HS (cm)
DSAI
<1
1-10
10-100
>100
Nov
Dec
Jan
Feb
Mar
Apr

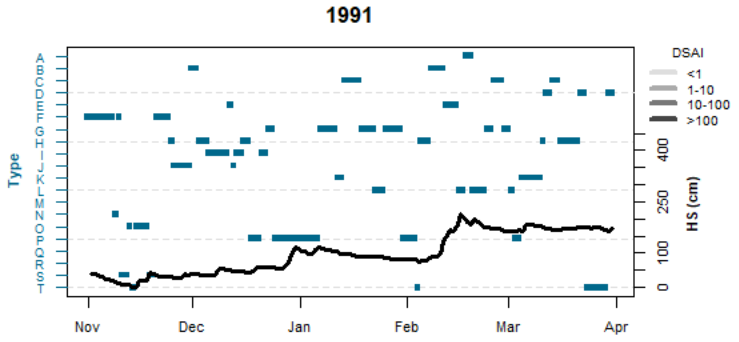
1991
Type
DSAI
<1
1-10
10-100
>100
HS (cm)
0
100
250
400
Nov
Dec
Jan
Feb
Mar
Apr

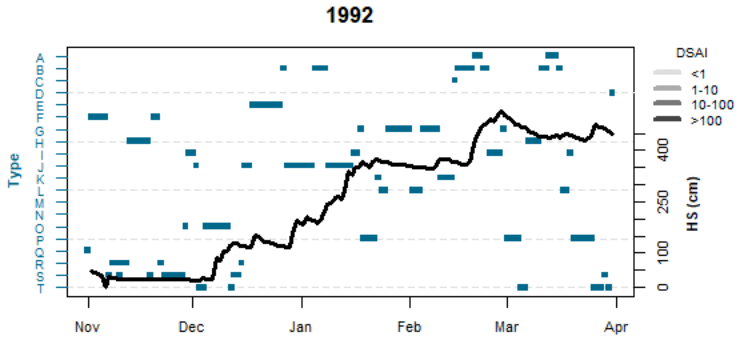
1992
Type
DSAI
<1
1-10
10-100
>100
HS (cm)
0
100
250
400
Nov
Dec
Jan
Feb
Mar
Apr

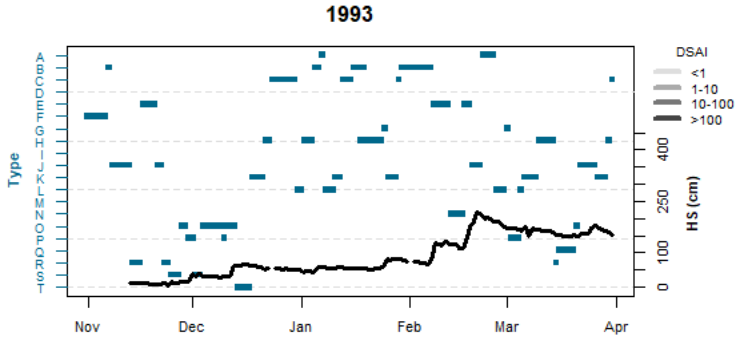
1993
Type
DSAI
<1
1-10
10-100
>100
HS (cm)
0
100
250
400
Nov
Dec
Jan
Feb
Mar
Apr

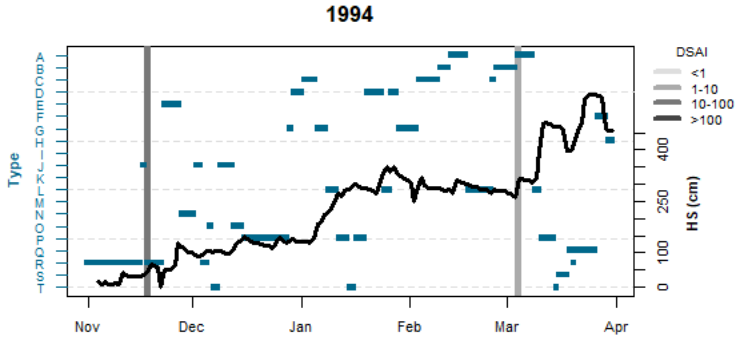
1994
Type
DSAI
<1
1-10
10-100
>100
HS (cm)
0
100
250
400
Nov
Dec
Jan
Feb
Mar
Apr

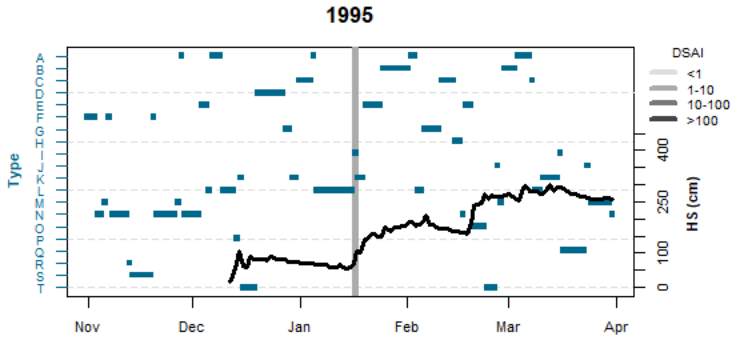
1995
Type
DSAI
<1
1-10
10-100
>100
HS (cm)
0
100
250
400
Nov
Dec
Jan
Feb
Mar
Apr

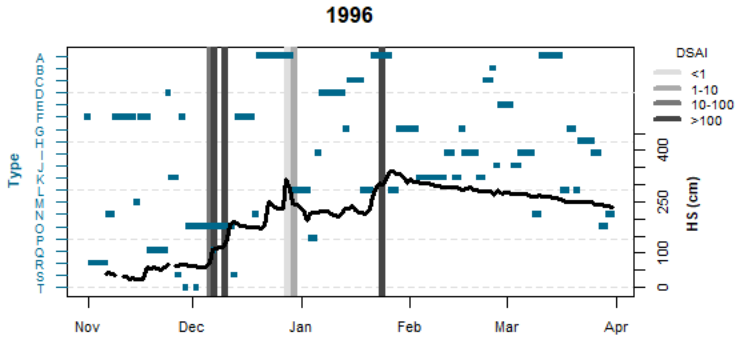
1996
Type
DSAI
<1
1-10
10-100
>100
HS (cm)
0
100
250
400
Nov
Dec
Jan
Feb
Mar
Apr

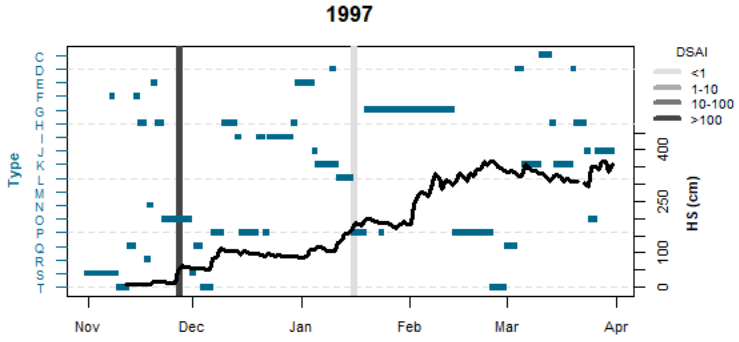
1997
Type
DSAI
<1
1-10
10-100
>100
HS (cm)
0
100
250
400
Nov
Dec
Jan
Feb
Mar
Apr

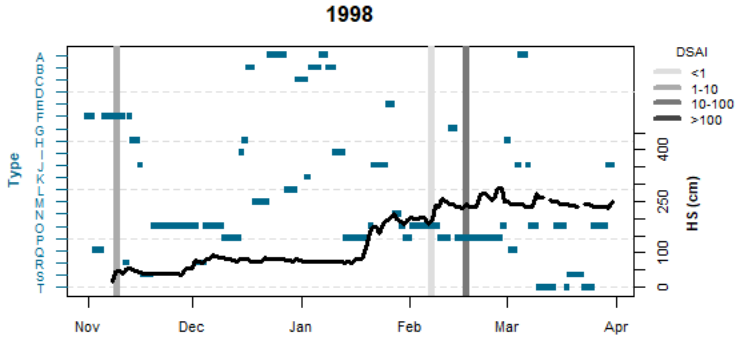
1998
Type
DSAI
<1
1-10
10-100
>100
HS (cm)
0
100
250
400
Nov
Dec
Jan
Feb
Mar
Apr

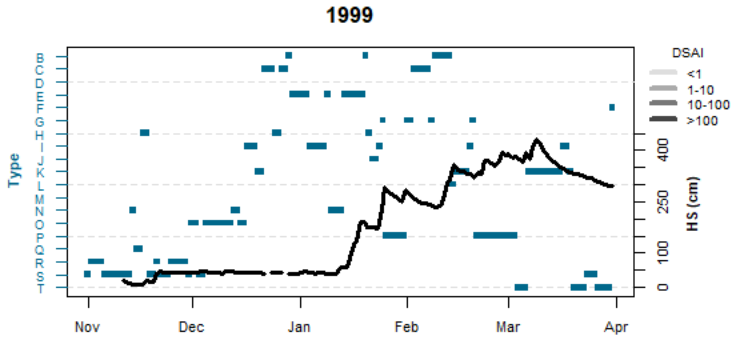
1999
Type
HS (cm)
DSAI
<1
1-10
10-100
>100
Nov
Dec
Jan
Feb
Mar
Apr

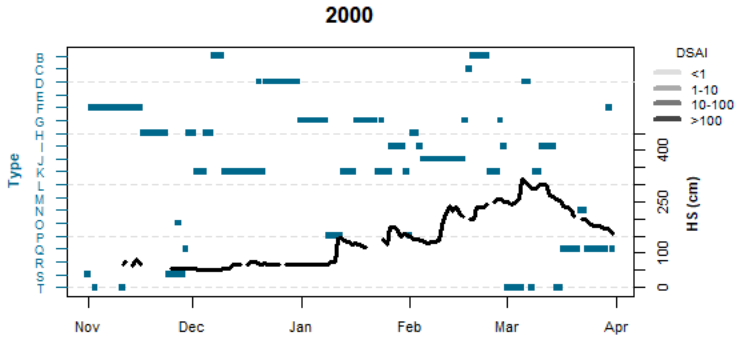
2000
Type
HS (cm)
DSAI
<1
1-10
10-100
>100
Nov
Dec
Jan
Feb
Mar
Apr

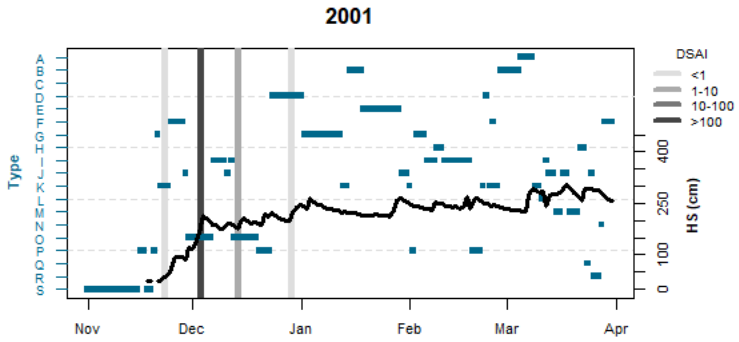
2001
Type
HS (cm)
DSAI
<1
1-10
10-100
>100
Nov
Dec
Jan
Feb
Mar
Apr

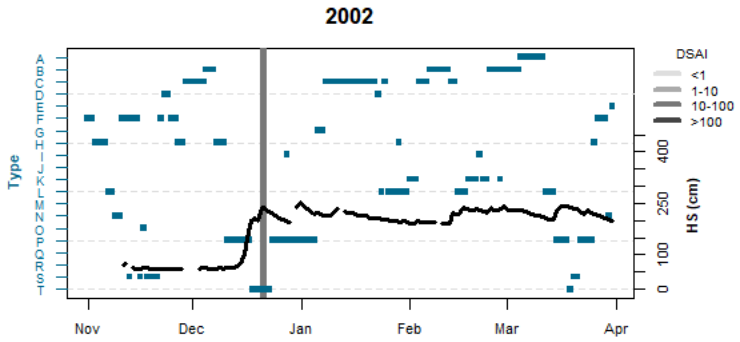
2002
Type
HS (cm)
DSAI
<1
1-10
10-100
>100
Nov
Dec
Jan
Feb
Mar
Apr

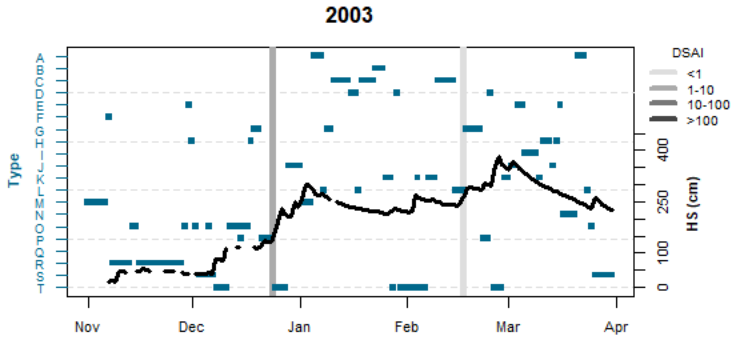
2003
Type
DSAI
<1
1-10
10-100
>100
HS (cm)
0
100
250
400
Nov
Dec
Jan
Feb
Mar
Apr

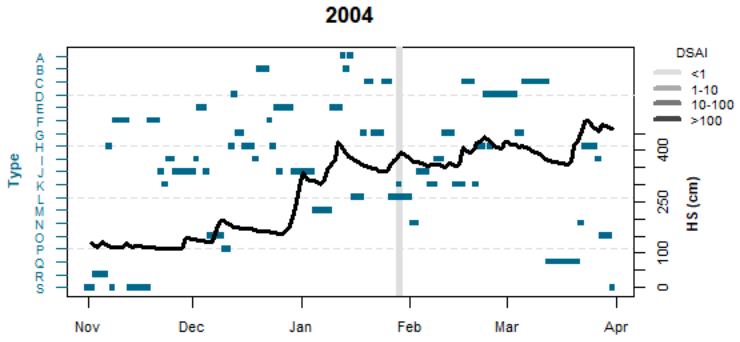
2004
Type
DSAI
<1
1-10
10-100
>100
HS (cm)
0
100
250
400
Nov
Dec
Jan
Feb
Mar
Apr

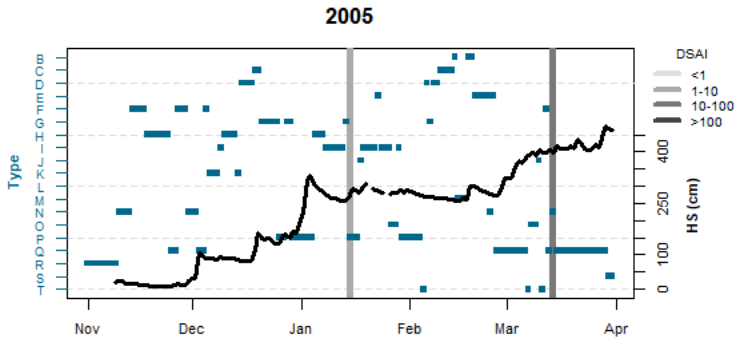
2005
Type
DSAI
<1
1-10
10-100
>100
HS (cm)
0
100
250
400
Nov
Dec
Jan
Feb
Mar
Apr

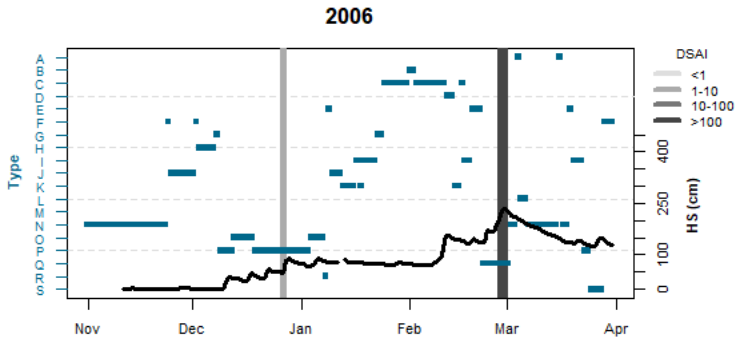
2006
Type
DSAI
<1
1-10
10-100
>100
HS (cm)
0
100
250
400
Nov
Dec
Jan
Feb
Mar
Apr

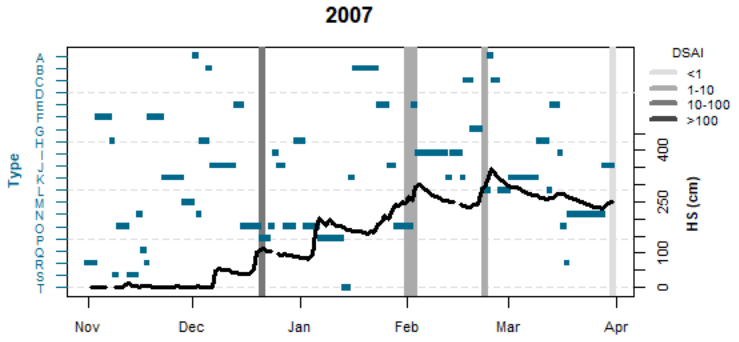
2007
Type
DSAI
<1
1-10
10-100
>100
HS (cm)
0
100
250
400
Nov
Dec
Jan
Feb
Mar
Apr

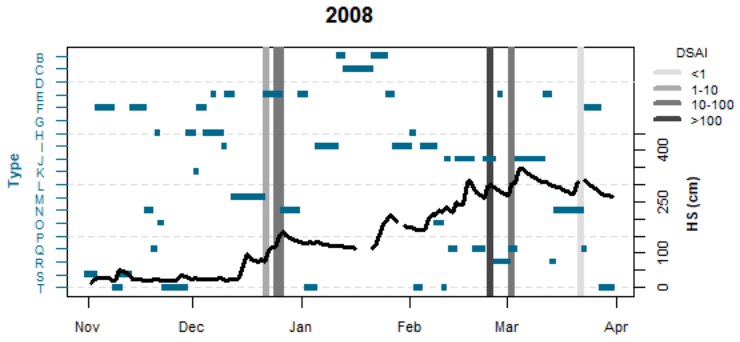
2008
Type
DSAI
<1
1-10
10-100
>100
HS (cm)
0
100
250
400
Nov
Dec
Jan
Feb
Mar
Apr

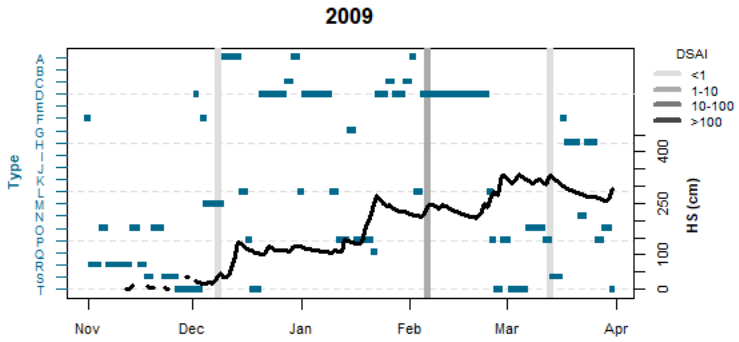
2009
Type
DSAI
<1
1-10
10-100
>100
HS (cm)
0
100
250
400
Nov
Dec
Jan
Feb
Mar
Apr

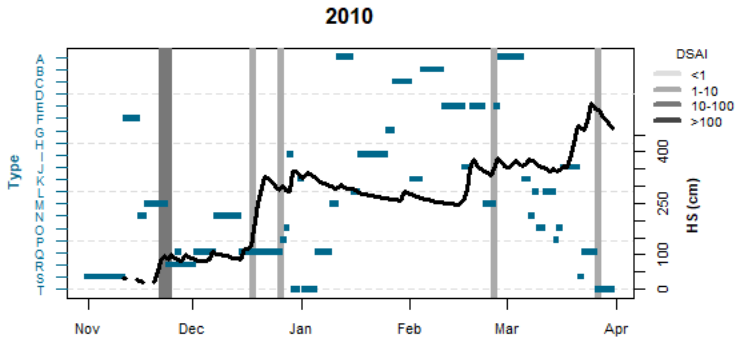
2010
Type
DSAI
<1
1-10
10-100
>100
HS (cm)
0
100
250
400
Nov
Dec
Jan
Feb
Mar
Apr

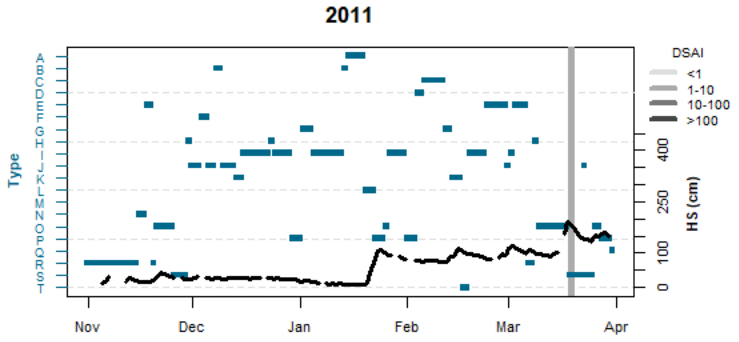
2011
Type
DSAI
<1
1-10
10-100
>100
HS (cm)
0
100
250
400
Nov
Dec
Jan
Feb
Mar
Apr

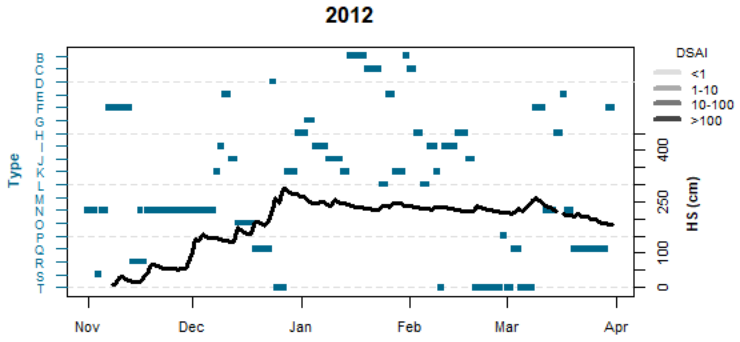
2012
Type
DSAI
<1
1-10
10-100
>100
HS (cm)
0
100
250
400
Nov
Dec
Jan
Feb
Mar
Apr

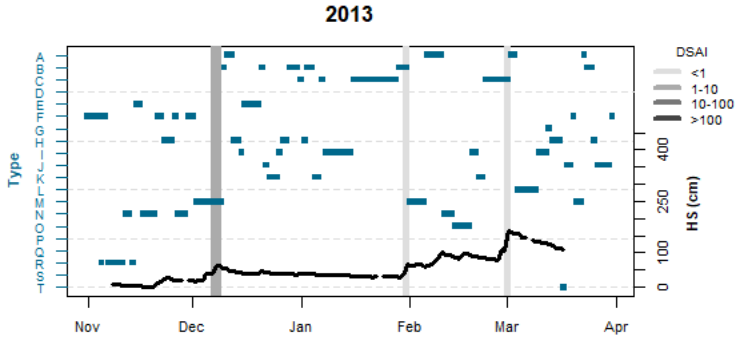
2013
Type
DSAI
<1
1-10
10-100
>100
HS (cm)
0
100
250
400
Nov
Dec
Jan
Feb
Mar
Apr

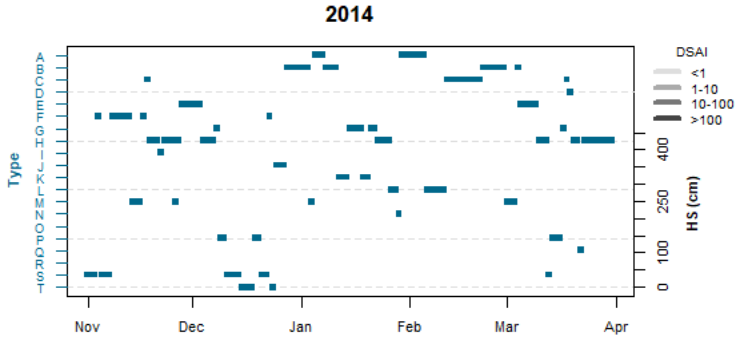
2014
Type
DSAI
<1
1-10
10-100
>100
HS (cm)
0
100
250
400
Nov
Dec
Jan
Feb
Mar
Apr

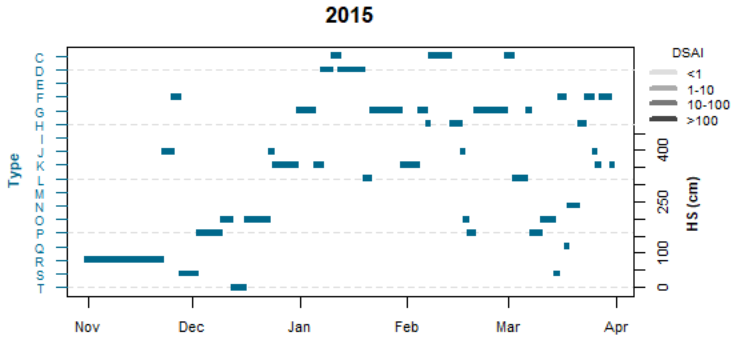
2015
Type
HS (cm)
DSAI
<1
1-10
10-100
>100
Nov
Dec
Jan
Feb
Mar
Apr

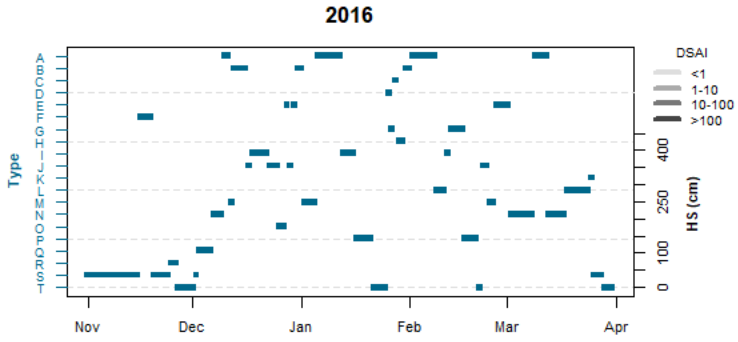
2016
Type
HS (cm)
DSAI
<1
1-10
10-100
>100
Nov
Dec
Jan
Feb
Mar
Apr

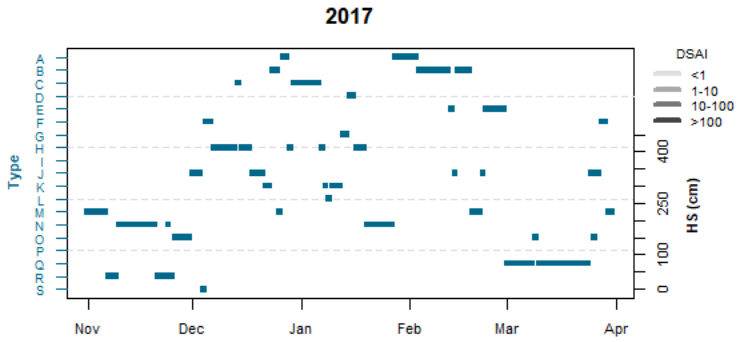
2017
Type
HS (cm)
DSAI
<1
1-10
10-100
>100
Nov
Dec
Jan
Feb
Mar
Apr

APPENDIX E

SENSITIVITY TO UNCERTAINTY IN AVALANCHE OBSERVATIONS

Daily avalanche observations compiled by professional ski patrol operations remain the most comprehensive avalanche record available. One key advantage to using this type of record is that most events are consistently recorded as they occur, whereas similar records compiled by backcountry avalanche centers depend largely on whether the avalanche damaged infrastructure or caused harm to a person. Despite this major advantage, there are still some important limitations of using ski patrol records. One such limitation is that the records are maintained primarily as a means to communicate general snowpack conditions between staff members, rather than to compile a list of exact measurements for every event. As a result, there is some uncertainty associated with what may otherwise seem straightforward observations, such as crown depth or relative avalanche size (R-size). Operationally, this uncertainty is negligible when the records are used on a day-to-day basis along with continuous, firsthand observations to assess stability. However, the amount by which a long-term study of avalanche events is impacted by measurement uncertainty is unclear. This section assesses the sensitivity of our research to measurement uncertainty in crown depth and R-size.

In order to assess the effect of measurement error on this research, we run a sensitivity analysis on the Bridger Bowl avalanche record. In this sensitivity analysis, we consider three different error rates, applied to depth and R-size for all events:

I. For every correct observation in the record, there is one incorrect observation.

II. For every two correct observations, there is one incorrect observation.

III. For every three correct observations, there is one incorrect observation.

We use the sample function in the statistical software R to randomly assign "errors" of -1, -0.5, 0, .5, or 1 foot for crown depth, and -1, 0, or 1 for R-size to each observation in the record. The sample function randomly selects the error value based on a specified probability distribution. Probabilities used for each of the three error rates (I-III listed above) are given for crown depth measurements in Table 1 and R-size in Table 2.

Table 1: Probability of assigning a given error in crown depth measurements for each error rate used in the sensitivity analysis.

Error Rate	-1'	-0.5'	0'	.5'	1'
I	0.125	0.125	0.5	0.125	0.125
II	0.0825	0.0825	0.67	0.0825	0.0825
III	0.0625	0.0625	.75	0.0625	0.0625

Table 2: Probability of assigning a given error in R-size for each error rate used in the sensitivity analysis.

Error Rate	-1	0	1
I	0.25	0.5	0.25
II	0.165	0.667	0.165
III	0.125	0.75	0.125

We assess the effect of measurement uncertainty by plotting histograms of crown depth and R-size for each error rate. There is very little change in the overall distribution of crown depths for any of the three error rates (Figure 1).

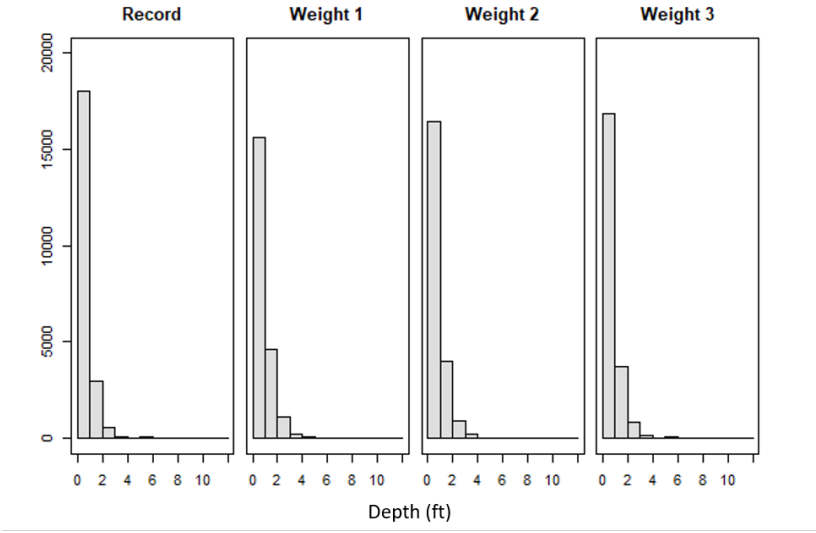

Figure 1: Histograms of crown depth in feet for the actual record (left), and error rates I-II (moving left to right).

Similarly, adjusting the R-size by +/- one size step, there is very slight change in the overall distribution of R-size for all events (Figure 2).

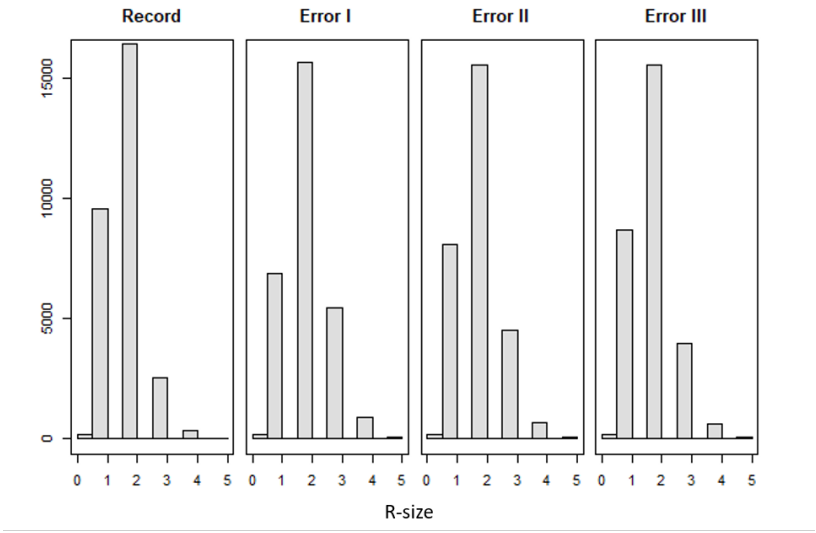

Figure 2: Histograms of R-size for the actual record (left), and error rates I-II (moving left to right).

Using the deep slab avalanche index (DSAI) described in the methods section, we identify the 1979, 1980, 1984, and 2011 seasons as major deep slab seasons in all three

error simulations (Table 3). In one of the three error simulations, the 1982 season is added in addition to the other four.

Table 8: List of seasons designated as major deep slab seasons for each of the three applied error rates.

Record	Major Seasons
Actual	1979, 1980, 1984, 2011
Error I	1979, 1980, 1984, 2011
Error II	1979, 1980, 1984, 2011
Error III	1979, 1980, 1982, 1984, 2011

This sensitivity analysis demonstrates that our analysis is robust to measurement uncertainty with respect to crown depth and R-size. Furthermore, while may be reasonable to assume a practitioner may misclassify size 1, 2, and 3 avalanches, it is far less likely that they would under-classify a size 4 or 5 event. Since the larger-magnitude events are weighted by several orders of magnitude larger than the small events, and since we are using the avalanche record only as a means to identify large-magnitude events, the impact of uncertainty with regards to R-size is likely much smaller even than what we have demonstrated in this sensitivity analysis. Thus, we acknowledge the uncertainty in the avalanche record, and implement an analysis that is not grossly affected by such measurement uncertainty.